POLITECNICO DI TORINO

Collegio di Ingegneria Meccanica, Aerospaziale, dell'Autoveicolo e della Produzione

Master's Degree Course in Mechanical Engineering

Master of Science Thesis

Experimental Investigation on the Dynamics of a Dummy Blade and Disk Coupled by a Dovetail Root Joint

Supervisors
Prof. Christian Maria Firrone
PhD. Zeeshan Saeed

Candidate
Meysam Kazeminasab

April 2021

Abstract

Vibration analysis is an important tool for understanding the dynamic characteristics of mechanical structures. In mechanical systems like turbomachinery bladed disk, a joint between two components can play a vital role to transmit dynamic information. In such a system, accurate prediction of joint characteristics is extremely significant in order to predict the responses by dynamic substructuring.

In every experimental impact test, spatial structural responses are collected by exciting at different places. The procedure is usually performed by measuring the time signal of response and the applied forces. These dynamic signals are recorded and processed in a Data Acquisition System wherein Fourier transforms and windowing operations are performed to filter out the noise in the signal to the best possible extent.

The main objective of this work has been to investigate collecting an experimental campaign by impact testing. The most common types of online signals that are utilized in Dynamic substructuring are Frequency Response Functions (FRFs), Coherence, and Power Spectral Density of input Force. The results corresponding to different impact points and also the response of various sensors have been compared. Moreover, we need to overcome all the pitfalls and uncertainties like double impact, averaging using different points for each average, mass loading effect and etc appeared during the experimental test in order to reach a good level of accuracy. In this thesis, the tests have been performed on a bladed-disk called VITAL in LAQ AERMEC lab. The blade and the disk each have been tested in a constraint-free condition which is realized by suspending them on flexible wires. The responses are measured by small tri-accelerometers and excitations are applied by a modal impact hammer. The data is collected using the Siemens Data Acquisition system called Simcenter Test.Lab and further post-processing has been done in MATLAB.

Keywords: *Dynamic substructuring, bladed disk, turbo-machinery, FRF, Coherence, experimental Impact test*

Acknowledgements

I would like to express my gratitude to my professors Christian Maria Firrone and Teresa Berruti for providing me the opportunity to work on this interesting topic in such a stimulating environment in AERMEC Laboratory. Moreover, I would also like to extend my deepest gratitude to my supervisor, PhD student Zeeshan Saeed, for introducing me to the field of vibration and for his dedication, patience and enthusiastic support through every aspect of this work.

Finally, I'm deeply indebted to express my very profound gratitude to my parents, family, and friends for providing me with unfailing support and continuous encouragement throughout my years of study and would not have been possible without them.

"Dedicated to the passengers of PS752 and their families."
R.P.

Table of Contents

List of Tables

List of Figures

Glossary

FRF Frequency Response Function

SISO single-input, single-output

SIMO single-input, multiple-output

DOF Degrees of Freedom

FRA Frequency Response Analyzer

DFT Digital Fourier Transform

FFT Fast Fourier Transform

RMS Root Mean Square

ICP Integrated Circuit Piezoelectric

MDOF Multi Degrees of Freedom

PSD Power Spectral Density

ASD Auto Spectral Density

CSD Cross-Spectral Density

Nomenclature

a_0	Mean value
a_n, b_n	Fourier of spectral coefficient
C	Damping matrix
F_0	External force vector
F	Force
i	imaginary unit, $i = \sqrt{-1}$
K	Stiffness matrix
k	Stiffness coefficient
M	Mass matrix
m	Mass
C_n, X_n	Modulus of Fourier coefficient
t	Time
ϕ_n	Phase of Fourier coefficient
f_s, ω_s	Sampling frequency
$\omega_m ax$	Nyquist frequency
f_{sine}	Frequency of sine wave
f_0, ω_0	Fundamental frequency
f_c, ω_c	Cut-Off frequency
T_0, T_c	Time span, pulse length, period

x, y, z Cartesian coordinate

$\dot{x}$ First derivative of displacement vector(Velocity)

$\ddot{x}, \ddot{z}$ Second derivative of displacement vector(Acceleration)

X_0 Complex vector

K_{dyn} Dynamic stiffness matrix

$x(t)$ Periodic function

ψ, ψ_r Eigenvector or mode shape

η, η_r Modal coordinate

ϕ, ϕ_r m-normalized eigenvector

$Y(\omega)$ Dynamic receptance matrix

ω^2 Eigenvalue for mode r

m_r Modal mass of r$^{th} mode$

k_r Modal stiffness of r$^{th} mode$

c_r Modal viscous damping of r$^{th} mode$

$H(\omega)$ Transfer function

$Y(\tau)$ Time lag

$S_{xx}(\omega)$ Power spectral density or Auto spectral density

$S_{xy}(\omega)$ Cross power spectral density

$R_{xx}(\omega), R_{xy}(\omega)$ Auto and cross-correlation function

H_1, H_2 Estimator

$\gamma^2(\omega)$ Ordinary coherence function

Chapter 1

INTRODUCTION

1.1 Vibration In Turbine

Turbine bladed disks are subjected in working condition to a broad spectrum of aerodynamic excitation forces which induce significant vibrations. One of the critical consequences of such high vibration amplitude is the bladed-disk failure caused by high cycle fatigue in turbo-machinery. This type of failure takes place when the blades are subjected to repeated excitation cycles and when the excitation force frequency equals the disk natural frequency, leading to the occurrence of resonance. Therefore prediction of system natural frequencies are crucial factor in order to avoid failure during real application. Experimental campaign analysis is a useful tool to perform impact test and measuring Frequency Response Function.

1.2 Thesis Approach And Aim

One of the most significant task in turbo-machinery is to predict dynamic characteristics including the mechanical joints at blade-disk (root joint) or blade-blade (shroud) interfaces accurately. These joints help dampening the vibration amplitudes. Identification or Measuring the interface degrees of freedom(DoF) accurately will be difficult due to size and weight of the blades and also geometry of interface inaccessibility.

The first and foremost step in experimental campaign analysis is to measure the excitation and the response of the structure under test. The structure must be excited by applied excitation force and resulting response vibrations, typically accelerations, which are both measured resulting in a Frequency Response Function data set. The FRF data measurement are very useful to identify natural frequencies, damping coefficients and mode shapes. The method has been chosen to excite the structure in order to get vibrating response in this project is impact hammer.

The aim of this thesis is focusing on conducting an experimental campaign by impact testing on our structure in different configuration. The experimental test has been set up to collect measured FRFs on a blade, disk and their assembly. Since this thesis is a part of a project on linear joint identification, all the measurements have been collected in this thesis utilized in the final project with the goal of joint identification of bade-disk. Therefore all the measurements are to be used in a substructuring context, so the test need to perform in such a way that to require high degree of accuracy and multi directional dynamics. During the test, all the difficulties and uncertainties should be avoided to the best possible extent. Their common occurrences will be discussed in the thesis.

Chapter 2

THEORY

2.1 Overview

The fundamental equations and their various forms will be introduced conceptually to provide insight into the relationships between the structure's dynamic characteristics and the frequency response function measurements. Despite the fact that in real application with multiple degrees of freedom(MDOF) and some degree of non-linearity, the superposition of single degree of freedom(SDOF) of linear models can be interpreted. Dynamic models are assembled for evaluating *dynamic behaviour* of components or systems. Depending on the principal objective of the analysis, the model can be designed in different ways.

The basic theoretical explanation of measuring frequency response functions will be covered here. Part one begins with theory of dynamic modelling which are include theory of Multi Degrees of Freedom system, Frequency Response Function, Coherence, Receptance and Accelerance model and translation to the other domain.

2.2 System With Multi Degrees of Freedom

The Dynamic equation of motion for a MDOF system which is describe behavior of system is expressed in following form:

$$[M]\{\ddot{x}\} + [C]\{\dot{x}\} + [K]\{x\} = \{F_0\}e^{i\omega t} \tag{2.1}$$

$$x(t) = \{X_0\}e^{i\omega t} \tag{2.2}$$

Substituted into equation (2.1), we obtain

$$\left([K] - \omega^2[M] + i\omega[C]\right)X_0e^{i\omega t} = F_0e^{i\omega t} \tag{2.3}$$

where K which is stiffness matrix, M is mass matrix, C is damping matrix,X_0 is complex vector, F_0 is external force vector and $x(t)$ is the steady state solution form of our system.
It will be defined $[K_{dyn}] = [K] - \omega^2[M] + i\omega[C]$ is the dynamic stiffness matrix which is a function of excitation frequency. Vector of the steady-state oscillation amplitudes is obtained as:

$$\{X_0\} = [K_{dyn}(\omega)]^{-1}\{F_0\} = [Y(\omega)]\{F_0\} \tag{2.4}$$

where $[Y(\omega)]$ is the receptance matrix.

This inversion is rather onerous from a computational point of view, especially in the case of systems with a very high number of degrees of freedom and also does not allow to highlight some important properties of the receptance matrix.

In the case of forced response, solution can be reach by applying direct modal transformation and premultiplying by $[\Psi]^T$ where $\{x(t)\} = [\Psi]\{\eta(t)\}$. We obtain a system of n decoupled differential equations of the type [1]:

$$\Big([k_r] - \omega^2[m_r] + i\omega[c_r]\Big)\,\eta_r(t) = \{\Psi_r\}^T\{F_0\}e^{i\omega t} \tag{2.5}$$

Here m_r is modal mass, k_r is modal stiffness, c_r is modal viscous damping of r^th mode, η_r modal coordinate (complex form) depend upon the normalisation of the mode shape vectors for their magnitudes. Solution form here is $\eta_r(t) = \eta_{r0}e^{i\omega t}$ and by using this solution in equation 4.5, after simplification equation 2.7 appeared. Clearly also the steady-state modal coordinates will be harmonic and therefore[1]:

$$\{x(t)\} = \{X_0\}\,e^{i\omega t} = \sum_{r=1}^{n}\{\psi_r\}\eta_r(t) = \sum_{r=1}^{n}\{\psi_r\}\eta_{r0}e^{i\omega t} \tag{2.6}$$

where η_{r0} is the amplitude of modal coordinate:

$$\eta_{r0} = \frac{\{\psi_r\}^T\{F_0\}}{k_r - \omega^2 m_r + i\omega c_r} \tag{2.7}$$

Therefore the vector of the steady-state oscillation amplitudes is expressed by the following formula[1]:

$$\{X_0\} = \sum_{r=1}^{n}\frac{\{\psi_r\}^T\{F_0\}\{\psi_r\}}{k_r - \omega^2 m_r + i\omega c_r} \tag{2.8}$$

This is valid also in the case of complex vector $\{F_0\}$ or in the case of n forcing not in phase with each other. At this point the receptance is defined complex function of excitation frequency, as:

$$Y_{jk}(\omega) = \frac{X_{j0}}{F_{k0}}\bigg|_{F_{i0}=0,\forall_i\neq k} \tag{2.9}$$

The fact is emphasized, far from marginal, which for a correct definition of receptance it is necessary that all the applied forces are zero, except that relating to the $k-th$ degree of freedom, that is $\{F_0\} = [0 \quad \cdots \quad F_{k0} \quad \cdots \quad 0]^T$. Note that j is relating to the measurement of response and k is regard to the node in which we apply the force. It can be observed that measuring FRF $Y(\omega)_{jk}$ is more convenient than measuring dynamic stiffness K_{dyn}. Equation of (2.8) can therefore be depicted in the following form:

$$\begin{Bmatrix} X_{10} \\ X_{20} \\ \vdots \\ X_{j0} \\ \vdots \\ X_{n0} \end{Bmatrix} = \sum_{r=1}^{n} \frac{[\psi_{1r} \quad \psi_{2r} \quad \cdots \quad \psi_{kr} \quad \cdots \quad \psi_{nr}]}{k_r - \omega^2 m_r + i\omega c_r} \begin{Bmatrix} 0 \\ 0 \\ \vdots \\ F_{k0} \\ \vdots \\ 0 \end{Bmatrix} \begin{Bmatrix} \psi_{1r} \\ \psi_{2r} \\ \vdots \\ \psi_{jr} \\ \vdots \\ \psi_{nr} \end{Bmatrix} \tag{2.10}$$

from which it is derived:

$$\{X_{j0}\} = \sum_{r=1}^{n} \frac{\{\psi_{kr}\}\{F_{k0}\}\{\psi_{jr}\}}{k_r - \omega^2 m_r + i\omega c_r} \tag{2.11}$$

which allows to write the expression of receptance as bellow:

$$Y_{jk}(\omega) = \sum_{r=1}^{n} \frac{\psi_{jr}\psi_{kr}}{k_r - \omega^2 m_r + i\omega c_r} = \sum_{r=1}^{n} \frac{\phi_{jr}\phi_{kr}}{\omega_r - \omega^2 + i2\zeta_r\omega\omega_r} \tag{2.12}$$

From this matrix equation we can extract any one FRF element, such a s $Y_{jk}(\omega)$, and express it explicitly in a series form:

$$Y_{jk}(\omega) = \sum_{r=1}^{n} \frac{(\phi_{jr})(\phi_{kr})}{\omega_r^2 - \omega^2 + i\eta_r\omega_r^2} \tag{2.13}$$

Receptance $Y_{jk}(\omega)$ is a complex function and can be represented graphically in modulus and phase. Furthermore, according to the place and direction of excitation and response, types of FRF can be defined:

- *Point Receptance* when coordinates of excitation and response are equal $j = k$
- *Transfer or cross Receptance* when coordinates of excitation and response are different $j \neq k$

By given the expression (2.12) it is easy to verify that the receptance holds reciprocity relation $Y_{jk}(\omega) = Y_{kj}(\omega)$ which distinguishes whether if the system is linear or not[1].

2.3 Frequency Response Function

Frequency response function (FRF) is a frequency based measurement function utilizing to identify the resonant frequencies, damping and mode shape of structure. As a matter of fact frequency response function related to a transfer function in frequency domain between the input and output of a system. Moreover FRF is a complex function which containing amplitude and phase. Their amplitude is the ratio of the input force to the response with a g/N unit and the phase is represented in degrees which depicts whether the response moves in and out of phase with the input. In other words, any function that has amplitude and phase can also be changed to real and imaginary terms as bellow[1] [2].

$$Amplitude = \sqrt{Imag^2 + Real^2} \qquad Phase = \tan^{-1}(\frac{Imag}{Real}) \tag{2.14}$$

2.4 Spectral Densities and Coherence

Coherence is function versus frequency which depicts how much of the output is due to the input in the FRF. In other words, coherence function indicates the degree of linear relationship between two signals as a function of frequency. It could be an indication of the FRF's quality. The accuracy of the FRF from measurement to repetition of the same measurement is evaluated.

In standard form we consider the input is X and output is Y, the FRF usually represented by H. Frequency response function is the crosspower S_{xy} of the input x and output y divided by the autopower S_{xx} of input [3].

$$H = \frac{S_{xy}}{S_{xx}} \tag{2.15}$$

Autopower S_{xx} is the complex conjugate $(a-ib)$ of the input spectrum multiplied by itself $(a+ib)$, which turns into an all real function, containing no phase. The crosspower S_{xy} is the complex conjugate of the output spectrum multiplied by the input spectrum, and contains both amplitude and phase [2].
For a harmonic excitation, the FRF is the relationship between the response $x(t)$ (output) to an the excitation $f(t)$ (input), the previous equation turn into:

$$H(\omega) = \frac{x(t)}{F(t)} \tag{2.16}$$

it is also possible to see in following figure.

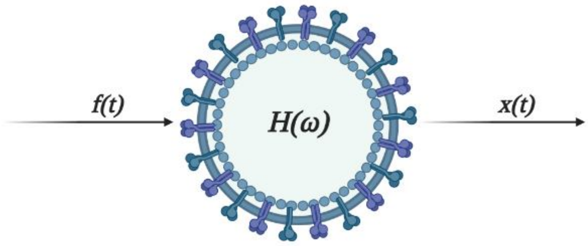

Figure 2.1: Frequency Response Function (FRF) for a harmonic excitation on a SISO (Single-Input-Single-Output) system.

In the analysis of the signals, two wave sources are said to be perfectly coherent with each other when they have constant phase difference, same frequency and same waveform.
In the experimental modal analysis, for the calculation of the frequency response function of a point the functions of auto-correlation and cross-correlation applied to the response signals (as well as the output signals) and excitation (i.e. the entrance). Signal $x(t)$ is the correlation of that signal with itself when measured after a time lag τ, $x(t+\tau)$ [3]:

$$R_{xx}(\tau) = \lim_{T\to\infty} \frac{1}{T} \int_{-T/2}^{T/2} x(t)x(t+\tau) \tag{2.17}$$

Which indicates how much the signal is related to itself. The Fourier transform of $R_{xx}(\tau)$ is called Power Spectral Density (PSD) or Auto Spectral Density (ASD) and is indicated [3]:

$$S_{xx}(\omega) = \mathscr{F}\{R_{xx}(\tau)\}$$

$$R_{xx}(\tau) = \frac{1}{2\pi} \int_{-\infty}^{+\infty} S_{xx}(\omega) e^{i\omega\tau}\, d\omega \tag{2.18}$$

$$S_{xx}(\omega) = \int_{-\infty}^{+\infty} R_{xx}(\tau) e^{-i\omega\tau}\, d\tau \tag{2.19}$$

Such definitions may also be generalized to combine two separate functions, such as the measurement of the so-called frequency response function (FRF). The

FRF is a transfer function that relates to at least one input output (for instance, the vibration response $x(t)$ to the random excitation force $f(t)$. In this case, the PSD is called Cross-Spectral Density (CSD) or, more often, cross-correlation, and relationships become [3]:

$$R_{fx}(\tau) = \lim_{T\to\infty} \frac{1}{T} \int_{-T/2}^{T/2} f(t)x(t+\tau) = \frac{1}{2\pi} \int_{-\infty}^{+\infty} S_{fx}(\omega)e^{i\omega\tau}\, d\omega \tag{2.20}$$

$$S_{fx}(f) = \int_{-\infty}^{+\infty} R_{fx}(\tau)e^{-i\omega\tau}\, d\tau \tag{2.21}$$

The CSD functions are complex functions (including real and imaginary parts, or magnitude and phase), whereas the PSD is a real function with magnitude only.

Measuring the FRF several times in order to find approximate reliable of structures transfer function. The repeatability of the individual FRFs is checked by estimating a coherence function, while the average is calculated using different estimator methods, depending on the desired end result.

The function $H(\omega)$ is a transfer function that represents the system. However, equation (2.16) is not valid unless the signals are harmonic. The meaning of autocorrelation and further developments for non-periodic signals was thus clarified in the couple of upper paragraph.

The convolution of the response with force can, however, be applied. It is possible to show that [3]:

$$|H(\omega)|^2 = \frac{S_{ff}(\omega)}{S_{xx}(\omega)} \tag{2.22}$$

and

$$H_1(\omega) = \frac{S_{xf}(\omega)}{S_{xx}(\omega)} \tag{2.23}$$

There are three different FRF estimators which equation (2.23) is one of them. This estimator $H_1(\omega)$ is the *conventional* FRF estimator and is determined by using the cross input-output spectrum and the input auto-spectrum. It is said to be unbiased with respect to noise on the output.

Another type of FRF estimator, $H_2(\omega)$, is reached by dividing the output auto-spectrum by the cross input-output spectrum:

$$H_2(\omega) = \frac{S_{ff}(\omega)}{S_{fx}(\omega)} \tag{2.24}$$

This estimator is said to be unbiased with respect to noise on the input.

Although both $H_1(\omega)$ and $H_2(\omega)$ estimators should give the same result, practically it will not happen due to some reasons:

- The signals include noise;
- The system relating the input and output is not linear;
- The measured output $x(t)$ is not a consequence of the input $f(t)$ alone, but also from other non-quantified external inputs.

Hence, the ratio of the two estimators can be defined as an indicator of the quality of the analysis:

$$\gamma^2(\omega) = \frac{H_1(\omega)}{H_2(\omega)} = \frac{|S_{xf}(\omega)|^2}{S_{xx}(\omega)S_{ff}(\omega)} \tag{2.25}$$

where $\gamma^2(\omega)$ referred to the ordinary coherence function, which can assume values in the interval [0,1]. Basically, the coherence can be seen as a measure of the *correlation* between two signals.

- A value of 1 at a specific frequency indicates that the FRF amplitude and phase are very repeatable from measurement to measurement.
- A value of 0 means that the tests should not be replicated. That is a potential *warning flag* that there is a measurement error Configuration.

When the amplitude of a FRF is very high, for example at a resonant frequency, the coherence will have a value close to 1 and when the amplitude of the FRF is very low, for example at an anti-resonance, the coherence will have a value closer to 0. This is because the signals are so low,their repeatability is made inconsistent by the noise floor of the instrumentation. Source of the problems will explain in the next chapter.

2.5 Receptance and Accelerance Models

The use of receptance Frequency Response Function (FRF) models has main key factors. The main factor is the design of experimental models within the frequency domain.Translating from the modal or physical to the frequency domain is straightforward, as this section will show. The transition from the frequency domain to the other domains is substantially more Complicated.It should be noted that although the formulation of the receptance is in use, there is no limitations placed once a frequency domain option is selected, as any formulation in the frequency domain is easily translatable.This section addresses the transition from the physical and modal domain to the frequency domain and explicitly to the formulation of the receptance [4].

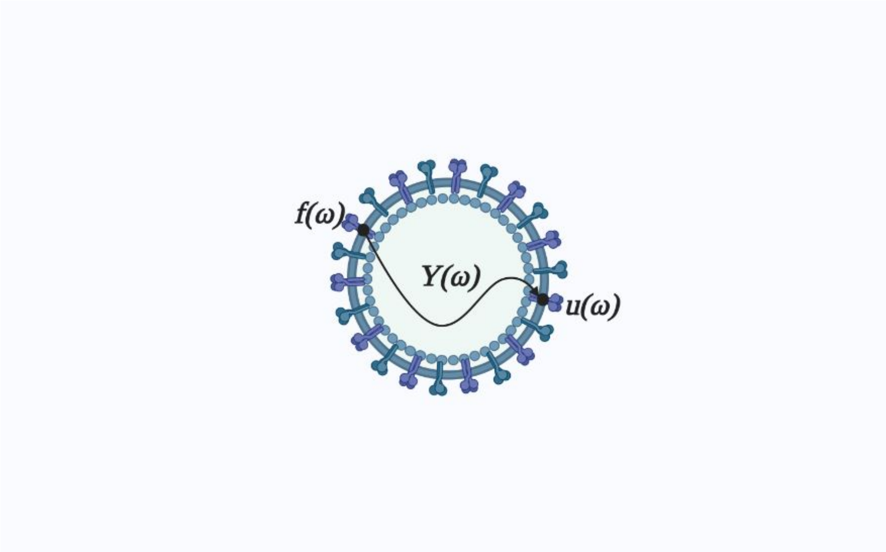

Figure 2.2: Receptance $Y(\omega)$ graphically shown. The input is a force $f(\omega)$ and the output is a displacement $u(\omega)$

Receptance is a measure of how much a structure moves for a unit input of force. Receptance also is the inverse of stiffness. As such, it is the transfer from a force $f(\omega)$ to a displacement $u(\omega)$ as illustrated in Figure (2.2) and described in Equation (2.26). The dependency on frequency ω is often omitted [4].

$$Y(\omega) = \frac{u(\omega)}{f(\omega)} \tag{2.26}$$

Another common representation form of FRF is accelerance which the definition is units of acceleration over force.

$$A(\omega) = \frac{\ddot{u}(\omega)}{f(\omega)} = -\omega^2 \frac{u(\omega)}{f(\omega)} \tag{2.27}$$

2.5.1 Translating from the Other Domains

Figure 2.3 provides a description of the various domains in which the dynamics of the substructure may be considered. Across the various domains, the substructure data can be derived either from numerical models, from experimentally measured data or from a combination of both.

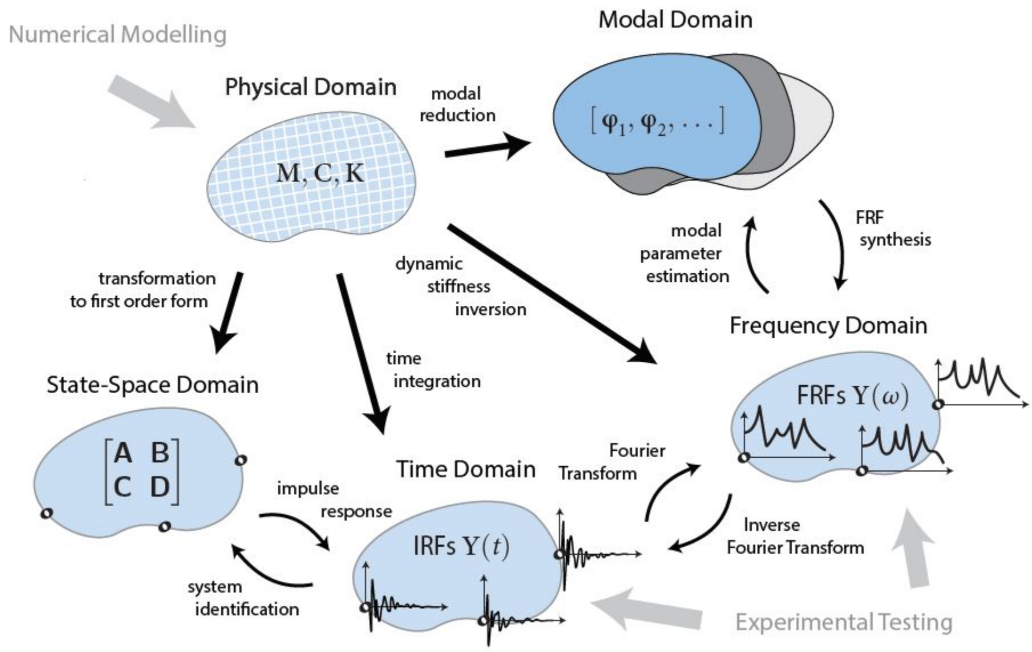

Figure 2.3: Five domains for structural dynamic simulation, approached from either a numerical modelling or experimental testing perspective, Some common conversions are indicated by arrows between the domains [4].

The Physical Domain

representation in the physical domain can be either discretized or continuous.The physical domain is the domain where the Finite Element approach is employed Equation (2.28) describes the physical domain's equilibrium equation [5] [6].

$$M\ddot{u}(t) + C\dot{u}(t) + Ku(t) = f(t) \tag{2.28}$$

Where the model matrices are the mass M, damping C and stiffness K matrices. $f(t)$ represents the external load on the system. Using the Fourier Transform to convert to the frequency domain by means of stating $u = ue^{i\omega t}$ Equation (2.28) becomes:

$$(K - \omega^2 M + j\omega C)u(\omega) = f(\omega) \tag{2.29}$$

$$Z(\omega)u(\omega) = f(\omega) \tag{2.30}$$

$$u(\omega) = Y(\omega)f(\omega) \tag{2.31}$$

Here $Z(\omega)$ represents the frequency dependent dynamic stiffness.$Y(\omega)$ is its inverse; the dynamic receptance. Equations (2.28) through (2.31) describes the translation from physical to frequency domain. The resulting receptance FRF is found to be:

$$Y(\omega) = (K - \omega^2 M + j\omega C)^{-1} \tag{2.32}$$

The FRFs $Y(\omega)$ can be measured for one or more structures or substructures. They contain substrucyures' dynamic behaviour in vs frequency. They are building blocks in frequency based substructuring. In chapter 5, some measurements will be shown for different substrucures and their configuration in the FBS context. While measuring them practically and accurately is discussed in Chapter 4 and 5.

Chapter 3

EXPERIMENTAL MODELLING

3.1 Introduction

We are going to evaluate the measurement techniques in this chapter. First of all, consideration should be granted to vibration measurement methods in general to show the meaning of the ones used here for our particular interest . Fundamentaly, two types of vibration measurement are[7]:

- When only one type of parameter is measured (usually the response levels)
- Where both input and response output parameters are measured.

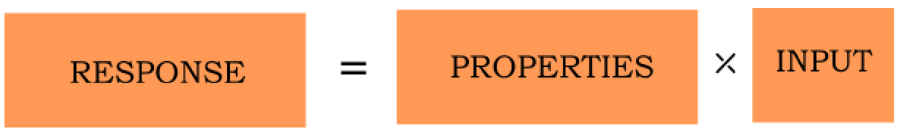

Figure 3.1: Relationship between response, properties, and input.

We can see that only when two of the three terms in this equation have been determined can we fully describe what happens in the test object's vibration. When we just calculate the response, we can not tell whether a very high response is due to a strong excitation of structural resonance. Nonetheless, all measurement forms have their uses, and in both cases, most of the equipment and instrumentation used are similar [7].

All of our attention here to the second type of measurement, where both excitation and response are measured simultaneously so that the basic equation can be taken to deduce the system properties directly from the measured data. There are two most common methods which both have advantages and disadvantages as following single-point excitation and excitation at several points on the structure. Measurements such as these are also referred to as *Mobility* measurements or *Frequency Response Function (FRF)* measurements. Responses were obtained directly using a single FRF excitation yield by dividing the *Measured Responses* by the *Measured Excitation Forces.* These are referred to as *SISO* (single-input, single-output) or *SIMO* (single-input, multiple-output) tests [7].

3.2 Test Planning

We will see that the type of approach we use to carry out the test and the data we measure will be of vital importance for undertaking's success. It is clear that there will need to be a comprehensive test preparation step before full-scale measurements are made and decisions taken concerning the methods of excitation, signal processing, and data analysis, as well as the proper selection of which data to measure, where to excite the structure and how to prepare and support it for those measurements. It is important to notice that recent advances in modal testing have resulted in a number of procedures for evaluating the optimal choice of different parameters, including positions for the exciter and response transducer. These methods are based on the pre-test existence of some type of theoretical model of the test structure, which they use to classify the most (and least) important or propitious areas of the structure from consideration of the various demands of [7]:

- support points (to minimize external influences).
- Excitation points (to ensure effective excitation of all modes).
- Response points (to ensure adequate coverage of all mode shapes so as to permit clear identification and discrimination of those in the test range).

3.3 Quality of Measured Data

The concern with quality assurance has now increased understanding of the need to ensure the highest reliability and consistency of the data that we assess and the results obtained from its subsequent processing. In the following procedure, we are going to evaluate some items in order to enable results to be obtained of the highest quality possible by the equipment and methods used [7].

3.3.1 Quality of Signal

The first concern is generally to obtain signals of adequate intensity and clarity and that is free from unnecessary noise. In addition to the obvious issues of proper transducer selection and conditioning electronics, it is often found that the dynamic range of the measured quantities is severe, especially when the frequency range covered is wide-more than a decade in frequency. What sometimes happens is that in one frequency range, there is a very broad signal component. In such cases, the frequency range of the measurements should be limited so that all components of interest have adequate signal strength to allow for their accurate measurement.

3.3.2 Fidelity of Signal

Another question, the transverse sensitivity properties exhibited by most accelerometers and other response transducers used in modal tests provide an example of this problem. Often, the transducer's motion is much greater in a direction perpendicular to its axis of measurement (than in the direction of measurement), with the consequence that the output is heavily polluted by the portion of transverse sensitivity, often giving somewhat misleading indications of the structure's motion. Certain conditions, including the incorrect marking or connection of transducers, cables, and channels to the data acquisition system, may lead to erroneous measurements. This is the test of the fundamental resonance and antiresonance pattern seen on the FRF curves. It has already been noted that resonances and antiresonances will alternate at any point FRF (excitation and response at the same DOF).In addition, the frequency of antiresonances in the FRF curve is closely related to the degree of separation between the two DOFs to which the FRF refers: excitation and response points which are well-separated on the test structure appear to have fewer antiresonances than those which have these two points presented far closer together [7].

3.4 Preparation of Structure

3.4.1 Free Support

The planning of the test structure itself is an important precursor to the entire process of calculating FRF. The first decision to make is whether to test the system under a *Free* condition or *Grounded* condition. In this thesis, a *Free Support* configuration is used. The *free* implies that the test object at each of its coordinates is not bound to the ground and is, in essence, freely floating in space. In this condition, the structure will exhibit rigid body modes that are dictated solely by its properties of mass and inertia, and where there is no bending or flexing at

all. In theory, any structure would have six rigid body modes, and each has a natural frequency of 0 [Hz]. By testing a structure in this free configuration, we can evaluate the rigid body modes and, therefore, the mass and inertia properties, which can be very useful data themselves [7].
Practically, it is not attainable to provide completely free support; the structure mechanism must be maintained in some way, but it is usually feasible to provide a suspension device that is similar to the free state. That can be accomplished by putting the test piece on very soft *springs*, as the light elastic bands might do, so that the rigid body modes, though no longer having zero natural frequencies, have very low values relative to those of the bending modes. In this case, very low means that the highest rigid body mode frequency for the lowest bending mode is less than 10 to 20 percent. If we achieve this type of suspension system, then we can still derive the rigid body (inertia) properties from the structure's very low-frequency behavior without having any major effect on the flexural modes, which are the focus of the test. Meanwhile, careful consideration should be paid to the risk of the suspension causing significant damping to only lightly damped test parts [7].
For this type of suspension, it should be noted that every rigid body would have no less than six modes, and it is important to verify that the natural frequencies of all these are sufficiently low until it is satisfied that the suspension system used is sufficiently soft [7].

3.5 Structure's Excitation

3.5.1 Hammer or Impactor excitation

The method of excitation imposed in this thesis is through the use of an impactor or hammer. The device consists of little more than an impactor, usually with a collection of specific tips and heads that help to expand the ranges of frequency and force level for the testing of various structures. The useful range can also be expanded by the use of various impactor sizes. Usually integral to the impactor is a load cell, or force transducer, which measures the magnitude of the force felt by the impactor and is believed to be the same and opposite to that encountered by the structure. The impactor excitation test is performed by a manual hammer when applied by hand Figure 3.2(a); otherwise, it can be applied by a spring-loaded pistol device, as shown in Figure 3.2(b). During the test, bounce back effect appeared by using a manual hammer when excitation points are located on the blade due to the higher blade motion, which is like a cantilevered beam behavior. The bounce-back effect always remains unless the impact were extremely fast in reverting the operator's hand. To overcome that problem, the Automatic hammer which, is developed, is applied at some points on the blade [7].

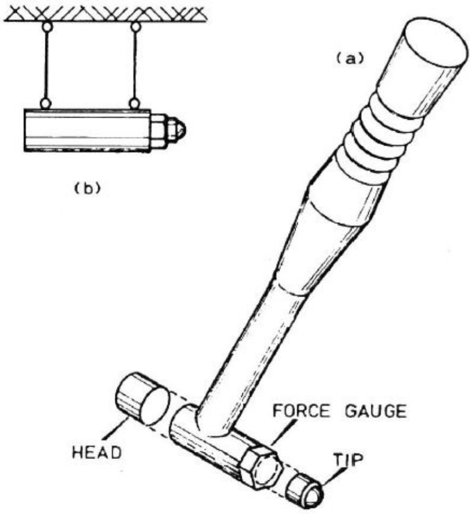

Figure 3.2: Manual hammer and impactor details, taken from [7].

Essentially, the magnitude of the impact is determined by the mass of the hammerhead and the velocity with which it is moving when it hits the structure. The operator must always control the velocity rather than the level of force itself, and so an acceptable way of changing the order of the level of force is by varying the mass of the hammerhead [7].
The frequency range which this type of device effectively excites is regulated by the stiffness of the contact surfaces and the mass of the impactor head. This will undergo a force pulse when the hammer tip hits the test structure, which is significantly that of a half-sine shape, as shown in Figure 3.3(a). It can be seen that a pulse of this kind has a frequency content of form illustrated in Figure 3.3(b), which is basically flat to a certain frequency (ω_c) and subsequently of diminished and uncertain power [7].

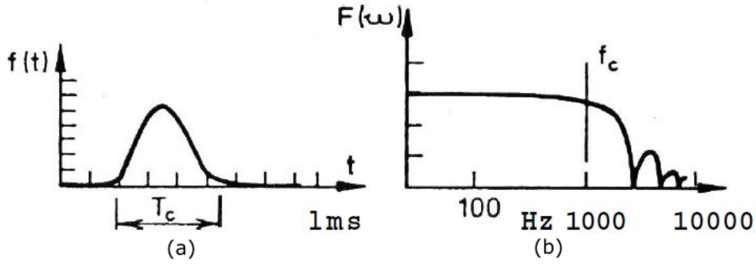

Figure 3.3: Typical impact force pulse and spectrum. (a) Time history; (b) Frequency spectrum , taken from [7].

Clearly, a pulse of this kind will be fairly ineffective at exciting vibrations in the above ω_c frequency range, so we need some control over that parameter. It can be seen that there is a direct relationship between the first cut-off frequency ω_c and the duration of the pulse T_c and it is important to cause a shorter pulse length in order to increase the frequency range. This, in effect, can be seen to be related to the stiffness of the contacting surfaces (not the hardness) and the impactor head mass. The stiffer the components, the shorter the pulse length, and the higher the frequency spectrum reached by the effect would be. Similarly, the higher the effective frequency range, the lighter the impactor mass. It is for this reason that a set of different hammer tips and heads are used to allow the frequency range regulation to be adopted. In general, as soft a tip as possible should be used to deliver all the input energy into the frequency range of interest; the use of a stiffer tip than appropriate would result in the injection of energy into vibrations beyond the interest range at the cost of those inside that range [7].
On a different point, one of the challenges of using a hammer to apply excitation is to ensure that each impact is exactly the same as the previous ones, not so much in magnitude as in location and orientation relative to the normal surface. At the same time, multiple impacts or *hammer bounce* must be avoided as these cause issues in the processing stage of the signal [7].
Another issue that must be addressed when using the form of excitation hammer is derived from the essentially transient nature of the vibrations in which the measurements are made. It is important to note the possibility of overloading during the excitation pulse, pushing the structure beyond its elastic or linear range [7].

3.6 Transducers

3.6.1 Accelerometers

The transduction is indirect in an accelerometer and is accomplished through means of an auxiliary or seismic mass in Figure 3.4(a) and (b). The force exerted on the crystals in this system is the inertial force of the seismic mass (i.e., $m\ddot{x}$). Therefore, as long as the body and the seismic mass pass together (i.e., $\ddot{z}$ and $\ddot{x}$ are identical), the transducer's output will be proportional to the body's acceleration ($\ddot{x}$), and thus the structure to which it is connected.A study of a simple dynamic model for this system in Figure 3.4(c) shows that the ratio ($\ddot{x}/\ddot{z}$) is essentially unity over a wide frequency range from zero upwards before the transducer's first resonant frequency is reached [7].

So to determine an accelerometer's working range, one needs to know its lowest resonant frequency. However, to some extent, this property may depend on the characteristics of the system to which it is being fixed, and indeed on the fixture itself. This frequency is given by $\sqrt{k/m}$ in the simple model. This value must be regarded as an upper limit (and hence not a conservative limit) because in most applications, the body of the accelerometer is connected to something that is less than rigid and so the transducer can have a lower resonant frequency than the one quoted [7].

As with force transducers, there is a problem with the cross or transverse sensitivity of accelerometers that can arise from imperfections in the structure of crystals and from contact through the casing. Modern designs are designed to mitigate these effects, and one configuration that appears to be better in this regard is the sheer form, which is shown in the sketch in Figure 3.4(b) [7].

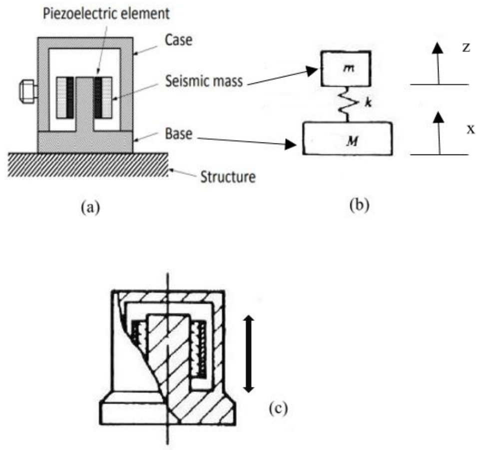

Figure 3.4: Transducer basics: (a) Compression-type of the piezoelectric accelerometer; (b) Shear-type of the accelerometer; (d) Simple dynamic model for accelerometer, taken from [7] [3]

3.7 Attachment And Location Of Transducers

3.7.1 Attachment

Most important is the correct location and installation of the transducers, especially accelerometers. There are various ways to mount the transducers onto the test structure's surface, some more convenient than others. Any of those methods are shown in Figures 3.5(a) and range from a threaded stud involving the necessary adjustment (not always possible) of the test structure, by different adhesives in combination with a stud, to the use of a wax which is the simplest and easiest to use. Such types of attachment become less effective as the functionality increases, although it is usually possible to determine the limits of each's utility and thus to choose the appropriate one in any specific case. Also shown in Figures 3.5(b) are typical frequency limits for each type of attachment. The especially high-frequency capability of the screwed stud connection can only be accomplished if the transducer is mounted exactly normal to the surface of the device so that the two components have a high stiffness contact. For instance, if the tapped hole axis is not normal on the surface, the resulting misalignment can cause a weak region of contact with a corresponding loss of stiffness and high-frequency range. The degree of local stiffening caused by its attachment to the structure is another factor when connecting the transducer. When this is applied to a fairly flexible plate-like surface, then there is a strong probability that the local stiffness will be considerably increased. The only possible solution to this problem is to transfer the transducer to another part of the structure [7].

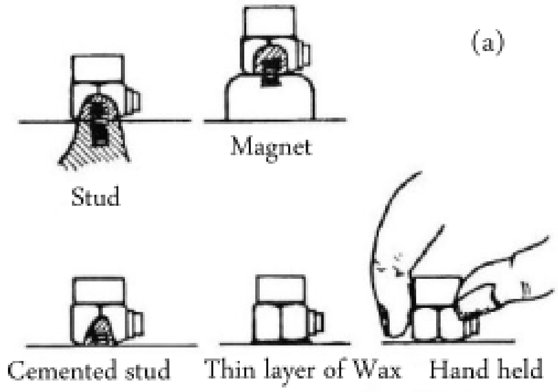

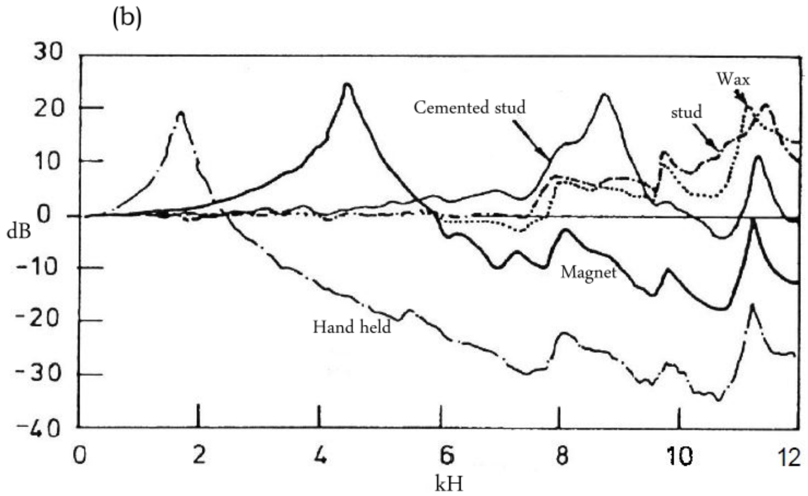

Figure 3.5: Accelerometer attachment characteristics. (a) Alternative attachment methods; (b) Frequency response characteristics of different attachments, taken from [7]

3.7.2 Location

By doing multiple driving point measurements at different points around our system, we can *survey* the structure to help decide the best position for excitation. Assume the three driving point Frequency Response Functions (FRFs) in Figure 3.6 as an example [2].

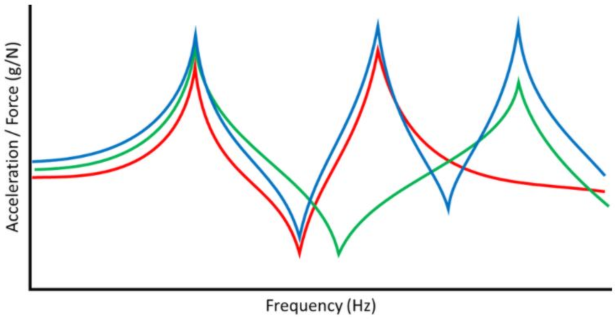

Figure 3.6: Three different driving point FRFs from the same beam structure, adapted from [2].

Figure 3.6 depicts which one of the three examples FRFs includes the most information about natural frequencies of the structures. The blue FRF shows three peaks, whilst the red and green FRFs show only two peaks each. By looking at and comparing the set of FRFs, we can infer that the position used to calculate the blue FRF is the three 's best driving point since the blue FRF contains the most peaks [2].

In the following explanation, three fundamental questions will cover as bellow:

- What is *Driving Point* measurement?
- Importance of *Driving Point*

What is Driving Point measurement?

A driving point measurement is a dynamic measurement in which the hammer (or shaker) force input and the accelerometer response output are measured at the same point on the structure and in the same direction [2].

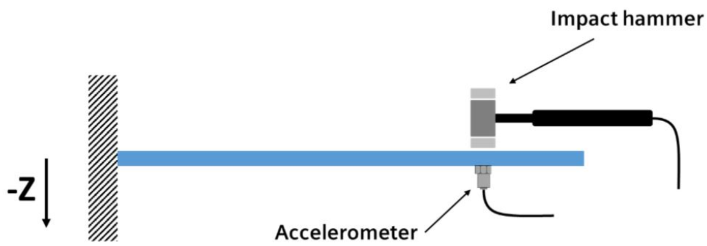

Figure 3.7: A driving point measurement on a cantilever beam. Both the force and response are being measured at the same location on the structure and in the same direction (-Z), adapted from [2].

Nonetheless, often collocating the impact and response measurement, as seen in Figure 3.7, may not be physically feasible, so a compromise needs to be made. For example, imagine measuring a driving point on a fuel tank or on another sealed vessel, where the interior surface is not accessible (see Figure 3.8).In this case, the accelerometer must be placed on the same surface that we will strike with the hammer and should be positioned as close to the position of the impact as possible. It is necessary to place the accelerometer where the impact itself will not be interfered with. Note that there should not be any contact between the impact hammer and accelerometer during the impact test, this will distort the FRF data we are trying to measure, and the consequence will be overloading the signals coming from the accelerometer [2].

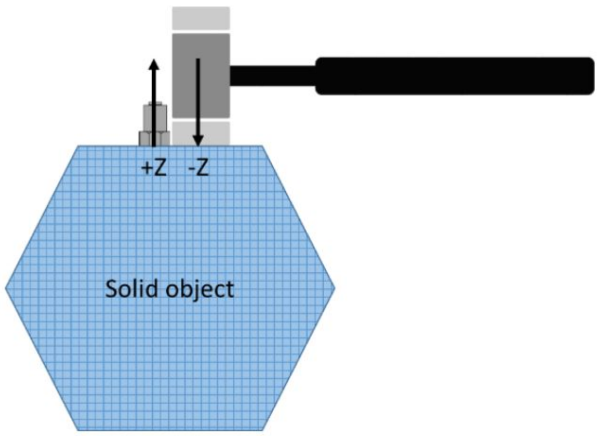

Figure 3.8: If required, place the accelerometer next to the impact spot, and as near as possible, adapted from [2].

Although it is important to calculate the force and the reaction at the same location and direction, the polarity of the two directions of measurement that differ, the hammer, for example, can be measuring in direction -Z, while the accelerometer is measuring in direction +Z. It also occurs in cases where the accelerometer is placed close to the place of impact as seen in Figure 3.8. The driving point calculation is accurate so long as both the hammer and the accelerometer signals are measured along the same axis [2].

Importance of Driving Point

The FRF driving point displays all the structure modes that are excited by impacting at a given spot. When impacting on a structure at a point does not properly arouse a specific mode type, the FRF may skip the peak corresponding to that mode. To find why let's looking for how the FRFs from Figure 3.6 were generated [2].

Consider the cantilever beam in Figure 3.9(a) below. Getting the red FRF has shown in Figure 3.9(b) by placing the accelerometer at point R and impacting at the same spot. Next, by moving the accelerometer and impact at point G, which generates the green FRF. Finally, move the accelerometer and impact to location B, and measure the blue FRF. As already mentioned, notice that there are three peaks in the blue FRF and only two in the red and green FRFs [2].

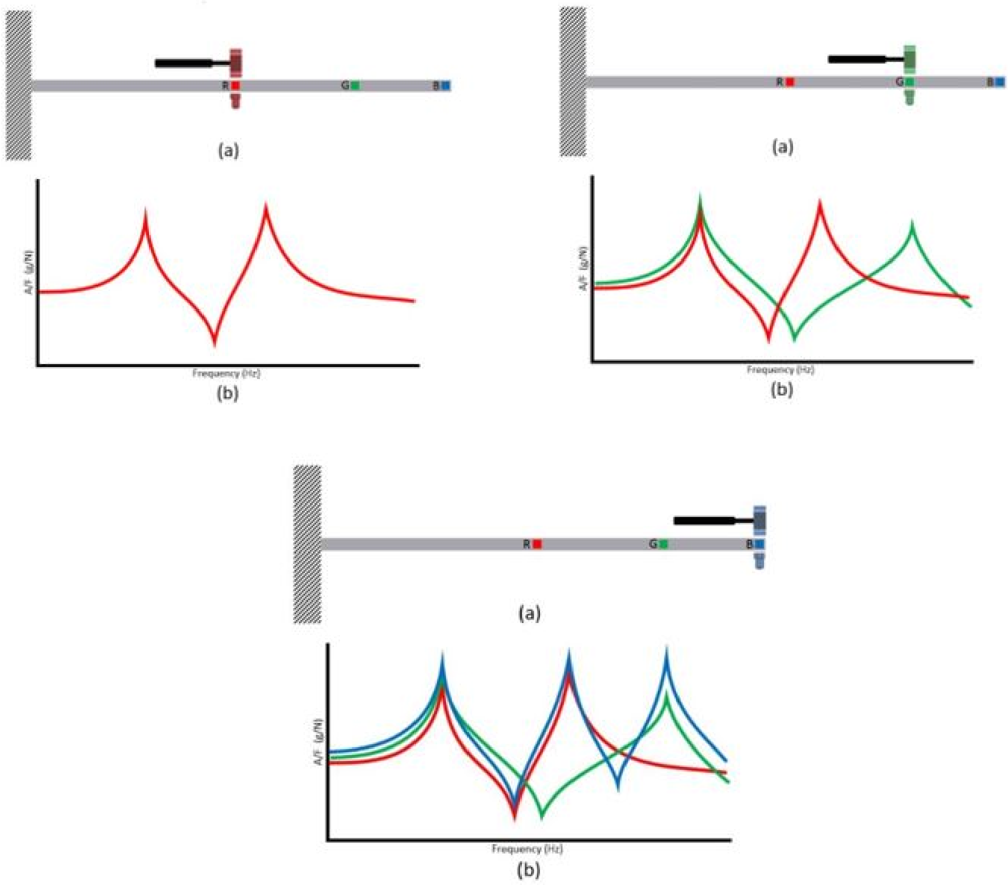

Figure 3.9: (a) Cantilever beam with three driving points R, G, and B; (b) driving point FRFs from each location, adapted from [2].

The first three vibration modes for the cantilever beam are represented in the following Figure 3.10 in order to better understanding.

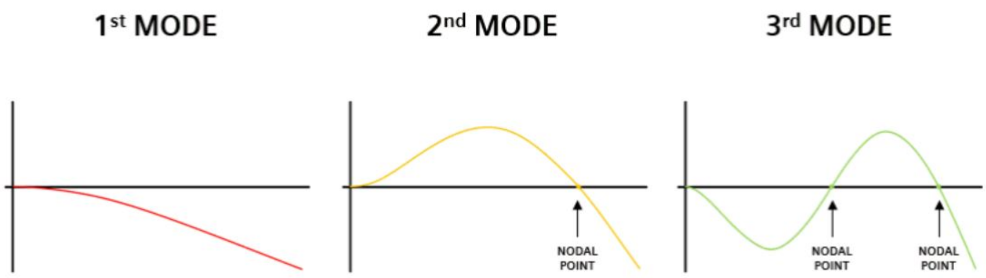

Figure 3.10: The first three mode shapes of a cantilever beam. The higher mode shapes feature points that do not move, called nodes, adapted from [2].

In the first mode, the whole beam is involved in the pattern of deflection; all points are moving. But there are points in the 2nd and 3rd modes that don't move at all. Such points in the deflection form that do not move are called nodes or nodal points. Overlaying our cantilever beam with the first three mode shapes (Figure 3.11), it becomes clear that the Red impact location is on top of a node in the 3rd mode shape, and the Green impact location is at a node of the 2nd mode [2].

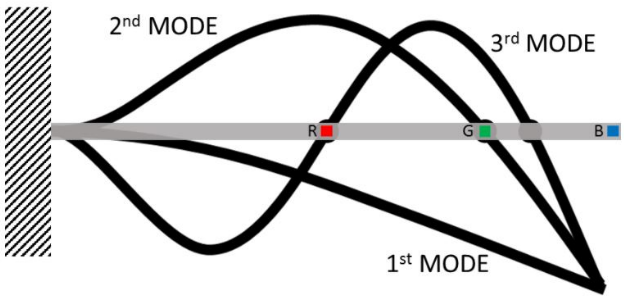

Figure 3.11: Nodal points in the 2nd and 3rd modes occur at Green and Red driving points, respectively. These modes will not be excited by impacting at these locations, adapted from [2].

Since nodal points are not involved in mode shapes, the effect of our structure at the Red and Green locations does not sufficiently excite the mode shapes that have nodes at these locations. As a result, the peaks that match the missing modes will not appear in the FRF [2].

It is the most important feature of a driving point measurement: A driving point FRF tells us which mode shapes are sufficiently excited by having an effect on our structure at that particular location. The modes that are excited to impact at that position will produce peaks in our FRF driving level, the modes that aren't excited about the place of the impact will not [2].

Through making multiple measurements of driving points at different positions around the structure and comparing the FRFs, we can say which position would better excite the modes we are interested in. This is known as a *survey of driving points* [2].

Carrying out a driving point survey helps avoid using an excitation nodal point. This is much more important for a practical structure with 2 or 3 essential dimensions since the nodal *points* from the simple example cantilever beam transform into nodal *lines* [2].

3.8 Analysers

3.8.1 Spectrum Analysers

The spectrum analyzer (or frequency analyzer, as it is often called) is an instrument type somewhat different from the FRA system (frequency response analyzer). Whereas the FRA was concerned with measuring only one frequency component at a time, the spectrum analyzer attempts to quantify all the frequency components present in a dynamic, time-varying signal simultaneously. Its output consists of a continuum, typically a discrete one with a finite number of components, which defines the relative magnitudes of a whole range of frequencies present in the signal. Maybe the easiest way to imagine the spectrum analyzer is as a series of FRA units, each tuned to a different frequency and running at the same time [7].

Over the past two to three decades, the latest generation of available optical spectrum analyzers has proved to be the workhorse of signal processing used in modal research. The digital spectrum analyzer (or Digital Fourier Analyser or Digital Fourier Transform Analyser) is able to calculate a broad range of incoming signal properties, including those needed for FRF measurements, all based on the Discrete Fourier Transform. To order to understand how to better use analyzers of this kind, the fundamentals of their operation need to be understood, and we will devote the next section to learning some of the key features [7].

3.9 Digital Signal Processing

3.9.1 Objective

The tasks of the spectrum analyzer that we are concerned with here are those of estimating the Fourier Transforms or Spectral Signal Densities given as inputs.

Here is presented the basic theory of the Fourier analysis to connect the two most important versions of the fundamental Fourier transformation between the time and frequency domains. This states in its simplest form that a function $x(t)$ can be written as an infinite sequence, periodic in time T [7]:

$$x(t) = \frac{a_0}{2} + \sum_{n=1}^{\infty} \left(a_n cos\left(\frac{2\pi nt}{T}\right) + b_n sin\left(\frac{2\pi nt}{T}\right)\right) \tag{3.1}$$

where a_n and b_n can be determined using $x(t)$ information through the relationships (3.2):

$$\begin{aligned} a_n &= \left(\frac{2}{T}\right) \int_0^T x(t) cos\left(\frac{2\pi nt}{T}\right) dt \\ b_n &= \left(\frac{2}{T}\right) \int_0^T x(t) sin\left(\frac{2\pi nt}{T}\right) dt \end{aligned} \tag{3.2}$$

In a situation where $x(t)$ is discrete and of a finite length, so that it is defined only at a set of N unique time values $(t_k; k = 1, N)$, we may write a finite Fourier series:

$$x_k(= x(t_k)) = \frac{a_0}{2} + \sum_{n=1}^{N/2} \left(a_n cos\left(\frac{2\pi nt_k}{T}\right) + b_n sin\left(\frac{2\pi nt_k}{T}\right)\right); k = 1, N \tag{3.3}$$

The coefficients a_n,b_n are Fourier or Spectral coefficients for the function $x(t)$ and they are often shown in modulus (and phase) form, $c_n(= X_n) = (a_n^2 + b_n^2)^{1/2}$ (and $\phi_n = tg^{-1}(-b_n/a_n)$). This is the type of the Fourier transformation we are concerned with during the practical application of the theory used in this subject. The signals (accelerometer or force transducer outputs) that arise in the time domain and in the frequency domain are the desired spectral properties. Illustration. Figure 3.12 shows the various types of time history encountered, their Fourier Series or Transforms or Spectral Density, and the approximate digitized (or discrete) approximations used and generated by the DFT analysis [7].

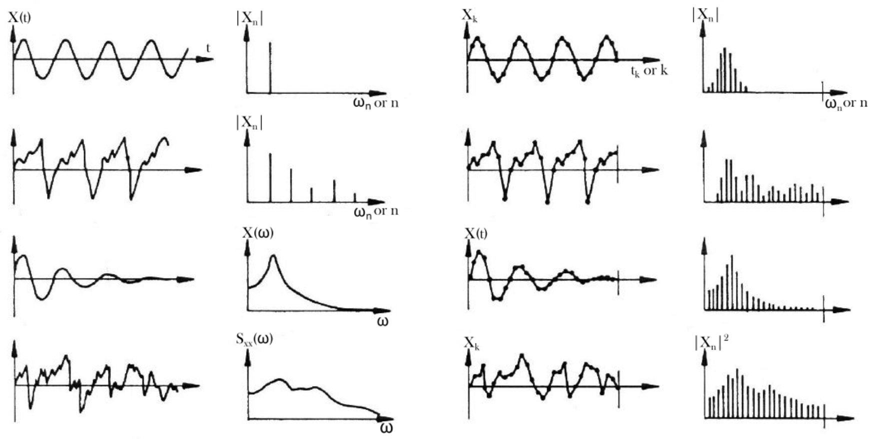

Figure 3.12: Time histories and their spectral analysis: continuous and discrete signals, taken from [7]

3.9.2 Basics of the DFT

In each case, the input signal is digitized (by an A-D converter) and recorded as a set of N discrete values, uniformly distributed in the time span T during which the measurement is carried out. Then, assuming that the sample in time T is periodic, a Finite Fourier Series (or Transform) is computed according to formula (3.3) above as an estimate to the required Fourier Transform. There is a basic relationship between the sample length T, the number of discrete values N, the sampling (or digitizing) rate ω_s and the range and resolution of the frequency spectrum $(\omega_{max}, \Delta\omega)$. The range of the spectrum is $0 - \omega_{max}$ (ω_{max} is the Nyquist frequency) and the resolution of lines in the spectrum is $\Delta\omega$, where

$$\omega_{max} = \frac{\omega_s}{2} = \frac{1}{2}\left(\frac{2\pi N}{T}\right) \tag{3.4}$$

$$\Delta\omega = \frac{\omega_s}{N} = \frac{2\pi}{T} \tag{3.5}$$

Since the transform size (N) is normally set for a given analyzer (and is typical, though not always, a power of 2: 512, 1024, etc.), the frequency spectrum covered and the resolution of the spectral lines is calculated solely by the time period of each sample [7].

The basic equation that is solved for the determination of the spectral composition :

$$\begin{Bmatrix} x_1 \\ x_2 \\ x_3 \\ \vdots \\ x_N \end{Bmatrix} = \begin{bmatrix} 0.5 \ \cos(2\pi/T)... \\ 0.5 \ \cos(4\pi/T)... \\ 0.5 \ \cos(6\pi/T)... \\ \vdots \, \vdots \\ 0.5 \ \cos(2N\pi/T) \end{bmatrix} \begin{Bmatrix} a_0 \\ a_1 \\ a_2 \\ \vdots \\ \vdots \end{Bmatrix} \ or \ \{x_k\} = [C] \{a_n\} \tag{3.6}$$

Accordingly, we use $\{x_k\} = [C]^{-1} \{a_n\}$ to calculate the unknown spectral or Fourier coefficients in $\{a_n\}$. Much of the effort to simplify the spectral analysis calculation is essentially dedicated to equation (3.6).

There are a variety of features of digital Fourier analysis that can give rise to incorrect results if not treated correctly. These are generally the result of the discretization approximation and of the need to limit the length of the time history. The special features of *Aliasing*, *Leakage*, *Windowing* will be addressed in the following sections [7].

3.9.3 Aliasing

Aliasing is an effect which causes distortion in a sampled signal's spectrum because the sampling rate is too small to properly capture the frequency content. Aliasing allows high-frequency data to appear at a lower frequency than it really is, as shown in Figure 3.13, thus assuming the frequency *false identity* or *alias* [2].
Some essential terms to know when talking about aliasing:

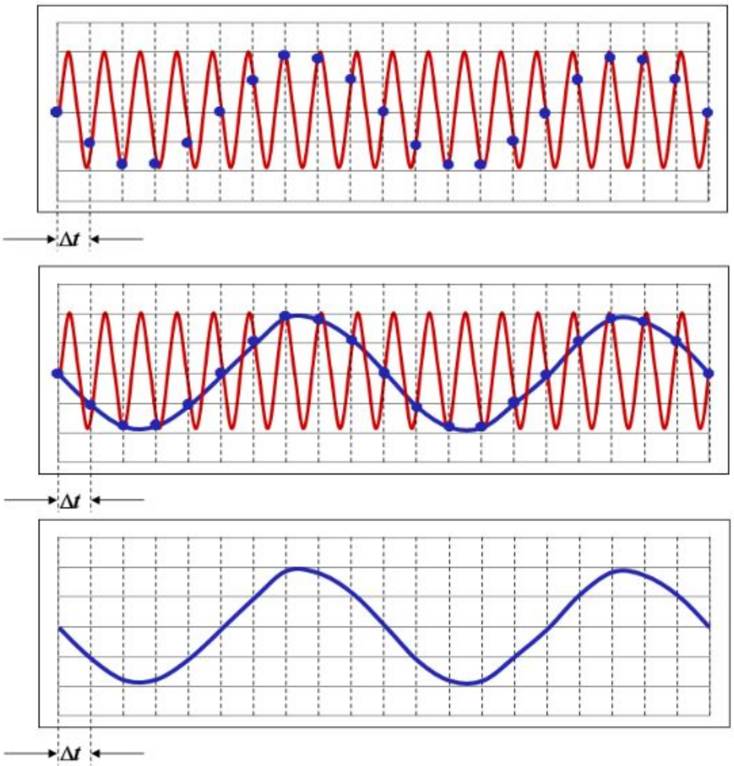

Figure 3.13: TOP: The red sine wave is the original signal. The blue dots represent how often the signal is being sampled. MIDDLE: The blue line is how the signal will appear due to the low sampling rate. BOTTOM: What the user will see in the time domain. Notice the acquired frequency is much lower than the actual frequency, taken from [2].

- **Sampling frequency (Hz):** The number of samples per second being acquired of an incoming frequency. The sampling frequency is two times the bandwidth.

- **Bandwidth (Hz):** The frequency range over which measurements will be taken. Bandwidth is defined as half of the sampling frequency.

- **Span (Hz):** The frequency range over which measurements will be taken and not be effected by the anti-aliasing low-pass filters (i.e., the alias-free region of the bandwidth). The span is 80% of the bandwidth.

- **Nyquist rate (Hz):** Minimum frequency at which a signal can be sampled without introducing frequency errors. The Nyquist rate is twice the highest frequency of interest in the sample.

To properly sample all of the desired frequency content of an incoming signal and thus prevent aliasing, sample at (or above) the Nyquist rate is needed. The sampling frequency when acquiring data is twice as high as the specified bandwidth. And all the frequency content below the specified bandwidth will be sampled at a rate that is adequate to capture the frequency content accurately. However, if the incoming signal includes frequency content above the defined bandwidth, for this higher frequency content, the sampling frequency (2x bandwidth) violates the Nyquist theorem [2].

A sine wave with an insufficient sampling (violating the Nyquist theorem) is shown in Figure 3.14(a). The frequency isn't properly identified.

In Figure 3.14(b), the correct frequency is shown by a sine wave with sufficient sampling. f_s represents the sampling frequency, f_{sine} represents the frequency of the sine wave.

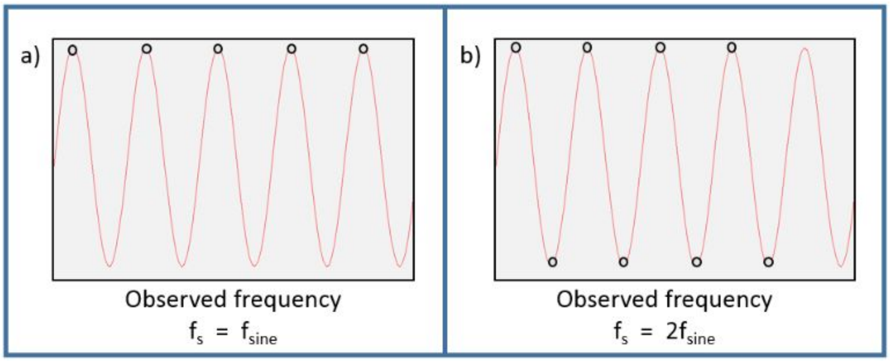

Figure 3.14: a) When sampling at the same frequency as the incoming signal, the observed frequency is zero Hertz. b) When sampling at twice the frequency of the sine wave, the observed frequency is f_{sine}, the true frequency of the sine wave, taken from [2].

When violating the Nyquist theorem, spectral content above the bandwidth is mirrored about the frequency of the bandwidth. This means that the frequency content X [Hz] above the bandwidth appears below the bandwidth by X [Hz]. Thus, higher frequency content appears to be at a lower frequency or an *alias* frequency [2].

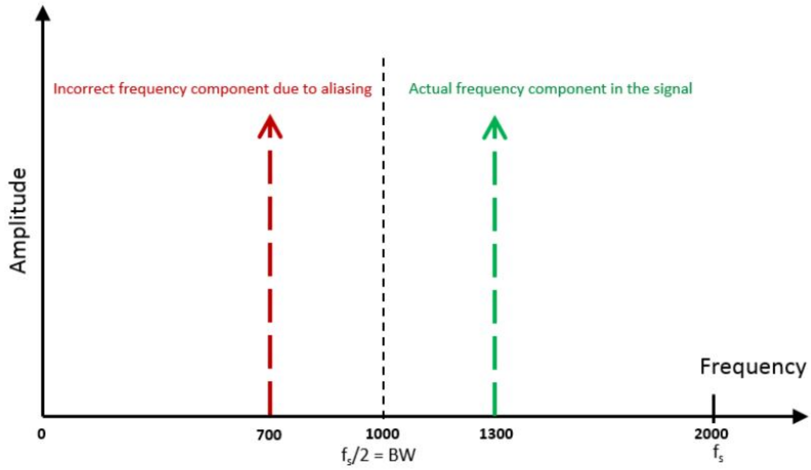

Figure 3.15: Aliasing causes frequency above the bandwidth to be mirrored across the bandwidth, taken from [2].

In this example, the frequency here is that of 1000 [Hz]. The actual frequency component in the signal is at 1300 [Hz]. The frequency over the bandwidth is 300 [Hz]. At 700 [Hz], 300 [Hz] would be mirrored under the bandwidth. Figure 3.15.

The solution to the problem is to use an anti-aliasing filter which subjects the original time signal to a low-pass, sharp cut-off filter. An anti-aliasing filter is a low-pass filter that removes spectral content that violates the Nyquist criteria (also known as spectral content above the specified bandwidth). The ideal anti-aliasing filter would be shaped like a *brick wall*, completely attenuating all signals beyond the specified bandwidth Figure 3.16 [2].

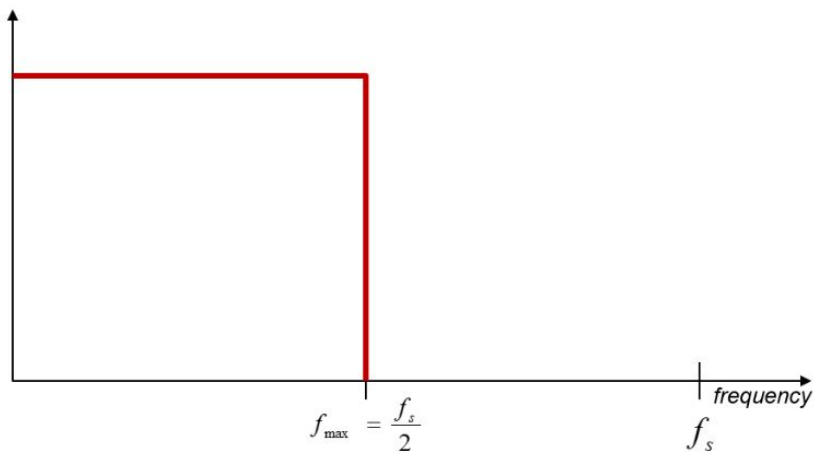

Figure 3.16: The ideal anti-aliasing filter would be shaped like a wall: cutting off all frequencies beyond the specified bandwidth ($f_s/2$), taken from [2].

This *wall form* filter is difficult to have in reality. Instead, a very sharp analog filter is used, which has a -3dB roll off at the bandwidth and attenuates all frequencies above the bandwidth to zero by 20% [2]. Figure 3.17.

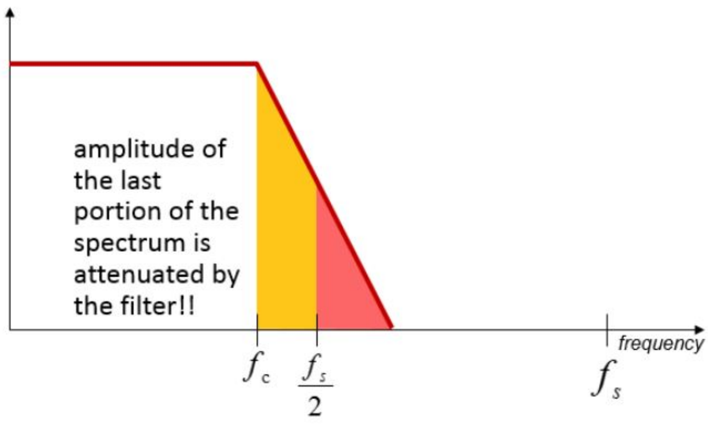

Figure 3.17: The anti-aliasing filter has a -3dB roll off point at the bandwidth, taken from [2].

This is why the *trustable*, alias-free region of the spectrum is from zero Hz to 80% of the bandwidth. This alias-free range is called the frequency span.

$$Span = 80\% Bandwidth \tag{3.7}$$

3.9.4 Leakage

The Fourier series given by equations (3.1) or (3.3) shows that $x(t)$ can be represented by a series of harmonic components with frequencies $f_1 = f_0, f_2 = 2f_0, f_3 = 3f_0$ and $f_n = nf_0$, where $f_0 = 1/T_0$ is both the fundamental frequency and the resolution in Hz (spacing of the frequency components).
Fourier analysis works over a function $x(t)$ with period T_0. However, this does not mean that only one period of signal exists; on the contrary, Fourier's analysis assumes that signals repeat infinitely in time. If the signals are truly periodic, this is not a problem since there cannot be any components in the signal at frequencies between those calculated in the Fourier analysis. s. However, there are many real situations in which this is not the case, either because the signal being acquired has a non-integer number of periods during the measurement period or because the signal is of the random type. Actually, unless there is full control over the source signal and perfect synchronization with the acquisition clock, in most practical situations, it is not possible to guarantee an integer number of periods is being acquired [3].

Let us analyze two contrasting situations, shown in Figure 3.18: in situation (a),n integer periods of a sine wave are measured during an integer period of time nT; in situation (b), $n+0.5$ periods of the same sine wave are measured during a non-integer period of time $(n+0.5)T$ [3].

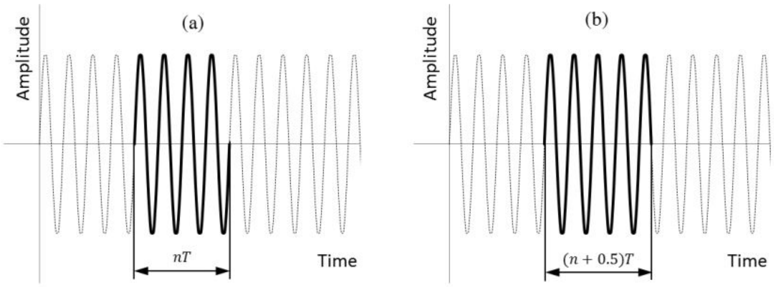

Figure 3.18: Acquisition of a sine wave during (a) an integer number of periods; (b) a non-integer number of periods, taken from [3].

Since only a finite portion of the signal can be measured and the Fourier transform assumes that time signals are periodic and repeat infinitely in time, what the Fourier Transform will *see* is what is shown in Figure 3.19 instead [3].

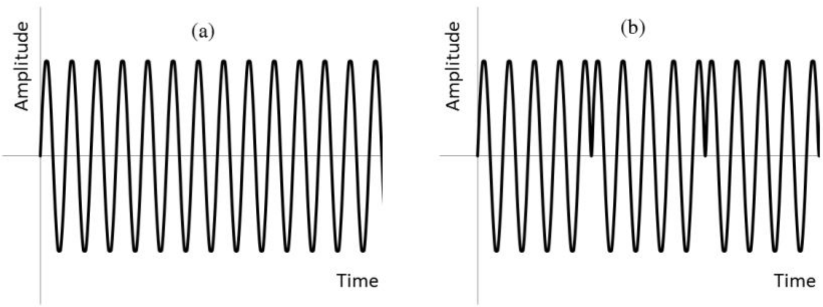

Figure 3.19: What the Fourier transform sees after the acquisition of the sine waves shown in Figure 3.18, taken from [3].

Figure 3.19(b) is no longer a harmonic signal; thus, when applying the Fourier transform, the signal is shown in Figure 3.19(b) will be regenerated as a sum of sine waves that will be translated into spectral components in the frequency domain. In practice, what happens is that the fundamental frequency is shown with a smaller amplitude with spreading to neighboring frequencies. The phenomenon of spreading of the true spectrum components to other frequencies is called *leakage* and is illustrated in Figure 3.20 [3].

This phenomenon can be seen as a distribution of the energy contained in the fundamental spectral line (which is the same in the particular examples shown in Figures 3.18 and 3.19) to contiguous frequencies as if the peak melted and leaked to the sides. No window is applied to the time signal. Leakage occurs and is highly visible: the amplitude is different from its true value, and spreading of the true spectrum components to other frequencies is accentuated [3].

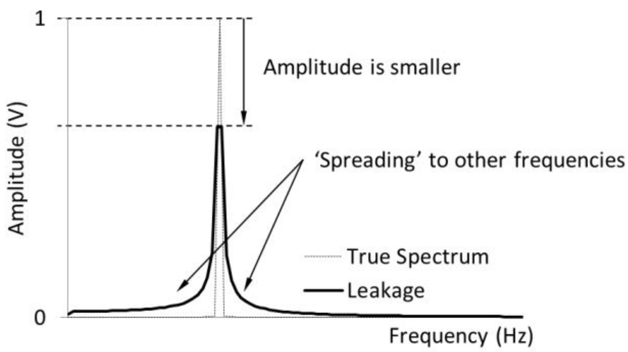

Figure 3.20: Overlapping of the true power spectra (dashed line) with the one obtained when the number of periods is a half integer (solid line), taken from [3].

Leakage has a major problem in many digital signal applications processing, including measurement of FRF and ways to avoid or Significant refinements to our techniques, are reducing its impacts. There are different possibilities which include [7]:

- One of the possibilities is changing the duration of the measurement sample length to match any underlying periodicity in the signal, which means changing T in order to *capture* an exact number of cycles of signals. Note that this solution will be effective to remove leakage only if the signal being analyzed is periodic, which is not easy to determine.
- Another method that does not completely remove the leakage effect but decreases it is increasing the duration of the measurement period T so that the separation between the spectral lines the frequency *resolution* will be finer.

3.9.5 Windowing

To avoid or at least minimize the leakage phenomenon, a function known as the *window* is multiplied by the time signal before the Fourier Transform is performed. The objective is to obtain a smooth decay to zero at the limits of the recorded time period, so that the resulting signal is continuous and approximates more closely to a periodic one.

Windows are typically shaped as functions that start at a value of zero, move to a value of one, and then return to a value of zero over one frame. The captured signal is multiplied by the window, as shown in Figure 3.21 [2].

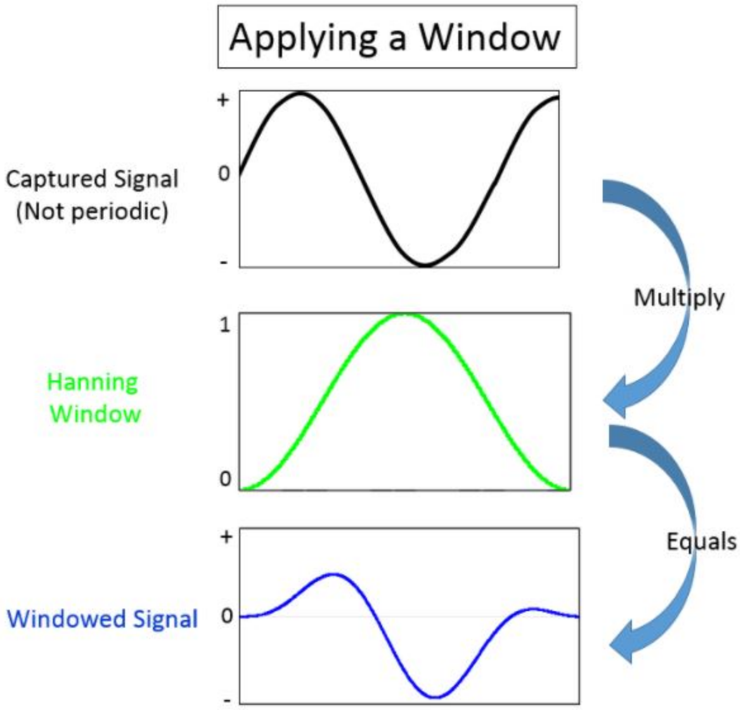

Figure 3.21: A signal (top) is multiplied by a window (middle), resulting in a windowed signal (bottom), taken from [2]

The benefit is not that the captured signal is perfectly replicated. The main benefit is that the leakage is now confined over a smaller frequency range, instead of affecting the entire frequency bandwidth of the measurement. Note that With the leakage spread over a smaller frequency range, doing analysis calculations like RMS yields more accurate results [2].

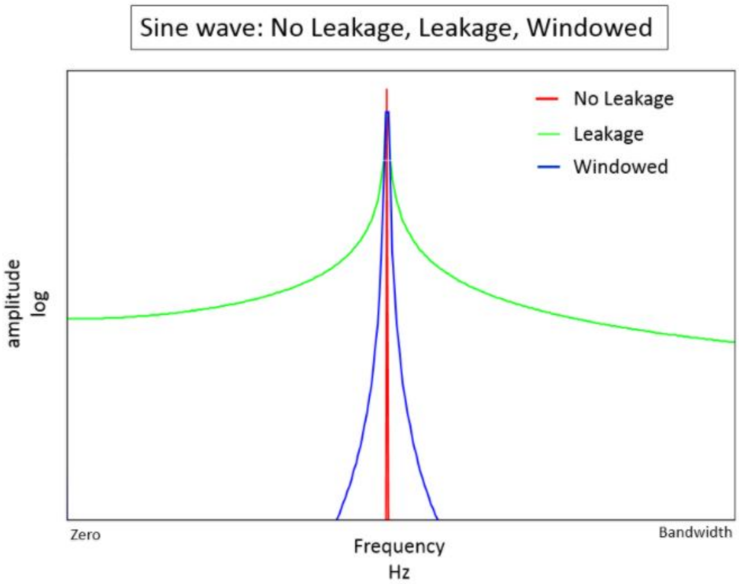

Figure 3.22: Periodic sine wave without leakage (red), a non-periodic sine wave with leakage (green), and windowed non-periodic sine wave with reduced leakage (blue), taken from [2].

In experimental measurements, there are often many different frequencies present. Without a window being applied, these frequencies would leak into each other, making determining the true amplitude of individual peaks very difficult, if not impossible. In Figure 3.23, the leakage of two tones with and without a window is overlaid [2].

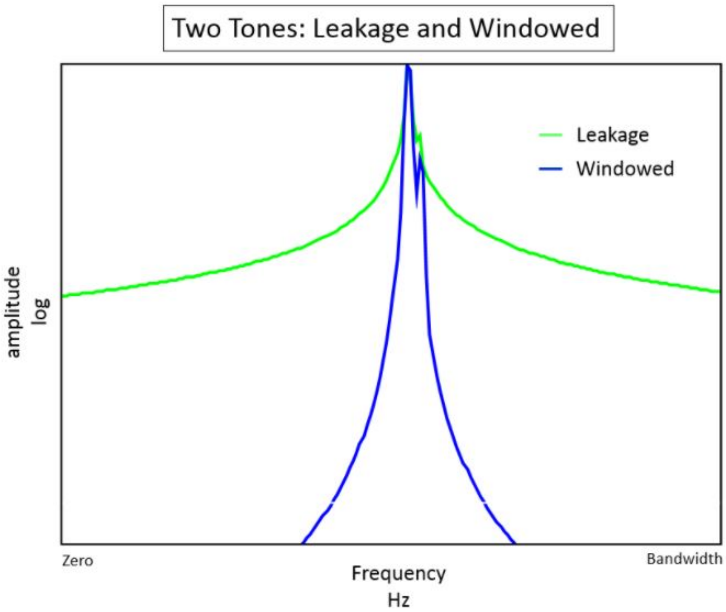

Figure 3.23: Two tones with leakage (green) and with window applied (blue), taken from [2].

There are many different windows, each optimized for particular situations. In our experiment the type of window used is exponential one. [2].

Exponential: In impact tests, exponential windows are frequently used. To prevent leakage, they are used to ensure that the accelerometer response decays to zero, Figure3.24 within the measurement time.

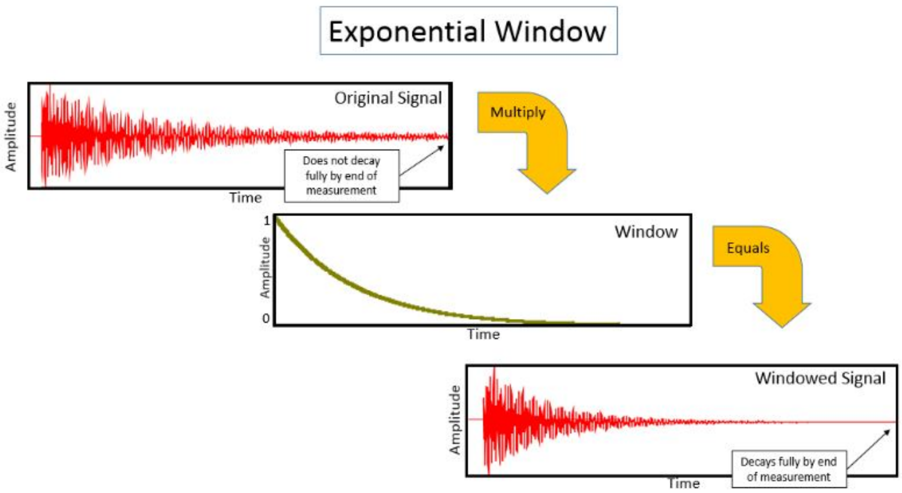

Figure 3.24: The accelerometer signal (upper left) of a modal impact test is multiplied by an exponential window (middle) to ensure the windowed signal decays completely to zero (lower right) to avoid leakage[2].

The exponential decay parameter, which has a value between 0% and 100% determines how much the exponential window's initial value is decreased by the end of the measurement. A decay parameter of 25%, for example, means that by the time the measurement is completed, the window has decayed to a quarter of its original amplitude. An exponential decay parameter of 100% is the same as a Uniform window (or not applying a window). When doing modal impact testing, a decay of 100% is preferred if the signal decays to zero in the measurement time frame. Note that by decaying faster, artificial damping is added to the resulting measurement.

Chapter 4

EXPERIMENTAL SETUP

4.1 Overview

In this chapter useful information provided an overview about the Simcenter Testlab Siemens software and how performed experimental test. In this case, the experiment focus on the method of data acquisition through an impact testing performed on a specimens which is Bladed-Disk. This chapter will be divided into two parts:

1. First part designed to present all the necessary equipment to perform the test and how to work with Simcenter Testlab Siemens software environment;
2. Second part represented an explanation about how to perform the test in the laboratory on the Bladed-Disk;

All of the experiments performed in AERMEC Laboratory in Mechanical Department LABS in Politecnico Di Torino University; an experimental and numerical laboratory that carries out research in the field of structural mechanics of turbines and compressors, to carry out different vibration analysis.

4.2 Equipment

The equipment necessary for an Impact Test consists of:

- Data Acquisition System
- A hammer to excite the structure
- Accelerometers, for the response signal
- Connection cables

- Specimen to be tested
- Dummy Masses
- Computer with the Simcenter Testlab Siemens Software

In the following part a short explanation about each device is provided.

4.2.1 Data Acquisition System

The Simcenter SCADAS Mobile and SCADAS Recorder (formerly called LMS SCADAS) are part of a family of modular data acquisition devices used for capturing dynamic signals. Data Acquisition System which is utilized in this project includes 16 channels;one input force channel and 15 output response channels.

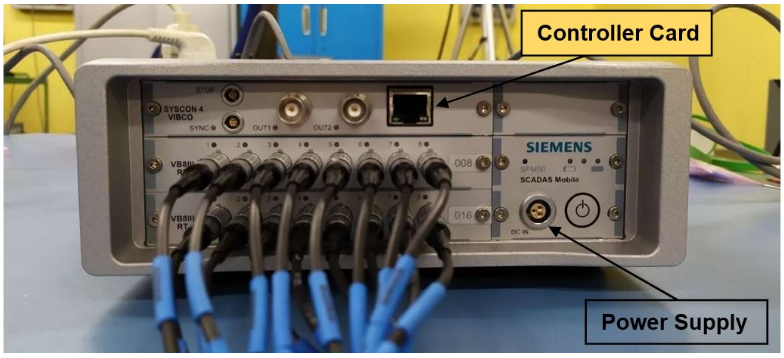

Figure 4.1: Simcenter LMS Scadas.

4.2.2 Manual Hammer

PCB® Model 086C03 impulse hammer is used in this project. All sensors in this system are classified as ICP® (Integrated Circuit Piezoelectric), low impedance, voltage-mode sensors. Hammer model selection involves determining the size and mass of the hammer structure which will provide the force amplitude and frequency content required for proper excitation of the structure under test. Small structures like compressor blades often require mini-hammers. Some very large structures may require a massive mechanical ram instrumented with a force-sensing impact head [8].

The hammer impulse consists of a nearly-constant force over a broad frequency range, and is therefore capable of exciting all resonances in that range. The hammer, size, length, material, and velocity at impact determine the amplitude and frequency content of the force impulse. The impact cap material generally determines energy content. The force spectrums of an impact on a stiff steel mass for hammers with their available tips are shown below [8].

Table 4.1: ICP Impact Hammer, adapted from [8]

Impact Force Hammer			
Hammer Configuration	Tip Extender	Plastic/Vinyl None	Plastic/Vinyl Steel
Hammer Sensitivity	mV/lb mV/N	10.53 2.37	10.92 2.45
Output Bias	10.4 volts		
Temperature	69° F, 21° C		
Relative Humidity	29 %		

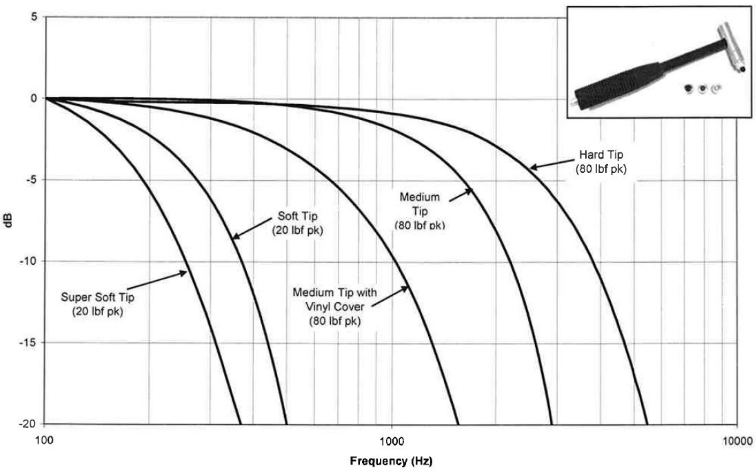

Figure 4.2: Family Impulse Hammer Response Curves, adapted from [8].

Figure 4.3: PCB® Manual Hammer Model 086C03.

One of the main errors accompanied with hammer impact measurements is a double hit measurement. In these cases the object is struck twice by the hammer, often unbeknownst to the measurer. As explained in section 3.5.1 during the test bounce back effect appeared by using manual hammer at some excitation points.To overcome that problem the Automatic Hammer which is developed in Politecnico Di Torino University is applied in some points on the blade.

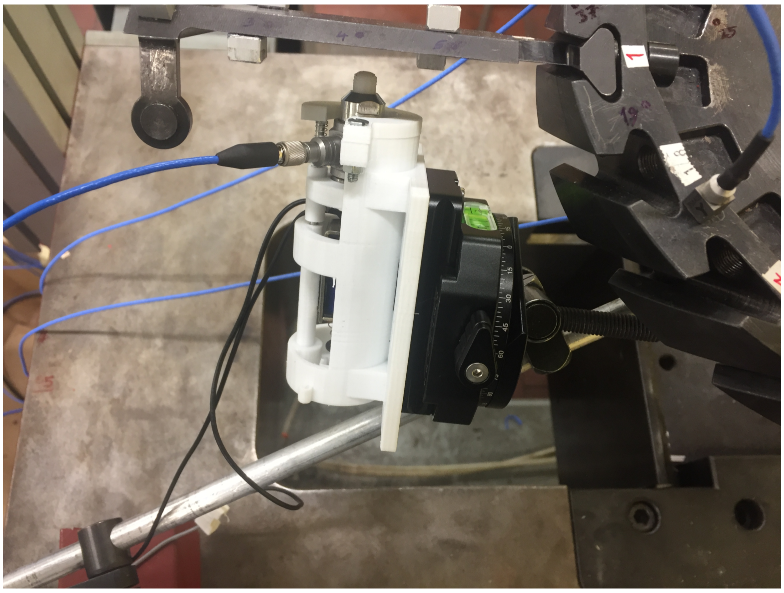

Figure 4.4: Automatic Hammer.

Automatic hammer has been built with electrical Arduino board connected to load cell which is framed to the structure with ability to have 6 DoF. Moreover the board also connected to laptop through USB cable and the load cell connected to data acquisition system. The baseline of the structure frame has able to fixed to the metal floor by magnet and after that the position of automatic hammer has been controlled with some clamps point in order to fix hammer in exact position.

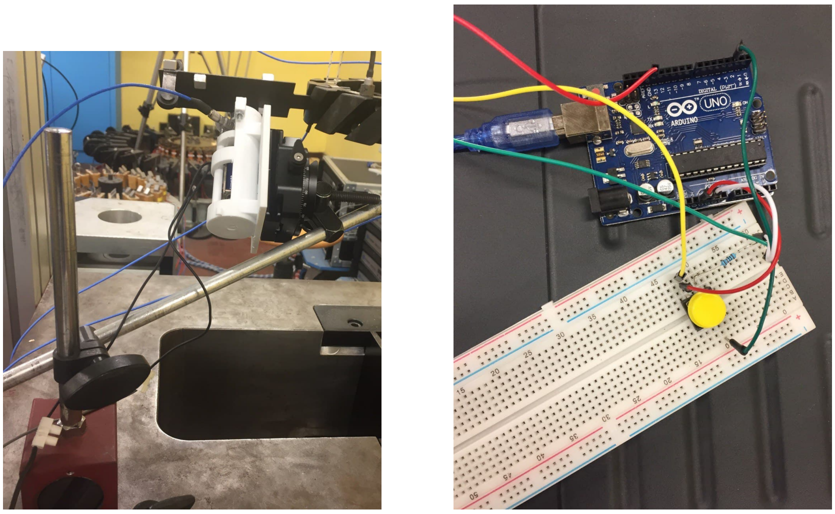

Figure 4.5: Automatic hammer

4.2.3 Accelerometer

Triaxial accelerometers provide simultaneous measurements in three orthogonal directions, for analysis of all of the vibrations being experienced by a structure. Each unit incorporates three separate sensing elements that are oriented at right angles with respect to each other. Five PCB® triaxial accelerometers Model 356A03 utilised in this project.

The mounting techniques which applied is Direct Adhesive Mount. Adhesive mounting is often used for temporary installations or when the test object surface can not be adequately prepared for stud mounting. Adhesive like hot glue and wax perform well for temporary installations whereas two-part epoxies and quick-bonding gels (super glue) provide a more permanent installation [8].

For restrictions of space or for convenience, most sensors can be adhesive-mounted directly to the test structure (an exception being units having integral mounting studs).Place a small portion of adhesive on the underside of the sensor. Firmly press down on the top of the assembly to displace any adhesive. Be aware that excessive amounts of adhesive can make sensor removal difficult. Also, adhesive that may invade the tapped mounting hole in the base of the sensor will compromise future ability to stud mount the unit [8].

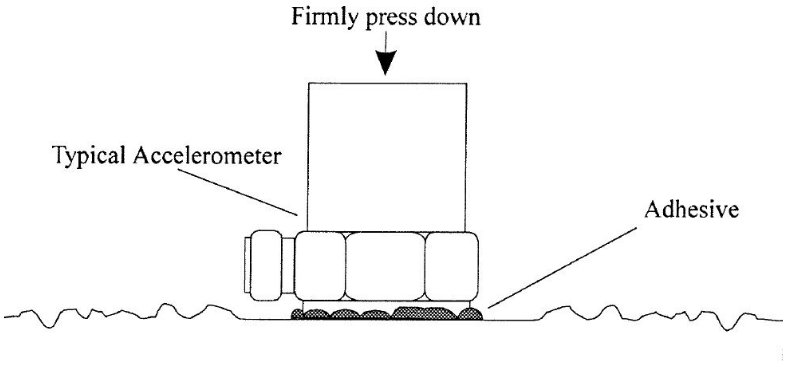

Figure 4.6: Direct Adhesive Mounting, adapted from [8].

Figure 4.7: PCB® Triaxial Accelerometers Model 356A03, adapted from [8].

4.2.4 Connection Cables

For each accelerometer, use a cable with an SMA connector on the sensor side and three circular push-up connectors related to X,Y and Z direction on the instrumentation side, to be connected respectively with the cables supplied together with the Simcenter LMS Scadas equipment. For better signal acquisition, isolate the metal parts of the circular push-up connectors by using paper adhesive tape.

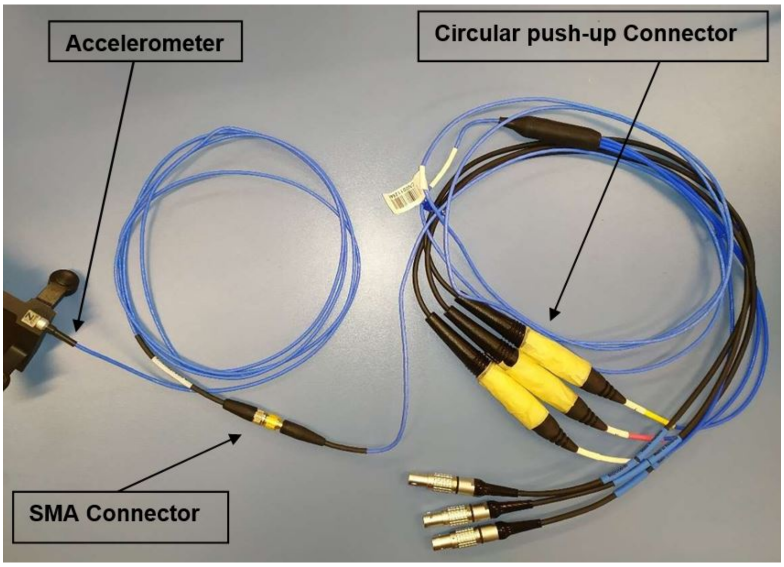

Figure 4.8: Connection cables Series 010G.

4.2.5 Test Object

The test-case is a Bladed-Disk with 18 blades having as many blade-disk joints (blade root joints) and blade-blade joints (shrouds). More information about how to perform the test and the pictures will be provided in section 4.4.

4.2.6 Dummy Mass

Dummy masses have affect to our result whenever we performed the test on couple system; Bladed-disk together. Although as already mentioned in 4.2.1 and 4.2.3 there are only 5 sensors and 15 channels used in the experiments, the problem will appear in numerical one when 10 sensors used with 30 channels which is not possible to perform the test experimentally with 10 sensors and 30 channels due to lack of our acquisition system requirement. So dummy masses play the role when system is coupled, for example when all 5 sensors located on disk in order to cancel the effect of the accelerometer's weight,dummy masses should add on the blade. Dummy masses are positioned on the blade in figure 4.10 in section 4.4.

4.3 Software

Simcenter Testlab Siemens software is utilized to perform this thesis. All the procedure and explanation about software provided in the appendix B.

4.4 Method of Performing Experimental Test

During the hammer test whenever there are various excitation points and position of sensors,two different method proposed for the test, move or rove either hammer or the accelerometer through measurement locations.

Roving the impact hammer is used in this project due to some advantages over roving the accelerometer.When shifting the accelerometer, the accelerometer at the various measuring points must be unmounted and remounted. Moving the accelerometer often changes the structure's mass distribution which can change the natural frequencies.

Moreover it is very important to setup the experiment in a proper way in order to minimizing any external errors due to operator or environment. So to reach that goal specific procedure applied as bellow:

1. All of five sensors mounted on hanging *Disk* or Free support 4.9 and all of the excitation points have already defined.

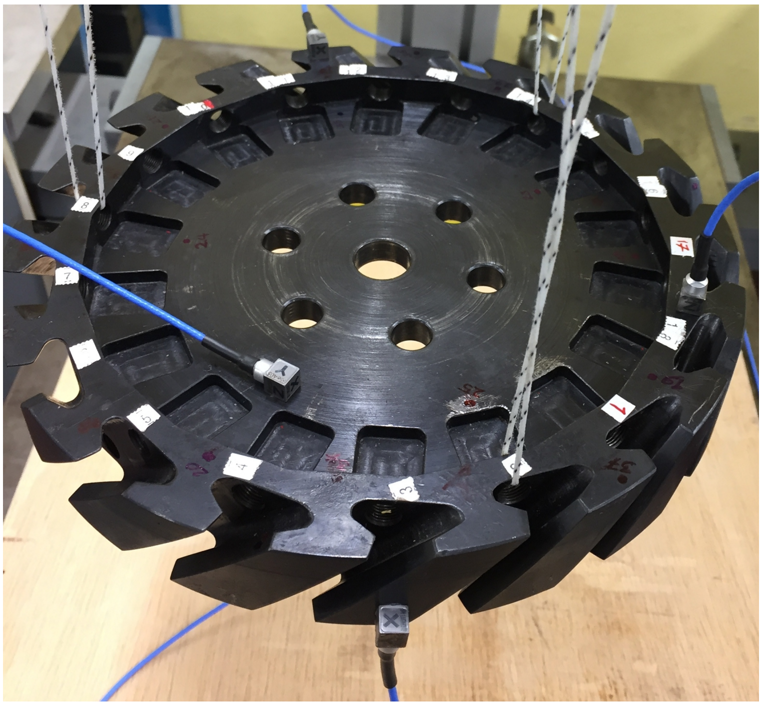

(a) Upper Face

(b) Lower Face

Figure 4.9: Disk test specimen with all located accelerometers

2. Adding blade to the disk by using bolt and spacer with $10N/m$ tightening torque and mounting dummy masses 4.2.6 on the blade. So this couple configuration named *blade+Disk* which is the sensors still remain on Disk and dummy masses are on the blade.

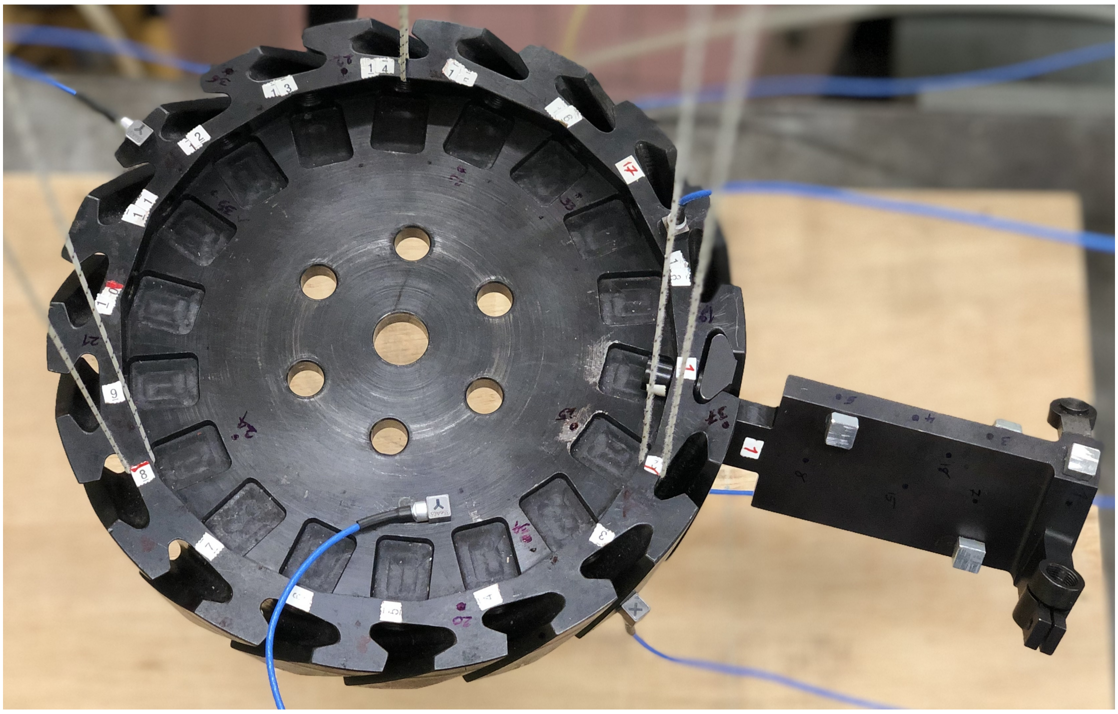

Figure 4.10: Coupled bladed disk system together with dummy masses and accelerometers.

3. In this configuration just need to swap dummy masses and sensors with each other. It means all the sensors moved on the blade and all dummy masses shifted to disk which is named *Blade+disk*.

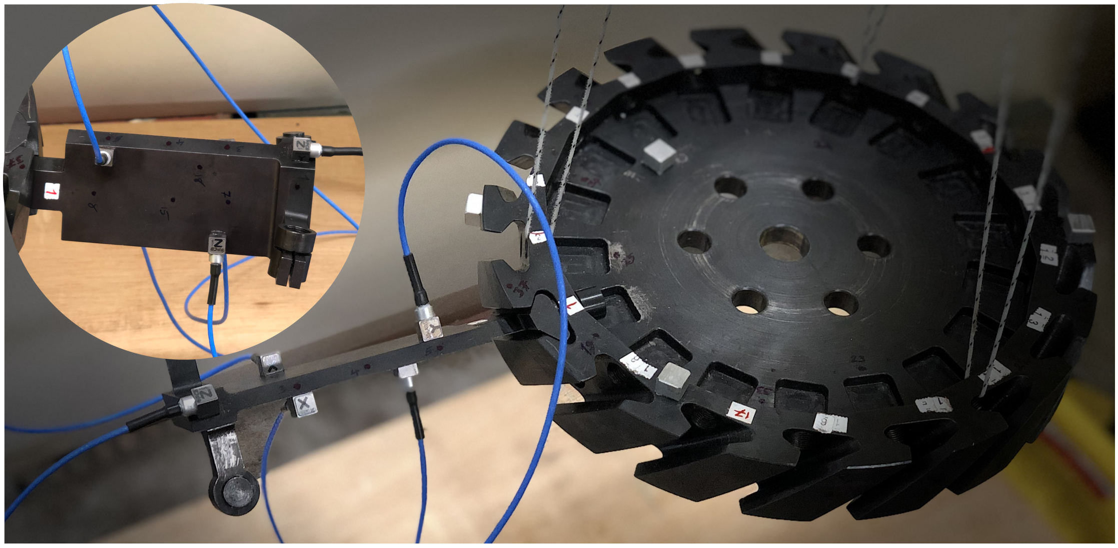

Figure 4.11: Coupled system together with all dummy masses and accelerometers.

4. The final configuration refer to Blade itself. So in this case all the sensors mounted on hanging *Blade*.

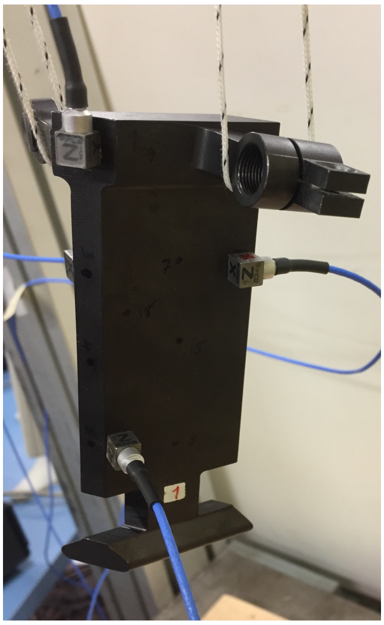

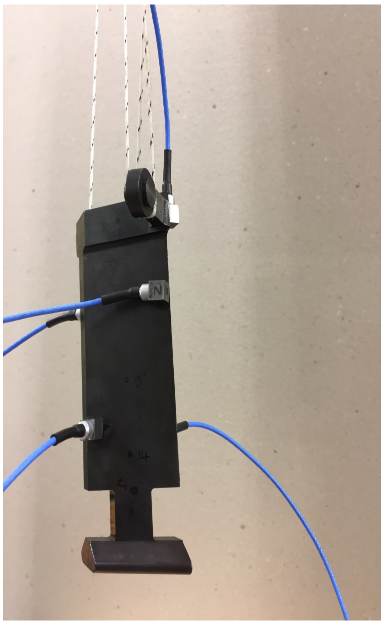

Figure 4.12: Blade test specimen with all located sensors

4.4.1 Roving Hammer versus Roving Accelerometer

The accelerometer measures in three directions, while the hammer measures in one direction only. If you move one or the other, you need to take the disparity into account.

Table 4.2 displays all the inputs and outputs for a 19 position check as an example relating to *Disk*.

Table 4.2: For a 19 measurement location impact test, there are 19 possible inputs and 57 possible outputs that can be measured for disk itself.

	A_{1x}	A_{1y}	A_{1z}	...	A_{19x}	A_{19y}	A_{19z}
F_{1x}							
F_{1y}							
F_{1z}							
$\vdots$							
F_{19x}							
F_{19y}							
F_{19z}							

After measuring the Frequency Response Functions (FRFs) between the 19 measurement excitation locations:

- There are 19 possible input locations for applying the input force. At any given location (1, 2, 3, 4,...,19) the force (F) can be applied in three possible directions: x, y, and z but in this thesis it's only applied in one direction which is z. Possible inputs are therefore $F_{1x}, F_{1y}, F_{1z}, ..., F_{19x}, F_{19y}, F_{19z}$.

- There are 57 possible output locations for measuring the acceleration response. At any given location (1, 2, 3, 4,...,19) the acceleration (A) can be applied in three possible directions: x, y, and z. Possible outputs are therefore $A_{1x}, A_{1y}, A_{1z}, ..., A_{19x}, A_{19y}, A_{19z}$.

The measurements must either have a complete row or complete column of the table shown in table 5.3 to have a correct mode shape, where the phasing of all measurement points is aligned properly.

Table 4.3: A complete row or complete column of the measurement table must be measured to ensure consistent phasing for the mode shape.

	A_{1x}	A_{1y}	A_{1z}	...	A_{19x}	A_{19y}	A_{19z}
F_{1x}							
F_{1y}							
F_{1z}							
$\vdots$							
F_{19x}							
F_{19y}							
F_{19z}							

A collection of measurements of the frequency response function which corresponds to any single column or row or column is needed.

Roving Accelerometer

Consider the case where the accelerometer switches between the 19 different positions when the hammer is being applied to the same position F_{1z}.
The accelerometer, measuring in three directions, is first located at place of measurement 1. The outputs A_{1x}, A_{1y}, A_{1z} are evaluated at the same time in relation to F_{1z}.

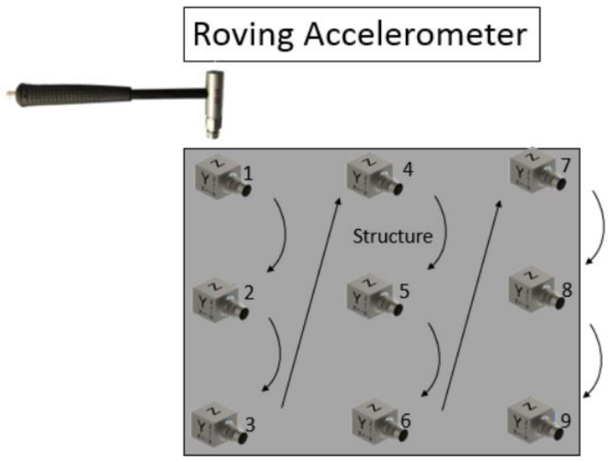

Figure 4.13: Roving accelerometer outputs with fixed hammer inputs, adapted from [2].

After measuring the three FRFs for location 1 the accelerometer is then shifted to location 2. The three outputs of position $2(A_{2x}, A_{2y}, A2z)$ are determined in the direction of z regarding the hammer input at location 1. This is continuing for positions 3 till 19.

After all 19 locations are measured, one complete row of the table is filled in as shown in table 4.4.

Table 4.4: Roving accelerometer modal test has one complete row: all outputs measured with respect to one input.

	A_{1x}	A_{1y}	A_{1z}	...	A_{19x}	A_{19y}	A_{19z}
F_{1x}							
F_{1y}							
F_{1z}	A_{1x}/F_{1z}	A_{1y}/F_{1z}	A_{1z}/F_{1z}	...	A_{19x}/F_{1z}	A_{19y}/F_{1z}	A_{19z}/F_{1z}
$\vdots$							
F_{19x}							
F_{19y}							
F_{19z}							

The full row with common reference ensures accurate phasing of all measurements, so that a proper shape of the mode can be measured.

Roving Hammer

Instead of roving the accelerometer, the hammer could be roved while the accelerometer stays fixed.

The accelerometer in this case measures outputs A_{1x}, A_{1y} and A_{1z}.The hammer impacts at F_{1z}, which happens to be perpendicular to the surface of the test object.The hammer is then moved to F_{2z}, F_{3z}, etc. This happens until impacts are done at all 19 locations as shown in Figure 4.14.

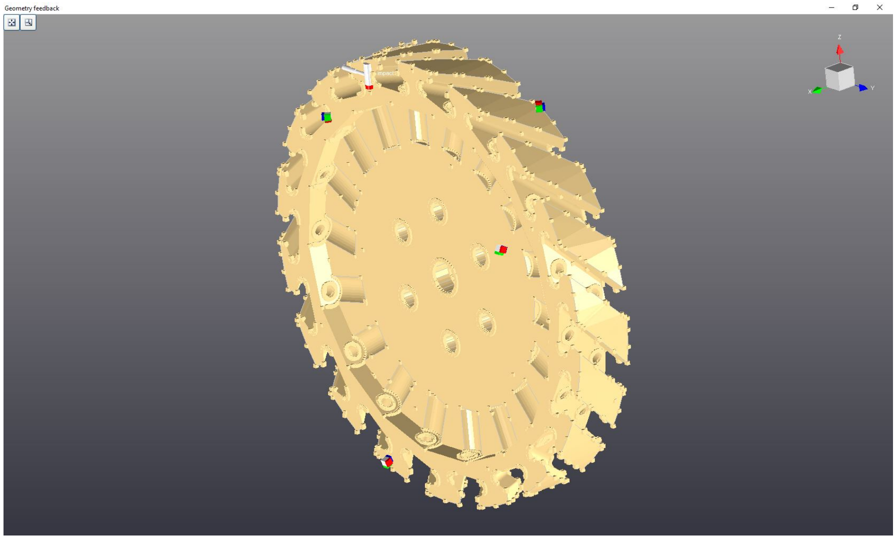

Figure 4.14: Roving impact hammer inputs with fixed accelerometer outputs on Disk.

The consequence of this test is NOT a complete row or column in the table following completion of the test, as seen in table 4.5.

Table 4.5: Roving hammer modal test DOES NOT have a complete row or column.

	A_{1x}	A_{1y}	A_{1z}	...	A_{19x}	A_{19y}	A_{19z}
F_{1x}							
F_{1y}							
F_{1z}	A_{1x}/F_{1z}	A_{1y}/F_{1z}	A_{1z}/F_{1z}	...			
$\vdots$							
F_{19x}							
F_{19y}							
F_{19z}	A_{1x}/F_{19z}	A_{1y}/F_{19z}	A_{1z}/F_{19z}	...			

There is NOT a complete row or column with test roving impact hammer. The impact hammer, instead of being used in all three directions, was used only in one direction at each different measurement spot.This is an easy oversight when using a modal impact hammer [2].

The only way to get all 3 directions from a roving hammer test is to impact in X, Y, Z directions at each point of the structure. This would provide a complete column in the FRF matrix for a single axis accelerometer that does not move and three columns for a triaxial accelerometer that does not move [2].

Since it's difficult (or near impossible) to impact in 3 directions in the middle of the plate we normally suggest using roving accelerometers when 3 directions are required. The other option would be to glue blocks at each node, impact the blocks in 3 directions and then use Modal Modification to remove the mass of the blocks at each node [2].

Chapter 5

RESULTS AND DISCUSSION

5.1 Overview

In this chapter the result of experimental activity will be provided for all four configuration as explained in section 4.4 and comparing the results of all sensors mounting on test objects and discuss about the results and all the difficulties we have faced during experimental test and what was causes and how to overcome those problems.

Five tri-axial accelerometers are positioned on the test object as explained in section 4.4. An instrumented hammer is used for the excitation during the FRFs measurement campaign. The impact excitation points never coincident with the measurement points where the accelerometers are located for practical experimental purposes.

5.2 The Test Campaign

The measurement campaign on the test objects of a blade, disk, and their assembly connected through a dove-tail joint are described. Five triaxial accelerometers are positioned on the blade and five on the disk. In order to decrease affect of fixed constrain in our results, the FRFs have been measured in free conditions. Measurement channels and models details are represented in the following table. The range of frequency bandwidth that we are interested is till 3000 Hz. Note that the impact experimental test has been performed base on average. It means that the number of hammer hit on the structure at the specific excitation point is five times. So the data collect after averaging of all those five times hitting.

Table 5.1: Measurement channels and models details

Description	**Disk**	**Blade**	**Assembly**
Number of response channels	15	15	30
Number of impacts	19	18	37

5.2.1 Error Sources

In order to build valid experimental models, there are different kinds of error sources which are necessary to be avoided. Some of them will be divided in three various categories: *Input and output errors*, *setup errors* and *signal processing errors*. The signal processing errors have already explained in section 3.9.

Input and Output errors

The conducted measurement performed by manual hammer or in some points automatic hammer and also accelerometers are affected by skill of operator. Some of those source of errors due to using those tools and to the operator skills.

1. **Location and Alignment:** Since the positions and directions of the DOF are specified, it is crucial that the hammer impacts and receptance are actually conducted at their respective locations and directions. Moreover it is important to hit and measure perpendicular to the structure's surface. Sometimes it is very difficult to hit same point with five time trying due to inaccessibility point or operator error.

2. **Force Magnitude:** In order to convey enough power into the auto-power spectrum (APS), the impact on the structure surface should be hard enough. This is to ensure that the signal-to-noise ratio of the sensor is valid. We have to try to forge a compromise between hard and soft impact for two specific reasons. First, both the accelerometers or the hammer, must not overload. second, linear transfer consider for experimental dynamic measurements. Note that hammer should not hit too hard which are cause local non-linearities that bring abou in force dependent transfer.

3. **Noise:** Noise is an inseparable part of sensors. H_1 and H_2 are two estimators can be used to minimize either input or output noise which explained in section 2.4.

Setup

Concerning to Set up the component to perform experimental dynamic measurements is vital to have proper measurement. Some those factors will be discuss below:

1. **Support Dynamics:** Choosing boundary condition is one of the first step has to made. As we have already mentioned in section 3.4 the model can either be implemented to a rigid interface or free-free models. As matter of fact, the free-free model is impossible to construct experimentally. The free condition means that the structure is, in effect, floating in space with no attachments to ground and exhibits rigid body behavior at zero frequency. Physically, this is not realizable, so the structure must be supported in some manner. Since this thesis is part of PhD student project, it is recommended to set up free-free models in order to have better compatible when working with Dynamic Substructures.

   Another important factor is that we have to be careful about support's construction for the component. To build a proper model which give us free-free behavior the stiffness of the support should be design in way that the support eigenfrequency should be low enough which it does not affect on the dynamics of the components.

   The support eigenfrequency is almost 10 times lower than the first mode of structure. Note that the support should have small damping as much as possible and should not be attached to prescribed interface of the components which is due to the local dynamics of the surfaces where they are attached.

2. **Added Dynamics:** There are another contribution that affects on the dynamics of component beside the support. Accelerometers and their cables add extra mass, stiffness and damping to the component. Stiffness and damping can be considered negligible but the mass effect can not.

3. **Sensor Placement:** Different way of attachment of accelerometer to the structure explained in section 3.7.1. It should be double checked that attachment is rigid and any motion between sensors and structure should be avoided as it can cause misleading receptance and damping.

Noise and Signal Processing

For each experimental measurements, singnal processing errors are inseparable part of each experiment. Most of those errors have been already mentioned with details in section 3.9.

1. **Aliasing:** Aliasing happen when a low sampling frequency is chosen which is inseparable part each measurement in signal processing errors. To overcome aliasing, choosing high sampling frequency for specific measurement. Note that the theoretical lowest sampling frequency is two times the highest signal

frequency. One of the solution is utilizing low-pass filters in order to minimize high frequency content.

2. **Leakage:** It is split into many finite time-blocks when measuring a potentially infinite time-signal block. The signal in this window is translated by Fast Fourier Transform into the frequency domain. FFT, in essence, believes that the time signal is infinite and accomplishes this by infinitely repeating the finite time-block. Although the signal amplitude also does not occur at the start and end of the signal, the same abrupt decreases or increases occur. This bring about high artificial frequency content. This problem is also called spectral leakage. This is circumvented by damping the beginning and ending of the signal such that they both approach an equal 0 in a process called windowing.

3. **Double Hits:** Double hit will happen during hammer impact test, when hammer tip touch the structure and structure rebounds into the hammer tip immediately. As a matter of fact, the second impact may only be milliseconds precisely after the first one and easy to miss on the data plot. Note that double hit contain misleading information and should be discarded by replacing new test round. We can observe double hit by viewing the amplitude of power-spectral density versus frequency or impact hammer force versus time history with zoom display feature during the data acquisition.

5.3 Disk

The disk depicted in figure 5.1 made of steel was hung on rubber bands, as shown in in figure 4.9, in the free-free constrain configuration. All of five triaxial accelerometers which are connected to 15 response channels, located along the disk moreover 19 excitation points (Input Channels) are specified to be hit by the instrumented hammer. We are going to evaluate some DoFs which almost represented the whole DoFs of the disk. Those DoFs are 19, 25, 27, 29, 36.

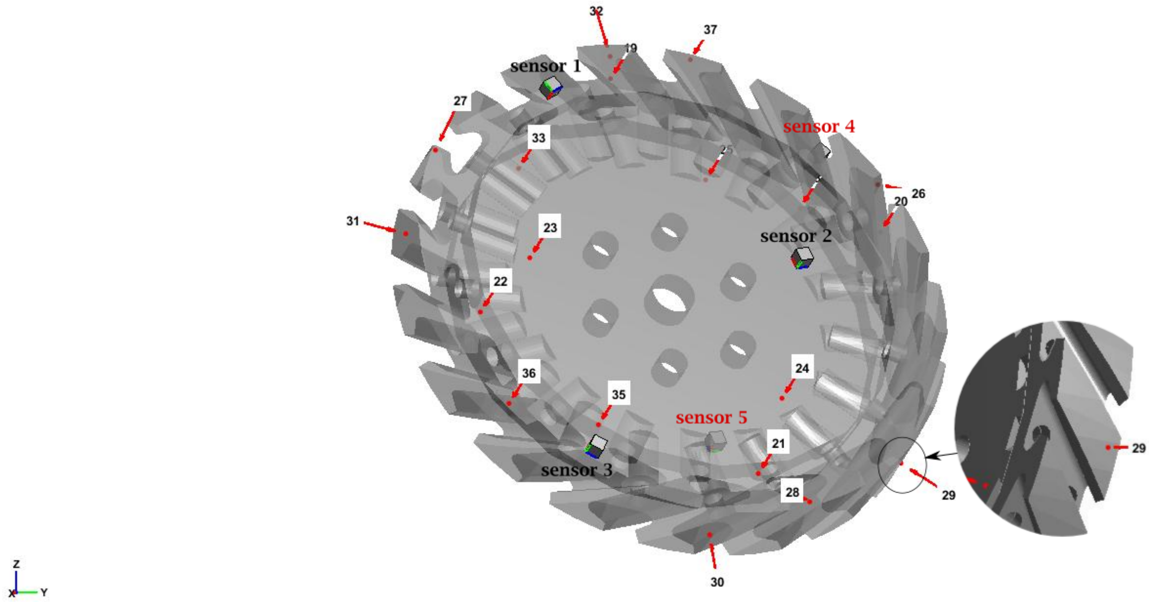

Figure 5.1: Setup for the disk. Each sensor has three response channels.

5.3.1 Input Force Spectrum

As we already mentioned in section 3.5.1 there can be some significant effects depending on which kind of tips have been used and how hard has been impacted the structure. Moreover if you are performing an impact test and every single hit for an average has a different level of input force, then the consequence is the spectrum excited by that impact will be dramatically different each time. The result of problem might have a significant effect in the coherence in high frequency range.

Moreover, often the local flexibility of the structure can play a vital role of the total time of the impact which cause an effect on the input spectrum force conveyed to the structure. This one will appear while the performed test that have dramatically varying stiffness's throughout the structure.

Basically, it would be better to notice that the input spectrum should be reasonably flat over the all frequencies with no significant drop-outs in the frequency spectrum. So we want the input spectrum to have sufficient, fairly even excitation over the frequency range of concern. If the input spectrum were to completely drop off to zero, then the structure would not be excited at that frequency which is not desirable.

By using hard metal tip to excite the structure over our frequency range of interest *3 kHz*, such that the input force spectrum does not drop off significantly by the end of the frequency range. As shown in Figure 5.2, the input power spectrum for all the excitation points roll off by approximately less than *-10 dB* over *3000Hz* which is acceptable value when you look at other characteristics like FRF and coherence.

As can be seen in the plot the highest input force imparted to the disk is corresponding to excitation point 29 which is located on the circumference of the disk, between two slot of the blade position refer to Figure 5.1. The reason is that in this case the hit applied laterally with much less flexibility with respect to hit when hammer applied vertically and more flexibility due to rubber bands. The lowest input force is also related to excitation point 25 which is located to inner part of the disk with lower thickness with respect to outer ring.

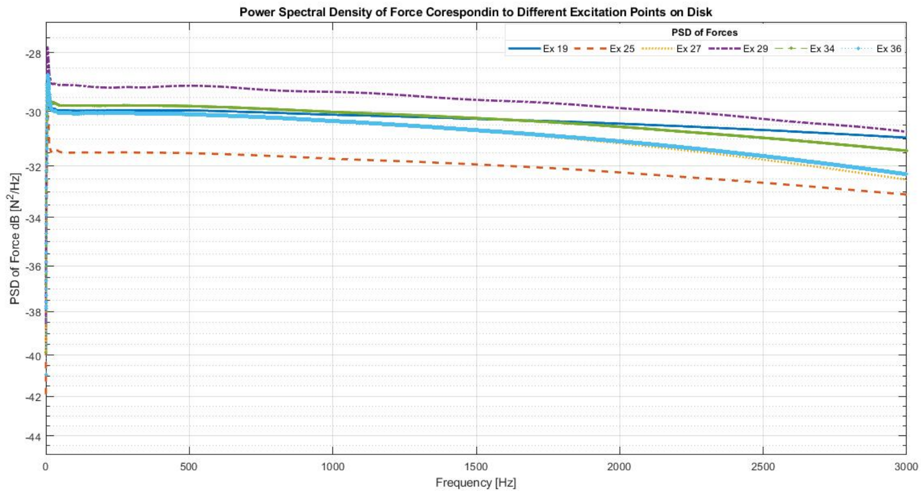

Figure 5.2: Power Spectral Density corresponding to excitation points on the Disk 19, 27, 29, 34, 36.

5.3.2 Frequency Response Function and Coherence

In this section the FRF and Coherence of excitation points 19, 27 and 29 will be investigated.
For the FRF we are going to see result of some sensors in three directions *x,y,z*.

As it shown in Figure 5.3 there are some peaks at low frequency around $[18-20]Hz$ which is rigid body modes. The rigid body modes will no longer have zero frequency because the structure constrained with soft elastic cords. However, if a sufficiently soft support system is used, the rigid body frequencies will be much lower than the frequencies of the flexible modes and thus have negligible effect. The first three flexible modes and damping ratio provided in the following table 5.2. Note that damping ratio calculated by 3dB or half power method.

Table 5.2: The fist three Modes of the Disk

Mode Number	1	2	3
Frequency [Hz]	1090.3	1969.4	2637.3
Damping ratio $\zeta(\%)$	0.03	0.04	0.02

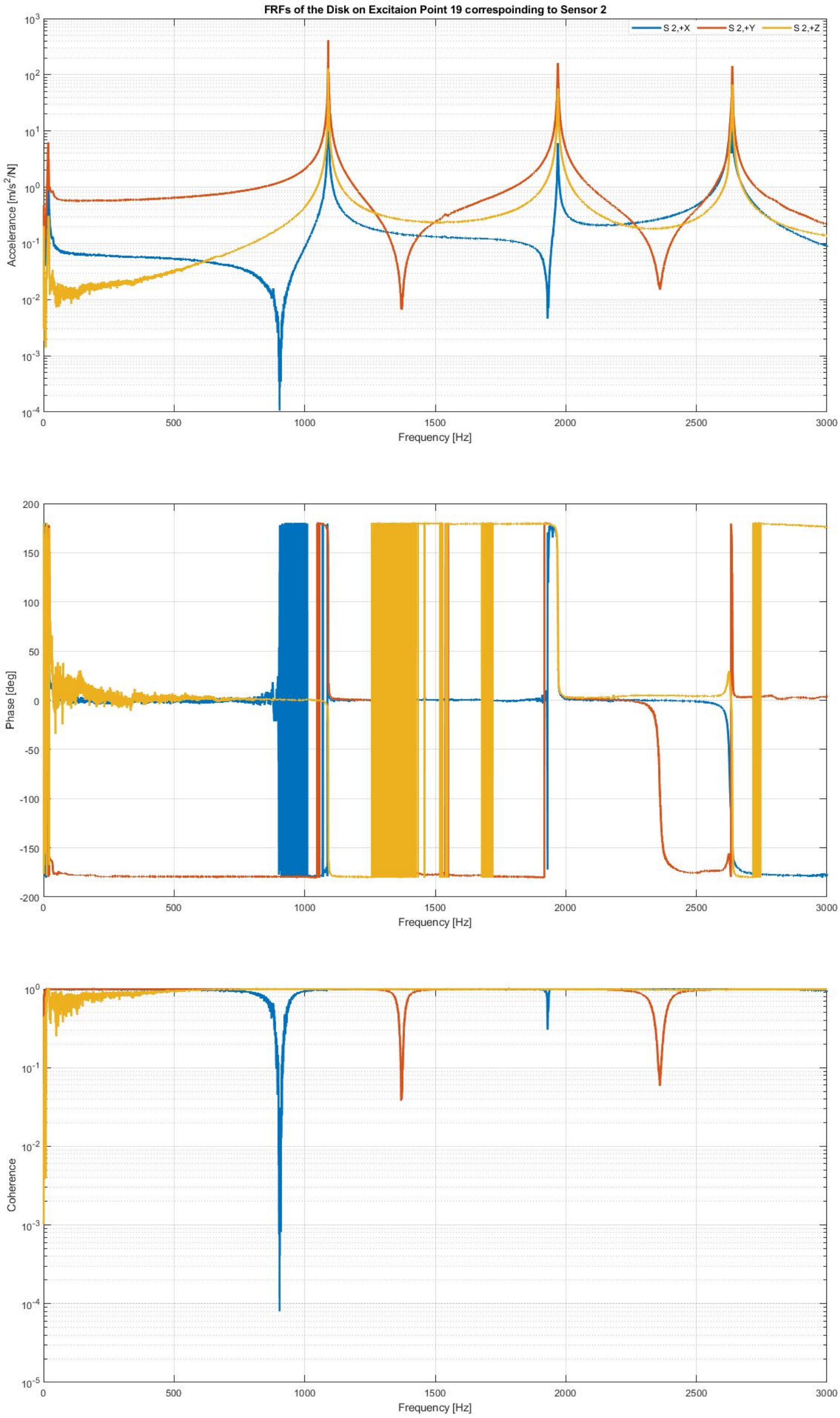

Figure 5.3: Frequency Response Function and coherence of the Disk on excitation point 19 corresponding to sensor 2 in three directions.

A proper excitation produces a vibration response that is perfectly correlated to the input excitation force which indicated through coherence graph that is close to one over the whole frequency range. To be sure about the data whether if it is valid or not, coherence should be monitored constantly through data acquisition. As it shown in Figure 5.3 the overall coherence should be close to 1 throughout frequency rage of interest. However, it is normal for coherence to be low at anti-resonance, in other words, structural nodes where the vibration responses are very low or drops in the coherence in anti-resonant regions are expected due to the fact that the structure has no response at these frequencies and therefore the response of the system is not coherently related to the measured input signal. At the beginning of +Z direction till $500Hz$ the response have noise which most likely there is little response in that direction at point 19.

Although the position of sensor 3 refer to Figure 5.1 is in a way that the response in +Z direction at point 27 does not feel enough response in that direction probably due to the impact at point 27 at root of the disk, the modes well separated with less noise at end of the bandwidth.

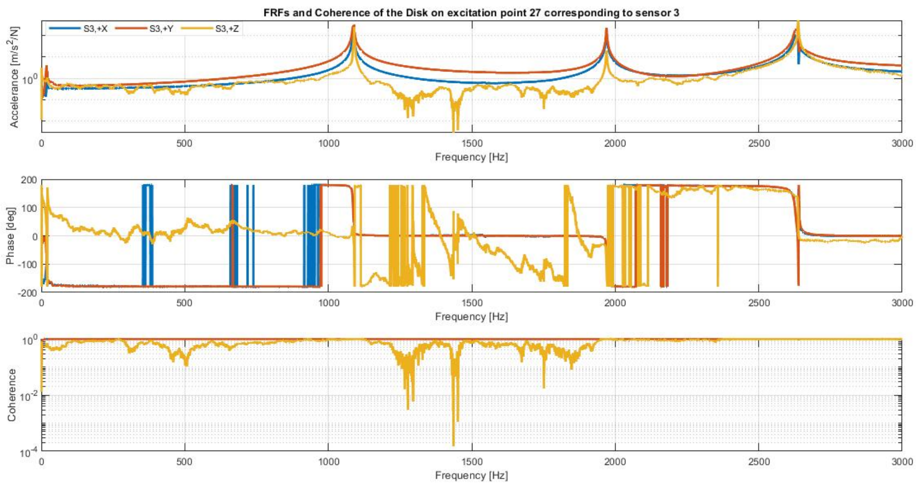

Figure 5.4: Frequency Response Function and coherence of the Disk on excitation point 27 corresponding to sensor 3 in three directions.

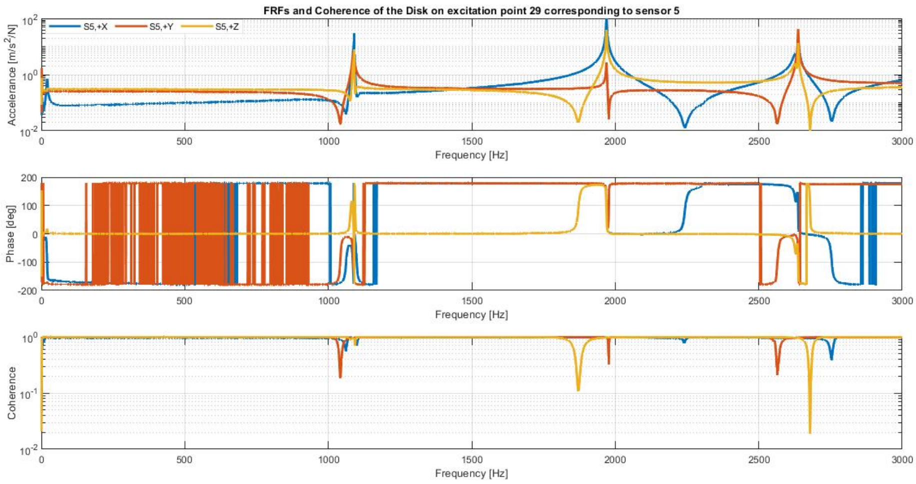

Figure 5.5: Frequency Response Function and coherence of the Disk on excitation point 29 corresponding to sensor 5 in three directions.

As shown in Figure 5.6 the level of consistency of average coherence value for all sensors is high enough except for sensor 3 in Z direction which specified by black arrow. Most of the averages relating to mean coherence value above 0.9 except for sensor 3, Z direction which the value is 0.7296 with respect to our threshold 0.8.

In Figure 5.7 the level of coherence mean value accuracy to each excitation points by considering all the sensors in Disk configuration are almost above of our threshold 0.8 except for excitation point 30 which the value is 0.6546 as depicted in following figure by arrow. The reason could be due to the direction of impact at point 30 which is laterally, Figure 5.1 and affected sensor 3 does not feel enough response in that direction.

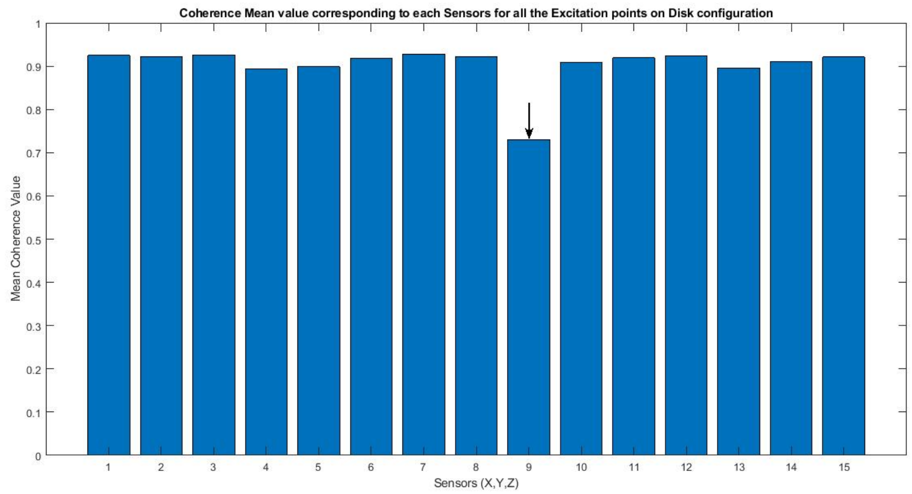

Figure 5.6: Coherence Mean Value corresponding to each sensors in X,Y and Z directions for all the excitation points on Disk configurations.

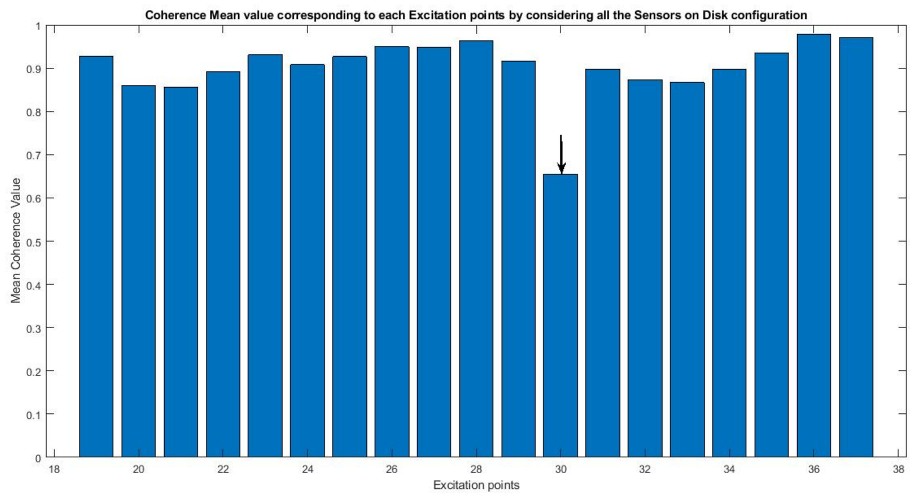

Figure 5.7: Coherence Mean Value corresponding to each excitation points by considering all the sensors on Disk configurations.

5.4 Blade

The blade shown in figure 5.8 made of steel was hung on rubber bands, as shown in in figure A.2, in the free-free configuration. All of five triaxial accelerometers with 15 response channels, located along the blade moreover 18 excitation points are specified to be hit by the instrumented hammer. We are going to evaluate some

DoFs which almost represented the whole DoFs of the blade. Those DoFs are 1, 2, 4, 15, 16, 17.

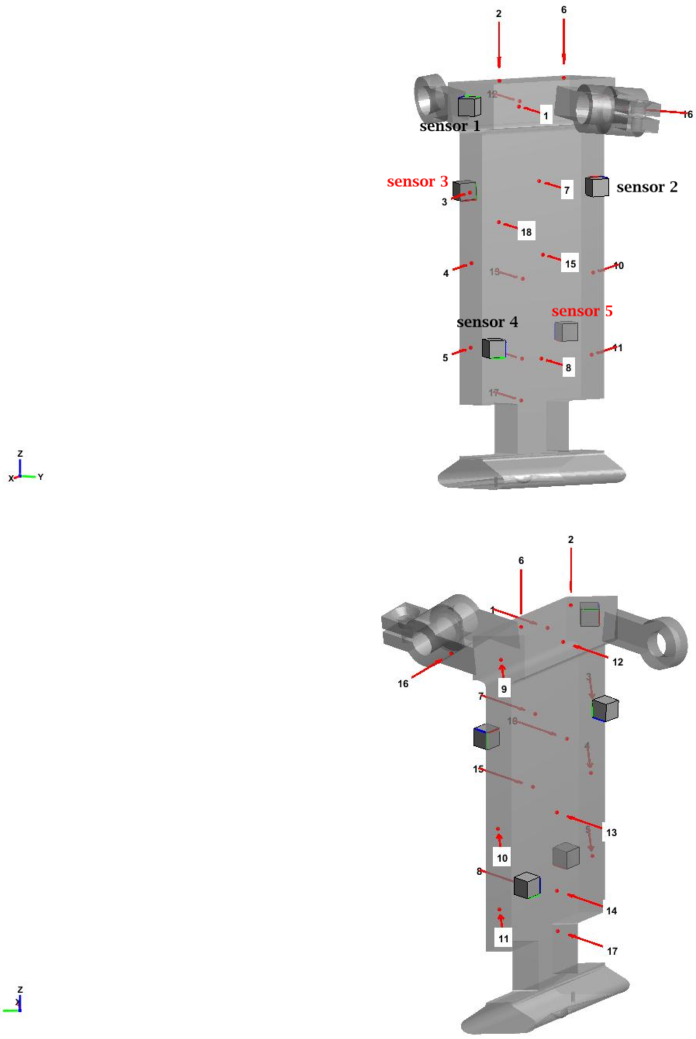

Figure 5.8: Setup for the blade front and back with all sensors

5.4.1 Input Force Spectrum

In the case of impact excitation on blade, the tip of the hammer determines the width of the excitation spectrum. As a rule of thumb the useful frequency range starts at 0 Hz and is limited to that frequency at which the magnitude is 20 dB less than the low-frequency magnitude, Figure 5.9 cover this rule.

As shown in Figure 5.9, the input power spectrum for all the excitation points roll off by approximately less than *-13 dB* over *3000Hz* which is acceptable value but the details will be discuss in next section by evaluating FRF and coherence.

Like before, the highest input force imparted to the blade is corresponding to excitation point 2 which is located on the top of the hanging blade. The reason is that in this case the hit applied vertically with much less flexibility with respect to hit when hammer applied from the side to the blade. The lowest input force is also related to excitation point 17 which is located close to root of the blade. The highest drop off in the level of amplitude is related to excitation point 4 which impacted laterally with very small area to impact.

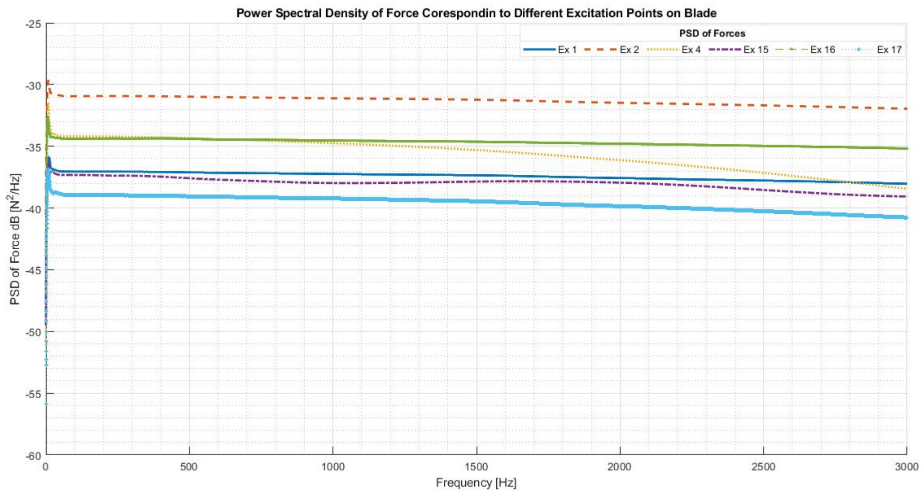

Figure 5.9: Power Spectral Density corresponding to excitation points on the Blade 1, 2, 4, 15, 16, 17.

5.4.2 Frequency Response Function and Coherence

FRFs and Coherence of excitation points 1, 2, 4, 15, 16 and 17 will be considered.

When the impact test conducting, the position of the input impact have a vital effect on the FRF results which can be seen in the coherence response function.

One of the biggest concern during the impact test is to ensure that the impact should be at the same location and same direction for each average. As shown before in Figure 5.8, the excitation point 1 is located on the blade in very narrow location in order to have clean hit on the exact position.

By referring to Figure 5.10, the FRF and coherence are shown and although the FRF looks reasonable, the coherence is seen to have some significant degradation throughout the whole frequency range. So this behaviour happened when the desire input locations have some slight variation with respect to actual location during impact test. So generally speaking those kind of poor measurement in coherence are due to the inconsistency of the impact location – whether it be not impacting the same location for each measurement or for not maintaining a consistent strike angle for each measurement.

The first three modes provided in the following table 5.3.

Table 5.3: The fist three Modes of the Blade

Mode Number	1	2	3
Frequency [Hz]	1199.9	2086.6	2745.6
Damping ratio $\zeta(\%)$	0.46	0.93	0.21

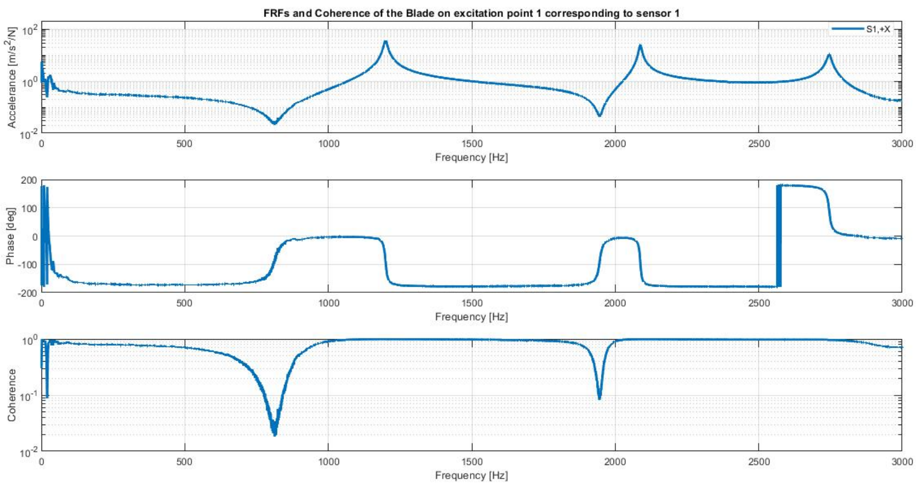

Figure 5.10: Frequency Response Function and coherence of the Blade on excitation point 1 corresponding to sensor 1 in three directions.

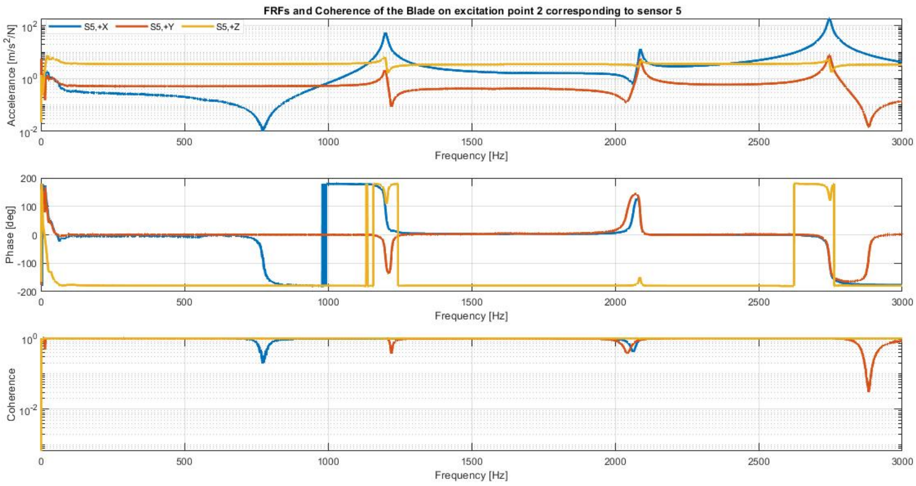

Figure 5.11: Frequency Response Function and coherence of the Blade on excitation point 2 corresponding to sensor 5 in three directions.

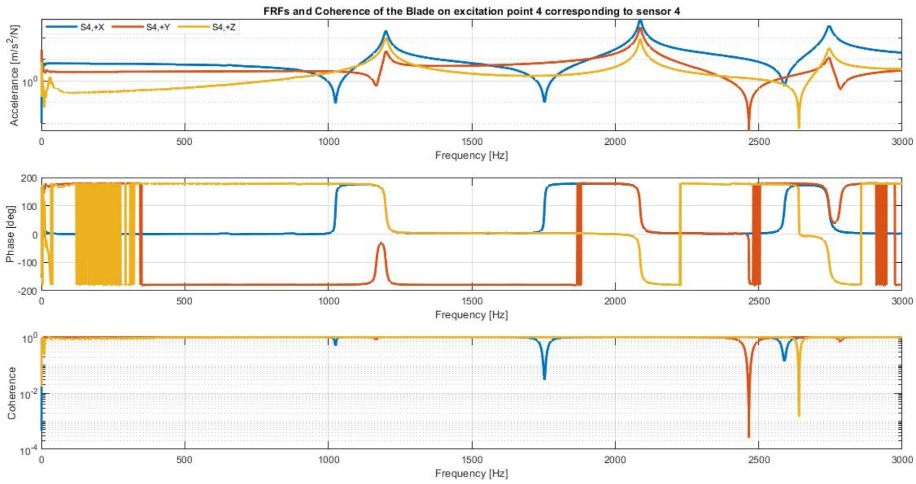

Figure 5.12: Frequency Response Function and coherence of the Blade on excitation point 4 corresponding to sensor 4 in three directions.

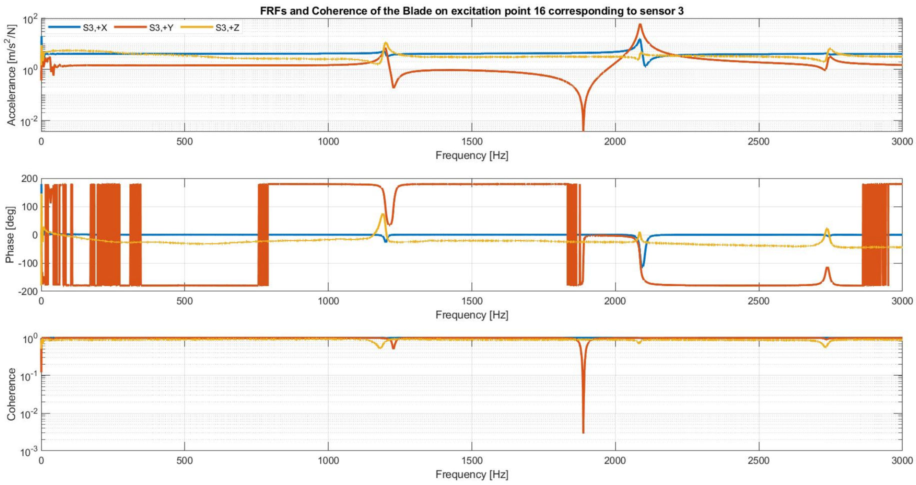

Figure 5.13: Frequency Response Function and coherence of the Blade on excitation point 16 corresponding to sensor 3 in three directions.

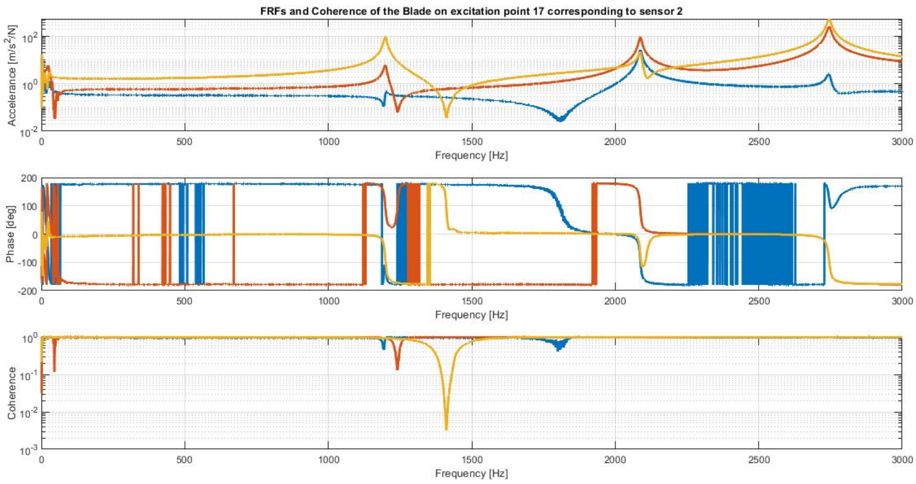

Figure 5.14: Frequency Response Function and coherence of the Blade on excitation point 17 corresponding to sensor 2 in three directions.

Lets consider excitation point 13 and 15 with considering response of sensor 3, X direction. As it depicted in Figure 5.8 the response coordinates are different from the excitation coordinated which specified by cross-point measurements. As shown in Figure 5.18 imaginary plot in cross-point measurement all the modes are not necessarily in phase with each other so the response can move either in phase or out of phase with the excitation. According to magnitude FRF in Figure 5.18 if two adjacent modes are in phase at a particular point, then an anti-resonance will

exist between them, otherwise If any two adjacent modes are out of phase, then their mass and stiffness lines will not cancel at the intersection and a smooth curve will appear instead.
When you excite a point which is near to the node point then the nearest mode corresponding to that node will not be excited or excite with low amplitude. In the following plot it seems there is node around point 15 which cause to get lower amplitude for mode 2 at that point and you can see mode 3 (red one) is barely discernible in imaginary plot.

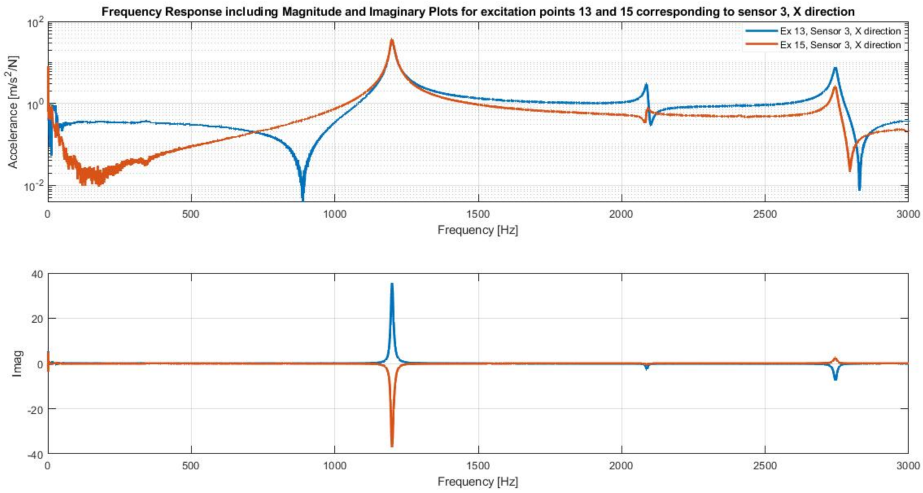

Figure 5.15: Frequency Response Function including Magnitude and Imaginary Plots for excitation points 13 and 15 corresponding to sensor 3, X direction.

In Figure 5.19 the level of consistency of average coherence value for all sensors is high enough except for sensor 3 in Z direction which specified by black arrow same as Disk one on Figure 5.6. Most of the averages relating to mean coherence value above 0.9 except for sensor 3, Z direction which the value is 0.7734 with respect to our threshold 0.8.

In Figure 5.20 depicted the level of coherence mean value accuracy to each excitation points by considering all the sensors in Blade configuration are almost above of our threshold 0.8 except for excitation point 15 which the value is 0.7500.

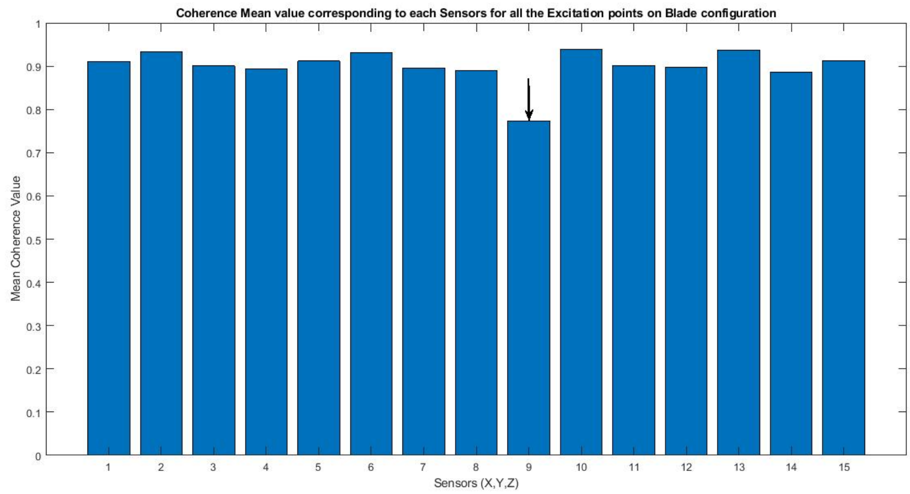

Figure 5.16: Coherence Mean Value corresponding to each sensors in X,Y and Z directions for all the excitation points on Blade configuration.

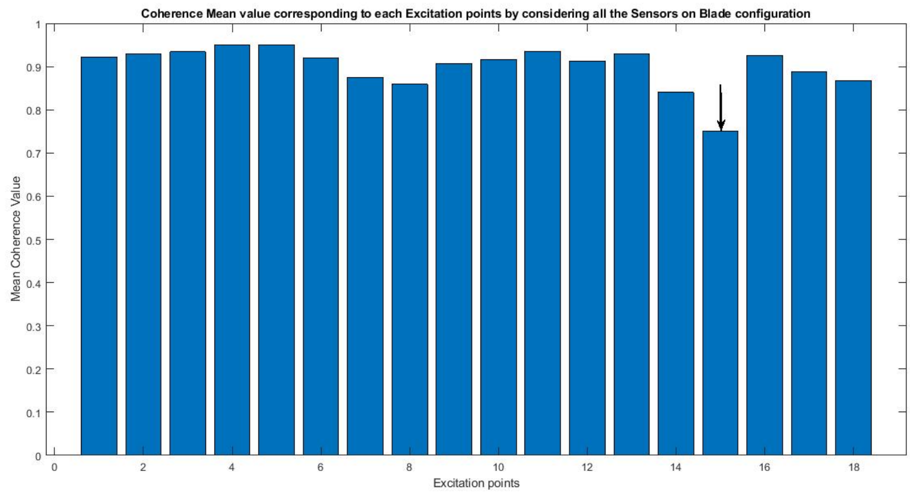

Figure 5.17: Coherence Mean Value corresponding to each excitation points by considering all the sensors on Blade configuration.

5.5 Disk with Blade

In this configuration the assembly system will be evaluated; disk plus blade couple together in order to perform test. Performing impact testing in assembled configuration have much more difficulties with respect to evaluate each one of them separately. In the first configuration all the accelerometers located on disk and dummy masses are on the blade and in the second setup the position of accelerometers and dummy masses will be swapped.

In the assembled configuration the poor measurement is unavoidable due to complexity of structure with many joints and possible nonlinear behavior. However, our test object is also behave in the same way, under particular situations we can avoid some pitfalls like double impacts. Needless to say that we would like to avoid double impact measurements at all costs but sometimes is unavoidable and we have to accept the measurement if the other factors like FRF, coherence and input force spectrum have proper results.

The coupled configuration as depicted in Figure 5.18, the blade is very flexible and prone to double impacts at some points during testing.

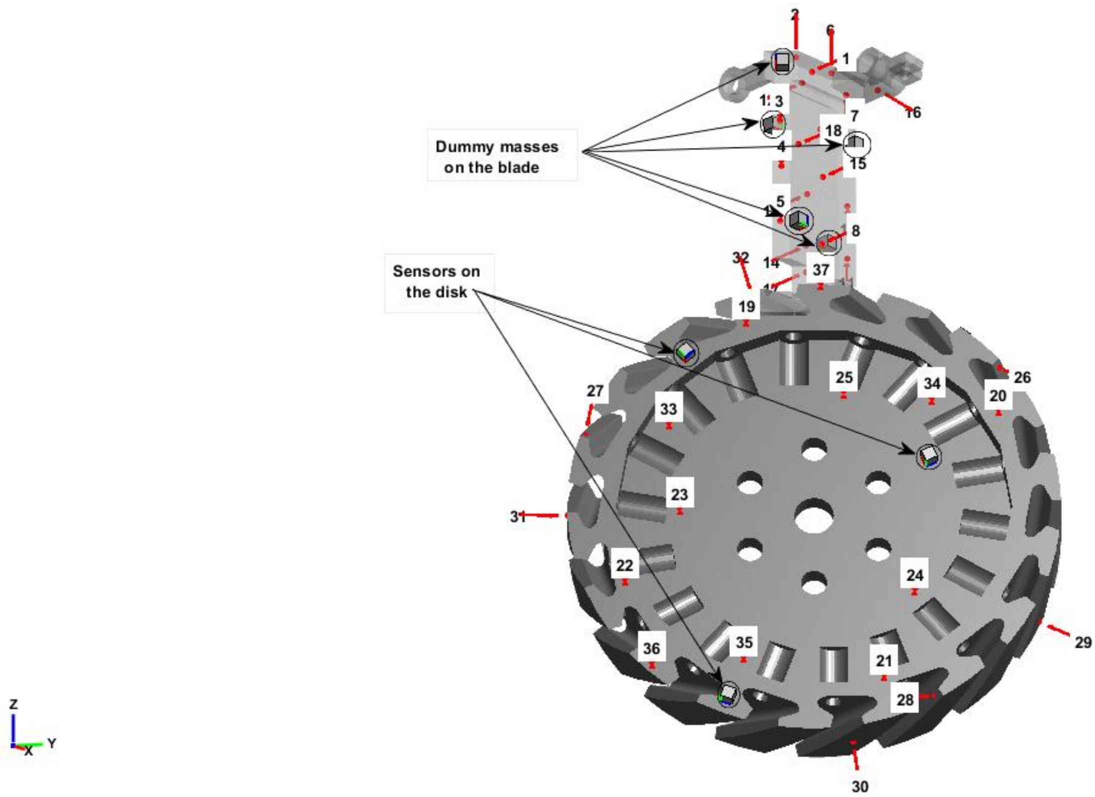

Figure 5.18: Setup for Assembly, disk and blade couple together.

5.5.1 Input Force Spectrum

First Configuration: First of all double impact showed in the first configuration when all sensors located on the disk and dummy masses are on the blade. Double hit occurs when the hammer hits the structure and structure rebounds into the hammer tip. The second impact may only be milliseconds after the first and easy to miss on the data display. Double hit would also result in erroneous results in some cases, which should be discarded and the test repeated. Excitation point 15 is one those points with double impact or multiple impact which is located on blade. The blue line in Figure 5.20 is corresponding to power spectral density of point 15 due to manual impact hammer with present of fluctuation over the frequency spectrum which is the effect of double or multiple impact. The red line is related to automatic hammer at same point, as mentioned before the frequency spectrum is reasonably flat over the entire frequency range with less than 20 dB rolloff over the entire frequency range as depicted in Figure 5.19.

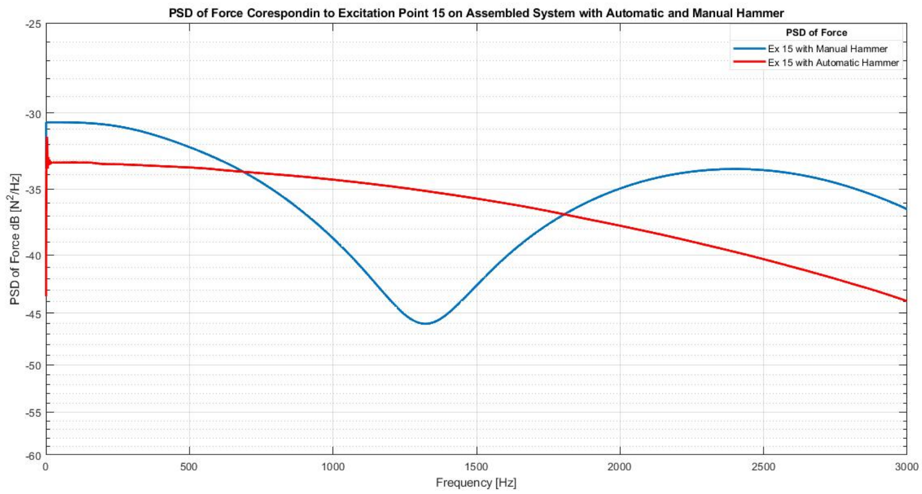

Figure 5.19: Comparison of Power Spectral Density corresponding to excitation point 15 on assembled system with manual and automatic hammer.

As we already mentioned in some excitation points the double or multiple impacts are unavoidable and at under specific circumstances, it might be reasonable to accept a measurement with double impact but the real concern here should be the sufficiency of FRF and Coherence. Here is power spectral density corresponding to excitation point 13 with double impact and excited by manual and automatic hammer in Figure 5.20.

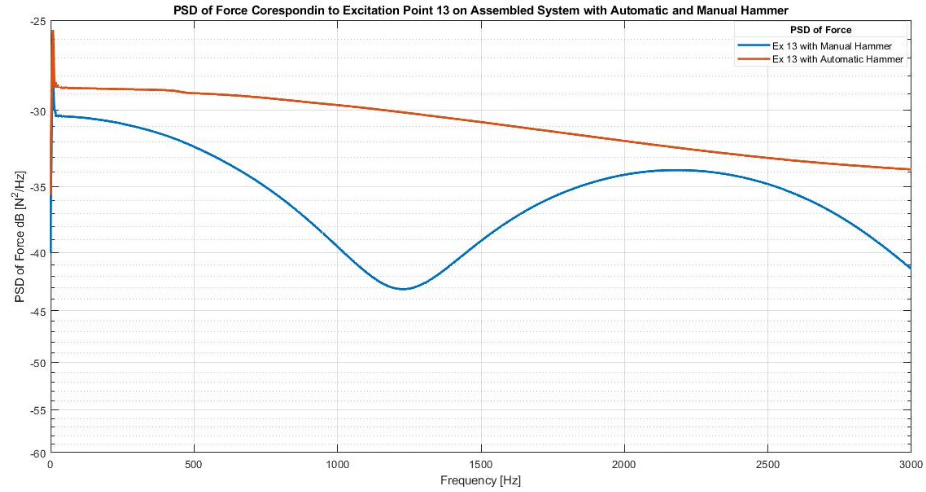

Figure 5.20: Comparison of Power Spectral Density corresponding to excitation point 13 on assembled system with manual and automatic hammer.

5.5.2 Frequency Response Function and Coherence

FRFs and Coherence of different excitation points will be considered in order to show the effect of double or multiple impact and in some cases the effect of windowing and more averaging in our results.

First Configuration: In this configuration the results of excitation point 15 will be examine and showing the effect of double impact and comparison between use of manual and automatic hammer.

As shown in Figure 5.21, The result of FRFs and coherence due to automatic hammer is quiet better with respect to manual hammer at excitation point 15. During the impact testing by hammer it is not possible to hit exactly at intended point with respect to automatic hammer with fixer position because of user's hand inaccuracy so there is a little bit shifting between two FRF graph at low frequency around $500Hz$ and high frequency band around $[1950 - 2500]Hz$. In FRF plot with using manual hammer there are also two additional peaks in the higher frequency range $1950Hz$ that were not well separated and clear but after excite by automatic hammer those modes became more clear. The anti-resonance were contaminated with noise at $2100Hz$ with manual hammer which cause poor coherence and generally the coherence level is better with automatic hammer.

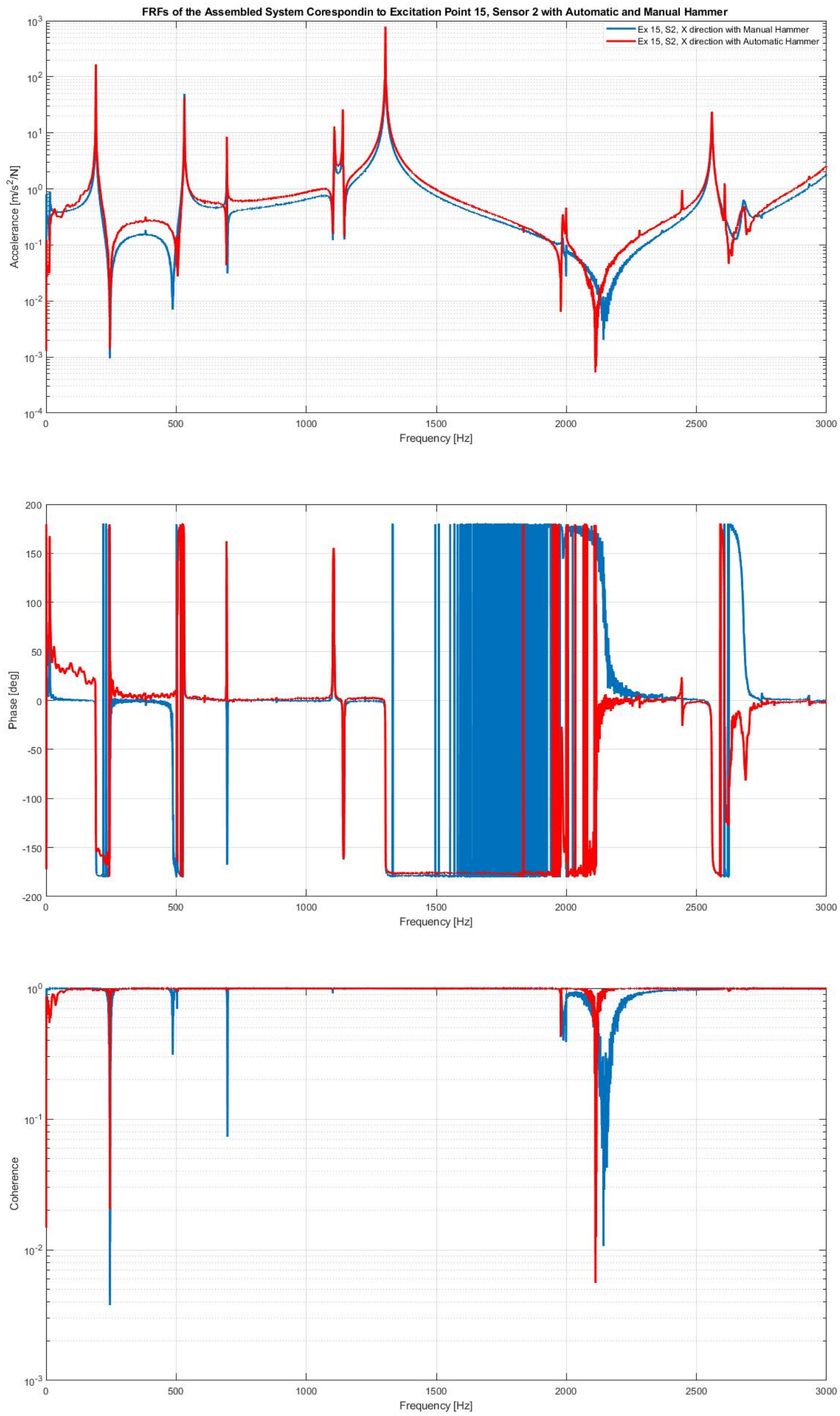

Figure 5.21: Frequency Response Function and coherence of the coupled system on excitation point 15 corresponding to sensor 2 in X direction with using Automatic and Manual Hammer.

As an indication whether if our results are correct or not we used the average coherence value for that excitation point and all mean coherence value corresponding to all sensors when we excite at point 15. If you look at the tale 5.4, both the mean value related to automatic hammer are better than manual one; the values are close to one which is the best value for coherence.

Table 5.4: Comparison of mean value coherence on point 15 corresponding to sensor 2, X direction with automatic hammer and manual hammer

Hammer Type	Manual	Automatic
Mean Coherence	0.9604	0.9806
Mean Coherence for all Sensors	0.9412	0.9745

The first nine modes and damping ratio provided in the following table 5.5.

Table 5.5: The fist nine Modes of the Assembly

Mode Number	1	2	3
Frequency [Hz]	191.25	531.4	695
Damping ratio $\zeta(\%)$	0.04	0.04	0.01
Mode Number	4	5	6
Frequency [Hz]	1108.75	1140.6	1304.4
Damping ratio $\zeta(\%)$	0.07	0.03	0.02
Mode Number	7	8	9
Frequency [Hz]	1986.56	2559	2676
Damping ratio $\zeta(\%)$	0.05	0.03	0.24

In Figure 5.22, The result of FRFs and coherence due to automatic and manual hammer depicted at excitation point 13. Clearly, there is not double impact with automatic hammer (red one) at point 13 but the measurement adequacy is quiet poor.

By looking at Figure 5.22 generally, the frequency response function recorded by automatic hammer is not particularly good as evidenced by the poor coherence at some frequencies over the spectrum with respect manual hammer (the blue one). Notice that the coherence is relatively poor particularly at the beginning of low frequencies till $1000Hz$.

Now let's consider the measurement where the double impact is observed in Figure 5.20. Now this measurement clearly has double impact on the input force excitation at point 13 and the input spectrum is not flat and has some variance over the frequency spectrum.

We have to notice that while we measure at the node of a mode then there will be no visible amplitude in FRF measurement related to that mode irrespective of if it is the excitation or response location. So by knowing that if the reference is located very close to the node of the mode then the amplitude of the FRF will be very low for that particular mode. By looking at Figure 5.22 the 9th mode around $2676Hz$ is an example of that. That amplitude is low compared to the 1st, 2nd or 3rd mode because the value of the mode shape for the input or output location is much smaller than that for the 1st and 2nd or 3rd mode, that's why the amplitude is much lower. However, in more complex structures it can be difficult, if not impossible, to choose a single reference point from which to view all of the modes. That is why we perform impact tests with multiple references so often. We can see all the modes from a collection of different referees this way.

In this case we can clearly see in table 5.6 that the result of manual hammer is much better than the automatic one.

Table 5.6: Comparison of mean value coherence on point 13 corresponding to sensor 3, X direction with automatic hammer and manual hammer

Hammer Type	Manual	Automatic
Mean Coherence	0.9839	0.8763
Mean Coherence for all Sensors	0.9733	0.8497

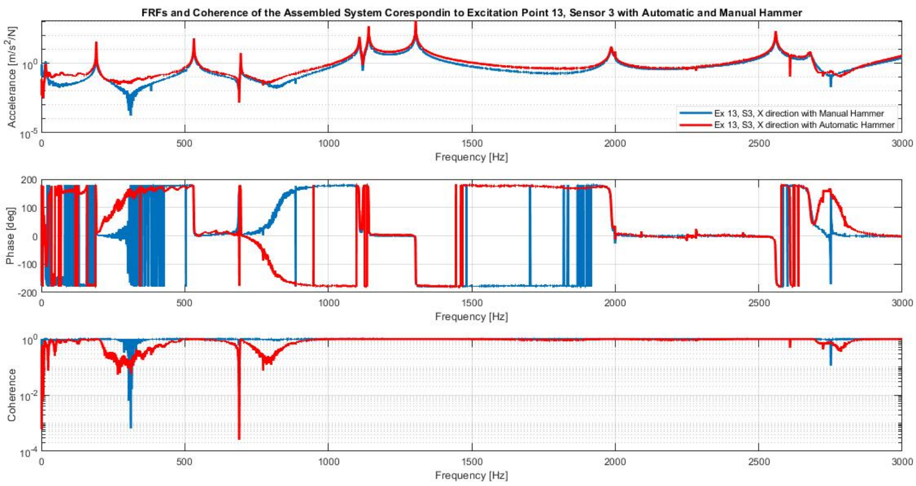

Figure 5.22: Frequency Response Function and coherence of the coupled system on excitation point 13 corresponding to sensor 3 in Z direction with using Automatic and Manual Hammer.

During the impact test in first configuration at some excitation points mean value of coherence was poor so we decide to perform impact testing for those points with more average hits and windowing in order to see the effect of those factors on our response. As mentioned before in section 3.9.5 the response signal is an exponential decaying function and may decay out before or after the end of the measurement. Applying response window depends on how the structure behave; if the structure is heavily damped, the response may decay out before the end of the time record which is our case study such that the response window can be used to remove the remaining noise in time record. On the contrary if the structure is lightly damped , the response may continue beyond the end of the time record so it must be artificially forced to decay out to minimize leakage. A general rule for setting the time constant, is about one fourth the time record length T.

In the following Figure5.23, two different excitation points are considered in order to show the effect of averaging and windowing on coupled system in the first configuration. Point 5 chosen from blade and point 21 chosen from disk.
For point 5 we consider 4 different cases which are: I)5 average hit with 100% exponential decaying or in other words no windowing. II)10 average hit with 25% exponential decaying window. III)10 average hit with 5% exponential decaying window. IV)10 average hit with 1% exponential decaying window.
For point 21 we had 5 cases: I)5 average hit with no windowing. II)10 average hit with 100% exponential decaying or in other words no windowing. III)10 average hit with 25% exponential decaying window. IV)10 average hit with 5% exponential decaying window. V)10 average hit with 1% exponential decaying window.
All the results shown in Figures 5.23 and 5.24 and table 5.7. FRFs amplitude plots for both points 5 and 21 are seem overlapped in the whole frequency range meanwhile it seems the coherence level become better after setup in the Testlab software to increase average hits from 5 to 10 and also applying decay window to our responses on those points. Table 5.7 provided the mean values of coherence due to different cases. As depicted in table the values became better after we used 10 averages with 25% windowing.

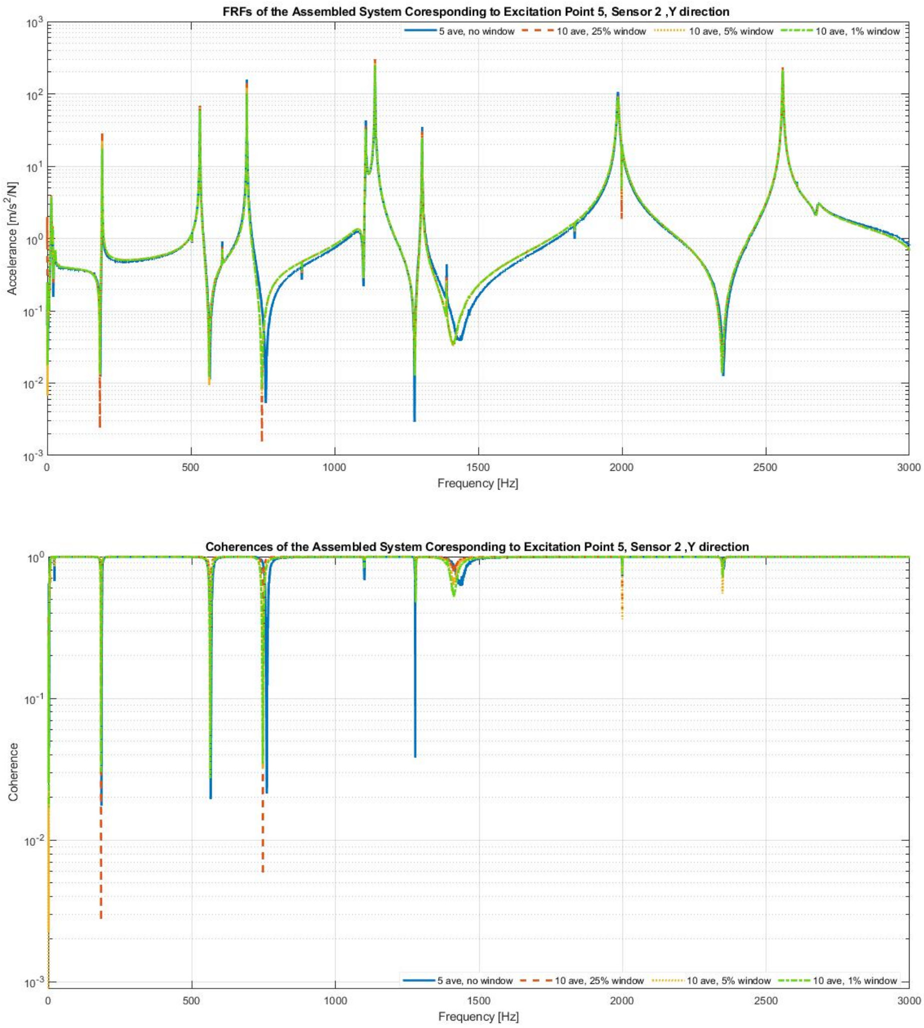

Figure 5.23: Frequency Response Function and coherence of the coupled system on excitation point 5 corresponding to sensor 2 in Y direction.

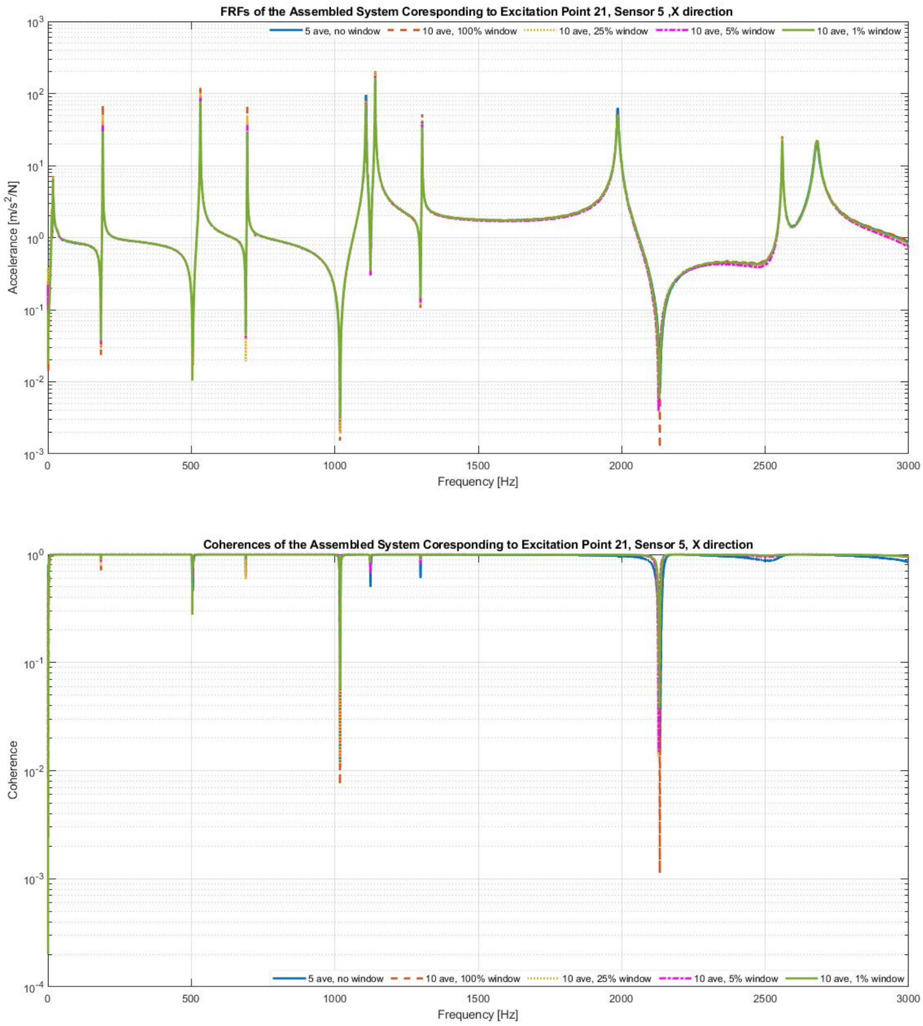

Figure 5.24: Frequency Response Function and coherence of the coupled system on excitation point 21 corresponding to sensor 5 in X direction.

Table 5.7: Comparison of mean value coherence on point 5 and 21 corresponding to sensor 2, Y direction and 5, X direction respectively

Mean Coherence	Point 5	Point 21
5 average, no window	0.9364	0.7768
10 average, no window	–	0.8469
10 average, 25% window	0.9504	0.8689
10 average, 5% window	0.9367	0.8574
10 average, 1% window	0.9394	0.8687

We have to note that the exponential window can also affect on damping and change the resulting frequency response because it has the effect of adding artificial damping to the system. In order to see how much is big that effect we compare damping ratio for both points 5 and 21 in the case that we do not have any window and the case that we have 25% window. Table 5.8 and 5.9 represent those data. As you can see windowing only affect on mode mode number 7 by adding artificial damping with portion of 0.02 before and after applying window which is small enough to neglect that effect.

Table 5.8: Comparison of damping ratio for point 5, corresponding to sensor 2, Y direction.

Mode Number	1	2	3
Damping ratio $\zeta(\%)$ when No window	0.08	0.06	0.03
Damping ratio $\zeta(\%)$ when 25% window	0.03	0.04	0.02
Mode Number	4	5	6
Damping ratio $\zeta(\%)$ when No window	0.10	0.04	0.03
Damping ratio $\zeta(\%)$ when 25% window	0.06	0.03	0.02
Mode Number	7	8	9
Damping ratio $\zeta(\%)$ when No window	0.11	0.04	1.15
Damping ratio $\zeta(\%)$ when 25% window	0.13	0.04	1.02

Table 5.9: Comparison of damping ratio for point 21, corresponding to sensor 5, X direction.

Mode Number	1	2	3
Damping ratio $\zeta(\%)$ **when No window**	0.09	0.06	0.03
Damping ratio $\zeta(\%)$ **when 25% window**	0.03	0.04	0.009
Mode Number	4	5	6
Damping ratio $\zeta(\%)$ **when No window**	0.09	0.04	0.03
Damping ratio $\zeta(\%)$ **when 25% window**	0.05	0.03	0.02
Mode Number	7	8	9
Damping ratio $\zeta(\%)$ **when No window**	0.12	0.04	0.3
Damping ratio $\zeta(\%)$ **when 25% window**	0.14	0.04	0.22

Second Configuration: When all the sensors moved on the blade and dummy masses swapped on the disk. In this setup we just only examine comparison between coherence mean value corresponding to each sensors for all excitation points and also for each excitation points by considering all the sensors in both first and second configuration.
As shown in Figure 5.25 the level of consistency of data for all sensors is high enough in order to use these data corresponding to these experimental test for post processing. All the averages relating to mean coherence value above 0.9 with respect to our threshold 0.8 and the level of consistency in second configuration is quiet better than the fist one for most of the sensors.
In Figure 5.26 the accuracy level of the data to each excitation points by considering all the sensors in assembly configuration is still remained above of our threshold 0.8. As depicted in following figure by arrow, the poor data specified by their color configuration. The lowest coherence averages relating to second assembly configuration when the sensors are on the blade and in this case poor coherence averages are relating to excitation point 17 with Mean Value 0.8447 which is located on the blade and nearest point to the root of the blade and it has very narrow space to access, in order to have clear impact but still above our threshold. Another excitation point in the first assembly configuration which has lowest mean coherence value is related to point 31 with Mean Value 0.8564 located on the circumference of the disk Figure 5.19.

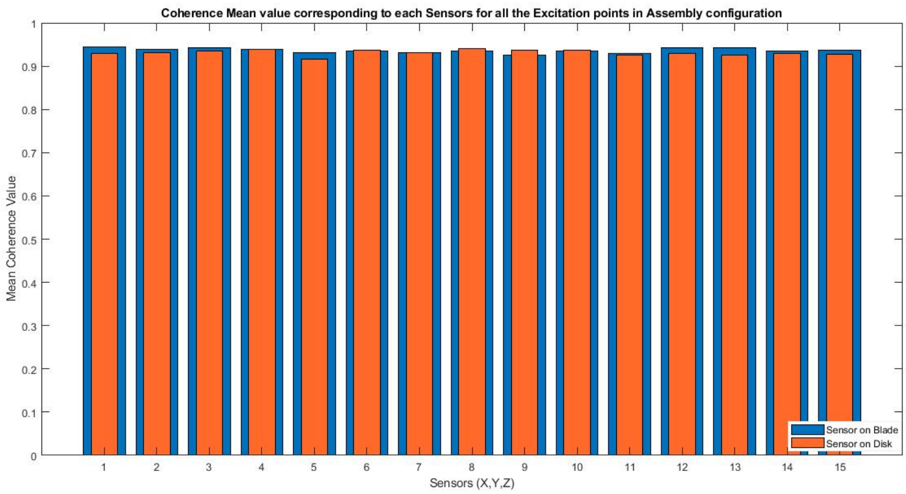

Figure 5.25: Coherence Mean Value corresponding to each sensors in X,Y and Z directions for all the excitation points in both Assembly configurations.

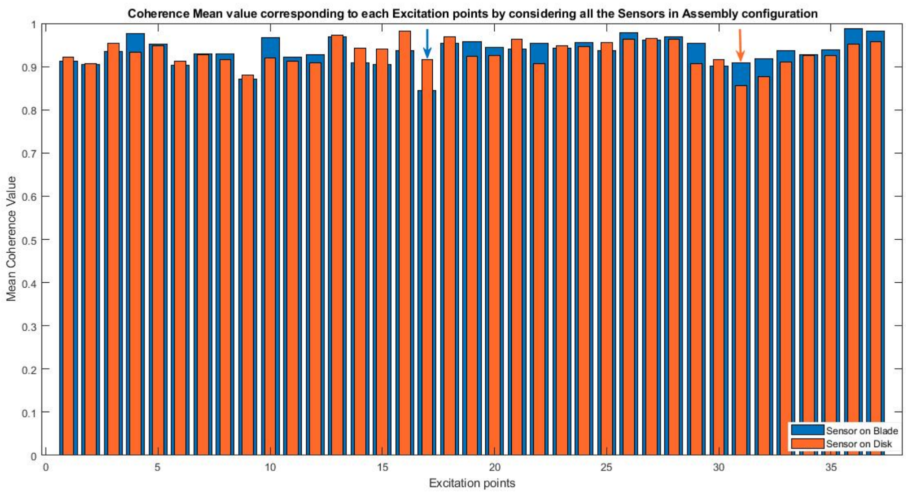

Figure 5.26: Coherence Mean Value corresponding to each excitation points by considering all the sensors in both Assembly configurations.

Chapter 6

CONCLUSION AND FUTURE WORK

Needless to say that vibration analysis allows to detect early signs of machine deterioration in order to repair machinery before catastrophic system functional failure takes place. Rotating machinery produces vibration during its normal operation as a consequence of friction and centrifugal forces of both the rotating parts and the bearings. As a result, vibration can be measured, recorded, trended, and in most cases even heard. Thus, we define vibration as a repetitive movement around a point of equilibrium characterized by its variation in amplitude and frequency.

In every turbo-machinery system the prediction of dynamic characteristics of mechanical joints are the key factor in vibration analysis, particularly at the inaccessible interfaces due to size of structure and geometry. With the aim of experimental campaign analysis by impact testing, the baseline of experiment has been set up in different configurations to measure the dynamics of a dummy blade and disk coupled by a dovetail root joint. The experimental test has been conducted to measure frequency response function on disk, blade and their assembly. Frequency response function is a frequency based powerful measurement function used to identify resonance frequency and damping which is a transfer function between input force and output response of a system. Another important tool to indicate the quality of our FRFs is Coherence. Coherence is a function which indicates the degree of linear relationship between two signals as a function of frequency.

In order to perform a test, the basic knowledge about the experiment should be provided and needed to have better understanding the concept of phenomenons during test. In every experiment, infrastructures is important to perform a test. In this thesis all the equipment which are necessary for an impact test checked during pretest setup. It has been tried to setup the experiment in proper way to minimize any external error due to environment of operator interfere. The method which is used in this test is roving hammer instead of roving accelerometer, all the accelerometer fixed in our structure.

Like every other experimental test errors will be appeared sometimes due to setup, input and output and signal processing. In this thesis we tried to avoid or at least minimized some of them. Input and output errors like location and alignment tried to minimize by double checked in our result at every impact. Another important error is related to how the structure setup. Support Dynamics, added dynamics and sensor placement are errors in this category. Free-free setup chosen for this experiment so it is very important to build a proper model which give us free-free behavior. It has been shown that the support eigenfrequency is much more less than the normal rule which is 10 times lower than first flexible mode. Double hits are unavoidable during impact test but here we tried to use new way to excite the structure with automatic hammer to avoid double impact at some points. Although in some excitation points the result of double impact with manual hammer is better than single impact with automatic hammer. The criterion here to compare the results is mean coherence value. In some points due to the poor coherence value more average hits and response window applied in order to improve our results. The good point is in most of excitation points, we did not use any window. Fortunately in each configuration, the level of accuracy mean coherence value are about our threshold.

A future investigation shall include a smart way define excitation points in our structure in order to avoid excite any nodal point or putting accelerometer close to nodes by using controllability and observability theory in the form of Hankel Singular Values. HSV offer a measure of the transmissibility energy from input to output for each state of a system. In structural dynamic systems this state is determined by the set of chosen DOF and the included eigenmodes. This is also possible to combine experimental results with numerical one based expansion method called System Equivalent Model Mixing (SEMM) is used to obtain expanded interface dynamics. The method uses numerical and experimental sub-models of each component and their assembly to produce the respective expanded or hybrid sub-models. By applying substructure decoupling to these sub-models, the joint can be identified.

Appendix A

Software

To perform an Impact Test, first make sure that you have turned on and correctly connected the LMS Scadas unit to your computer. So open the software by following the path:

Simcenter Testlab $\Rightarrow$ *Testlab Structure Acquisition* $\Rightarrow$ *Impact Testing*

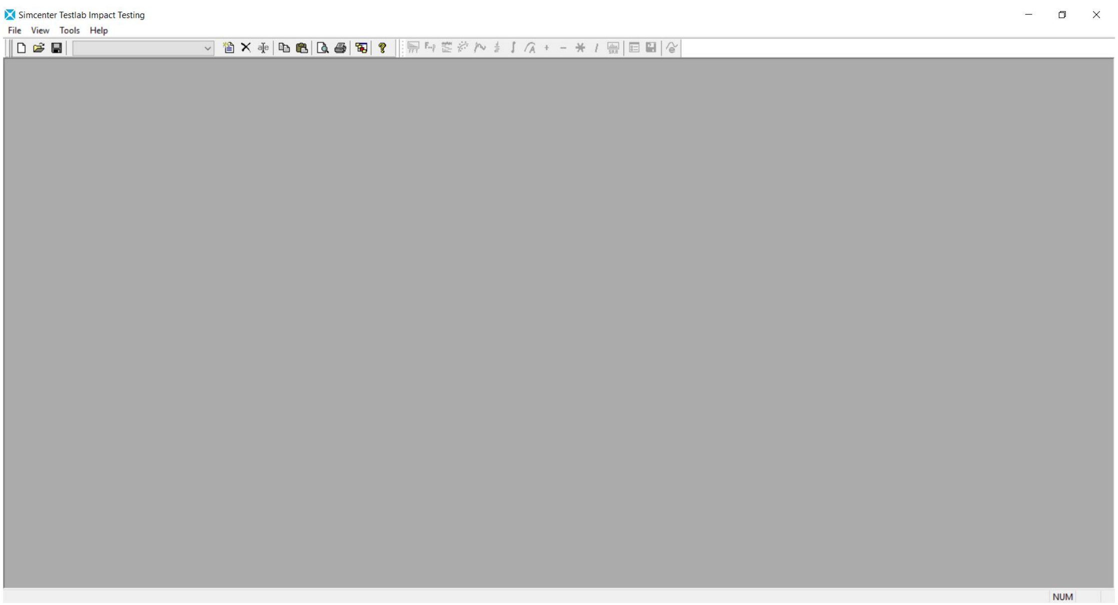

Figure A.1: Simcenter Impact Testing Initial Home Screen.

The preliminary steps have already done by bachelor student who did his thesis titled *Dynamic response measures user manual of the acquisition software and example of measurement results*, so in order to prevent rewrite the whole explanation will skip and just focus on all the procedures have done in this thesis.

As shown in Figure A.2. at the bottom of the screen you can move between the different worksheets of the software, of which a list is provided below:

- Documentation
- Navigator
- Channel Setup
- Calibration
- Impact Scope
- Impact Setup
- Measure
- Validate
- Post processing
- Geometry

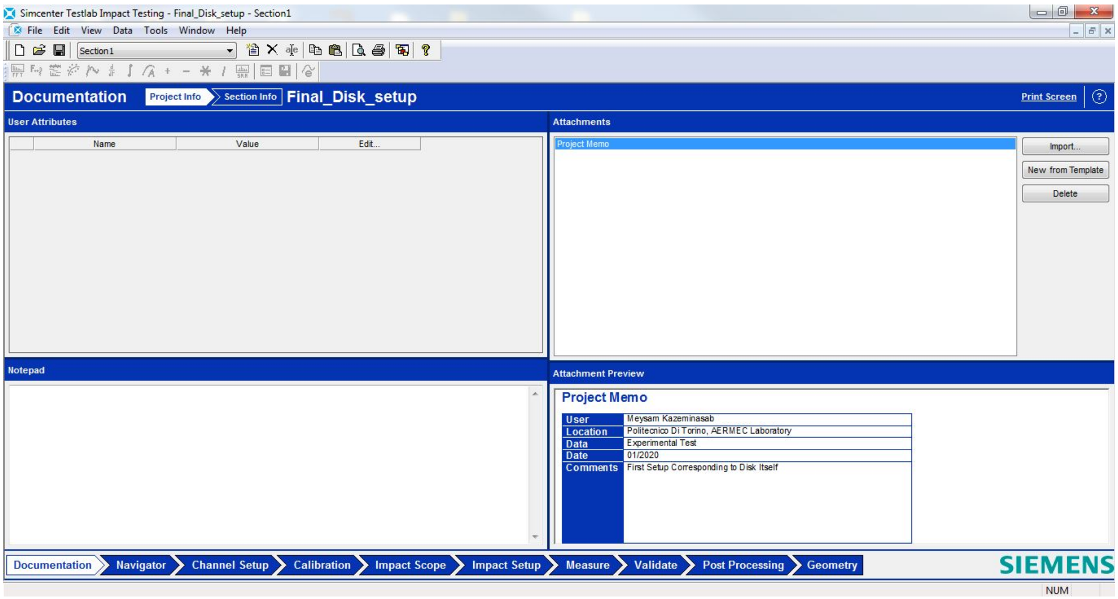

Figure A.2: Different Worksheets of The Software.

The first seven listed sheets will be analyzed concisely, useful for the analysis of frequency response function. In the following procedure, a brief explanation have provide about some of them.

A.0.1 Channel Setup

In the Channel Setup screen it is possible to set the measurement input and output channels. As already mentioned in section 4.2.1 the LMS Scadas has a maximum of 16 channels. Once the input channel has been declared (i.e. the hammer with instruments, on channel 1) and the 15 output channels (i.e. corresponding to 5 triaxial accelerometers). As an example the channel setup corresponding to Disk experimental setup will be depicted in Figure A.3.

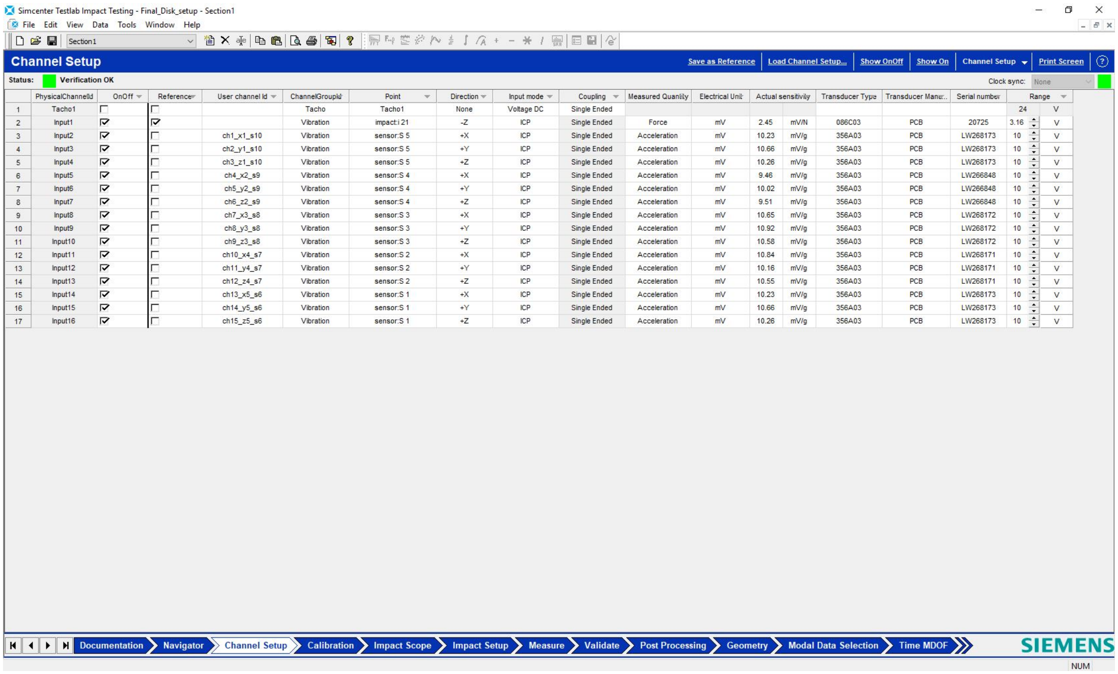

Figure A.3: Channel Setup Worksheet.

Once all the items have been completed and summarized in a table A.1 are the fundamental options to be set manually in the Channel Setup screen.

Table A.1: Fundamental Options of the Channel Setup Screen

	Impact Hammer	Accelerometer
Physical Channel ID	Input1	Input2,...,16
On/Off	On	On
Reference	Yes	No
Channel Group ID	Vibration	Vibration
Point	Impact	Sensor
Direction	-Z	+X,+Y,+Z
Input Mode	ICP	ICP
Coupling	Single Ended	Single Ended
Measured Quantity	Force	Acceleration
Electrical Unit	mV	mV
Actual Sensitivity	Variable[1]	Variable[2]
Transducer Type	086C03	356A03
Transducer Manufacturer	PCB	PCB
Serial Number	20725	Variable[3]
Range	Variable[4]	Variable[5]

[1] will be different corresponding to different hammer table4.1
[2] will be different corresponding to different direction and type of accelerometer.
[3] will be different corresponding to different type of accelerometer.
[4,5] will be variable due to position of impacts and accelerometer

A.0.2 Impact Scope

This window allows us to view the electrical input signals. On the Overview screen, the diagrams depicting these signals appear. Hitting the object on which the test is being carried out with a hammer.

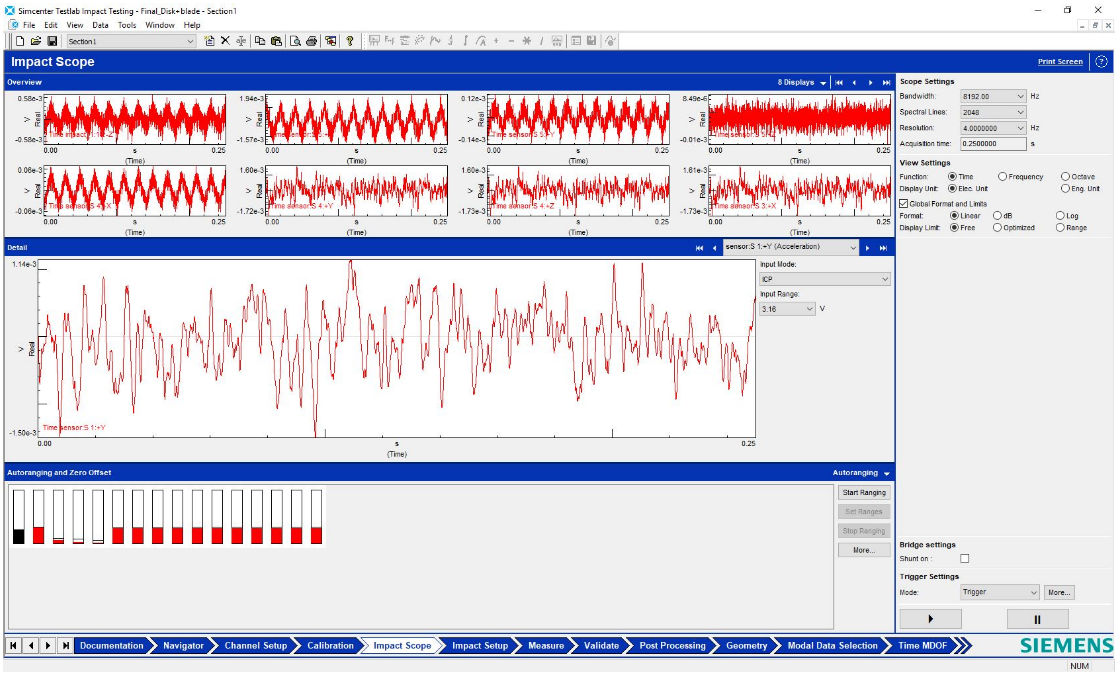

Figure A.4: Impact Scope Worksheet.

In the right section called *Scope Settings* you can change the values for the following fields:

- **Spectral lines:** represent the number of samples acquired;
- **Resolution:** represents the frequency relating to the period in which according to the theory each function can be thought of as periodic of period T_0 .This period represents the actual sampling time. Mathematically it can be defined as follows: indicate with ω_k the frequency of the $k-th$ harmonic and with ω_{k+1} that of the $(k+1)-th$ harmonic. Then the frequency resolution can be seen as the difference between the two successive harmonics $\Delta\omega_0 = \omega_{k+1} - \omega_k$ [1]
- **Bandwidth:** represents the product between the two previous ones.

In Simcenter Testlab under the Acquisition Setup tab there is a level bar which gives an indication of whether or not the data acquisition system is in overload. A white bar indicates the range is too large. Green bars indicate the range is set appropriately. Orange indicates that the signal is within the upper limit/overhead region. A red bar indicates the range is set too low and the channel is overloading [2].

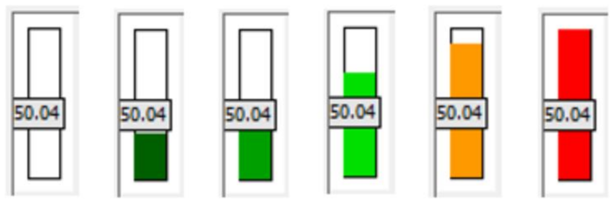

Figure A.5: Colors and Levels In The Bar Displays.

A.0.3 Impact Setup

This worksheet is to be completed once the Channel Setup has been completed before proceeding to the measurement screen. It is divided into three sub-screens:

- Trigger
- Bandwidth
- Windowing

All the data relating to these three options have been brought in the following table A.2.

Table A.2: Impact setup Information For All Configuration

	Scope Setting
Band Width	8192 Hz
Spectral Lines	2048
Resolution	4 Hz
Acquisition Time	0.25 s

A.0.4 Geometry

To create a model, starts by copying Cartesian coordinate of original disk and blade shapes in order to have wire-frame geometry which is close to the man shape of disk and blade. Designing the geometry in this way not only useful for visualization during the impact test(i.e. specified all the impacts and sensors position) but also it would be practical to animate the shapes when going through Modal Analysis.

The following procedures explains all the step by details [2].

Load in the Geometry Add-in to create a geometry in Simcenter Testlab by going to: *Tools* ⇒ *Add-ins* ⇒ *Geometry*.

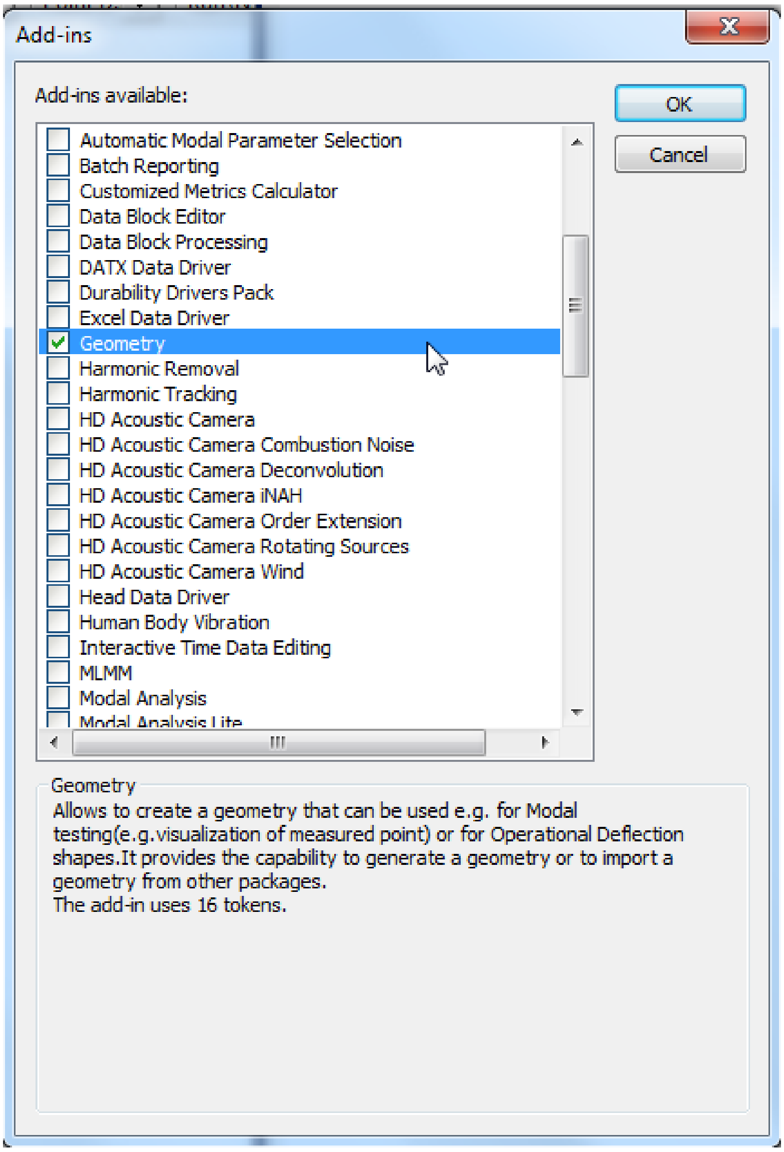

Figure A.6: Turn on the Geometry add-in [2].

Although it is possible to import a CAD model into the geometry worksheet, this section will describe creating a geometry from scratch. The worksheet on geometry consists of many minor-worksheets listed at the top of the worksheet on geometry.

The minor-worksheets include:

- Components
- Nodes
- Lines
- Surfaces
- Slaves
- Mesh area
- Torsional node

To create geometry some of those necessary parts will be explained. The example which is considered is a disk and all of the following procedure remains constant for blade itself and coupling system.

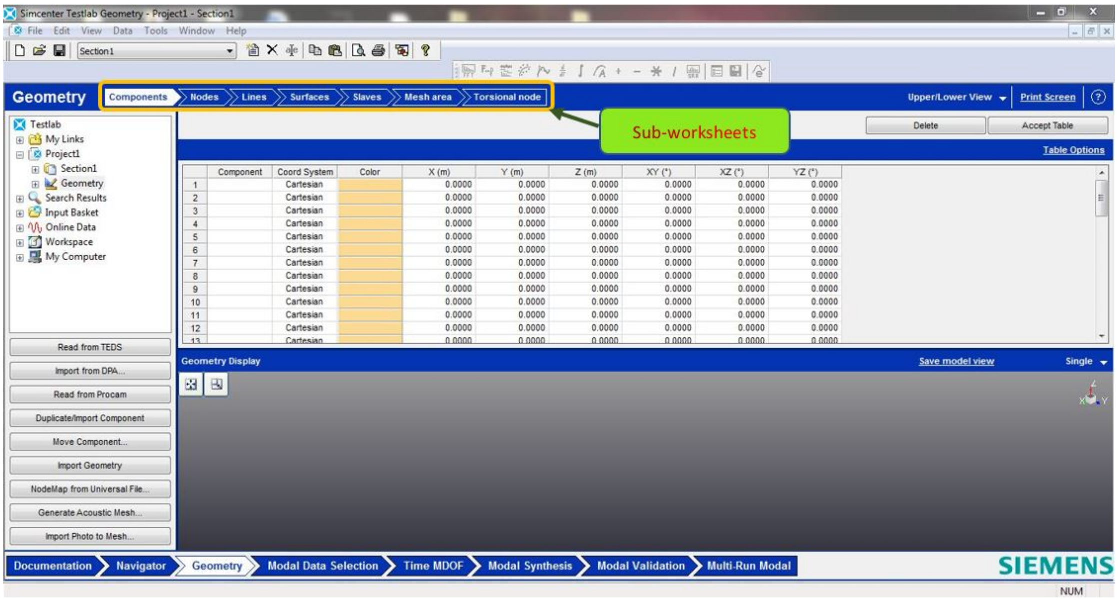

Figure A.7: The minor-worksheets always appear at the top of the Geometry worksheet.

Components

Start in the Components tab. For each component of the geometry, type in a name as seen in tree of *Geometry* in left side of page.Usage of different components of visualisation architecture helps as well as organisation. All the coordinate is collected from the original Disk and Blade shape.
Note that the created components include the *Circle* which is upper wireframe of the disk depicted with Orange ,*Circle down* is lower wireframe of the disk shown with Dark Blue, *Impact* which is the position of excitation points depicted with

Purple and *Sensor* which is the position of accelerometers depicted with Red in disk. The components of the disk are listed in the component table Figure 3.16. After making any changes to the geometry, press the *Accept Table* button (at the top right of the worksheet) to save the changes. Most buttons remain inactive until you pick *Accept Table*
One coordinate system can be specified for every part: either Cartesian, cylindrical, or spherical. The type of coordinate which is used in this part is Cartesian one.

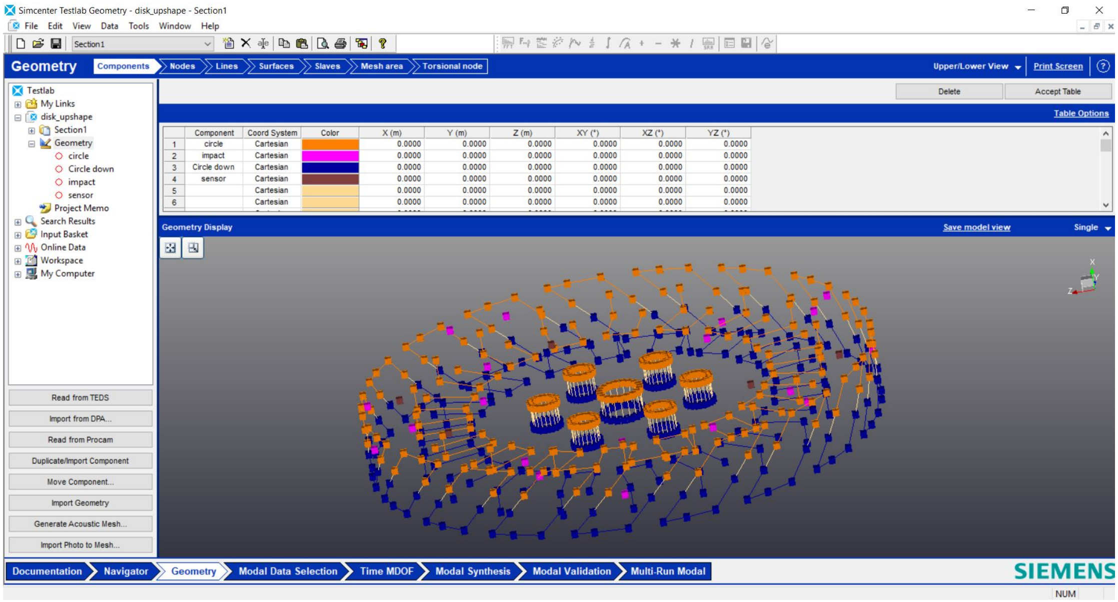

Figure A.8: Adding Components to the Geometry.

Once all components needed have been added, nodes can be specified for each component. The nodes on the part represent physical locations.

Nodes

Component by component nodes can be included in the tab Nodes. To bind nodes to a specific component, select the component in the tree on the left hand side of the computer.

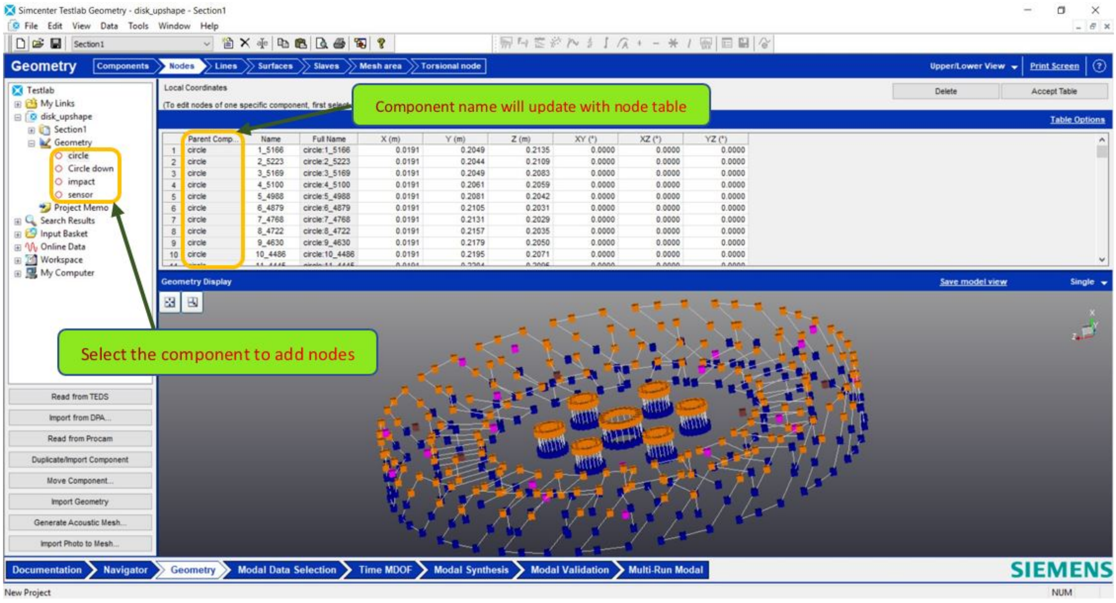

Figure A.9: The node worksheet. Select the component to add nodes to.

Fill in the *Name column*. Notice that the *full name* structure for each node is *Parent Component : Name*.

Fill in the X, Y, and Z coordinates for each node. This will place the nodes in space. You can chose to fill out with local or global coordinates (change this option under *Table Options*). It is also possible to rotate nodes about an axis using the XY, XZ, and YZ columns.

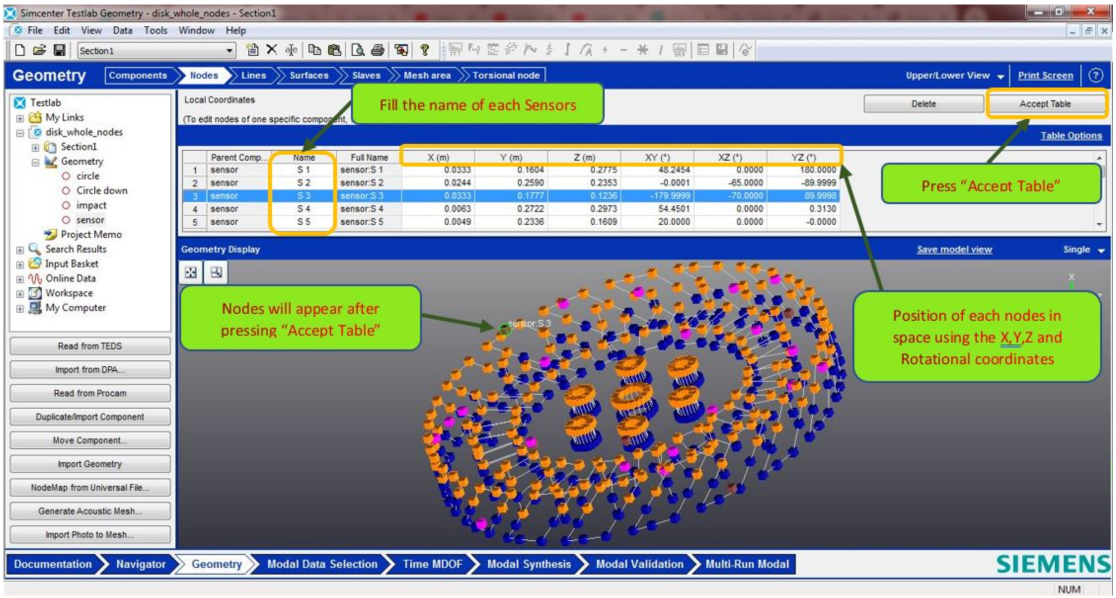

Figure A.10: Adding nodes to a geometry.

As always, when adding nodes click *Accept Table*. That will trigger the nodes to appear at the bottom of the screen in the geometry preview window.

Repeat this process until all components desired have nodes added.

Lines

To add lines, press the nodes in between. To create a continuous line you can continue to click between nodes. Once a line has been created, double click on the last node.

Once all the desired lines are added, press *"Accept Table"* to save your changes.

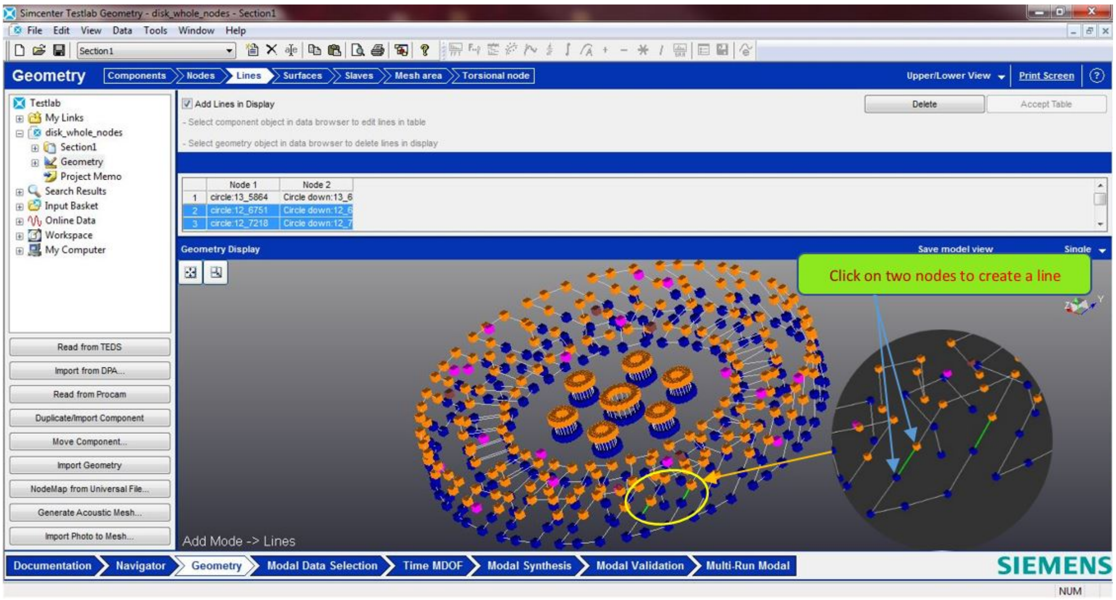

Figure A.11: Create a line by clicking node to node. When done creating the line, double click on the last node that the line should connect to.

After creating the wireframe separately for disk and blade,it is also possible to link together a wireframe and CAD geometry so that the modes can be animated on the full CAD geometry. In order to merge CAD design and wireframe follow the steps below:

1. Import the CAD file of the object under test.

   The *.stl* file is imported into the Geometry workbook.

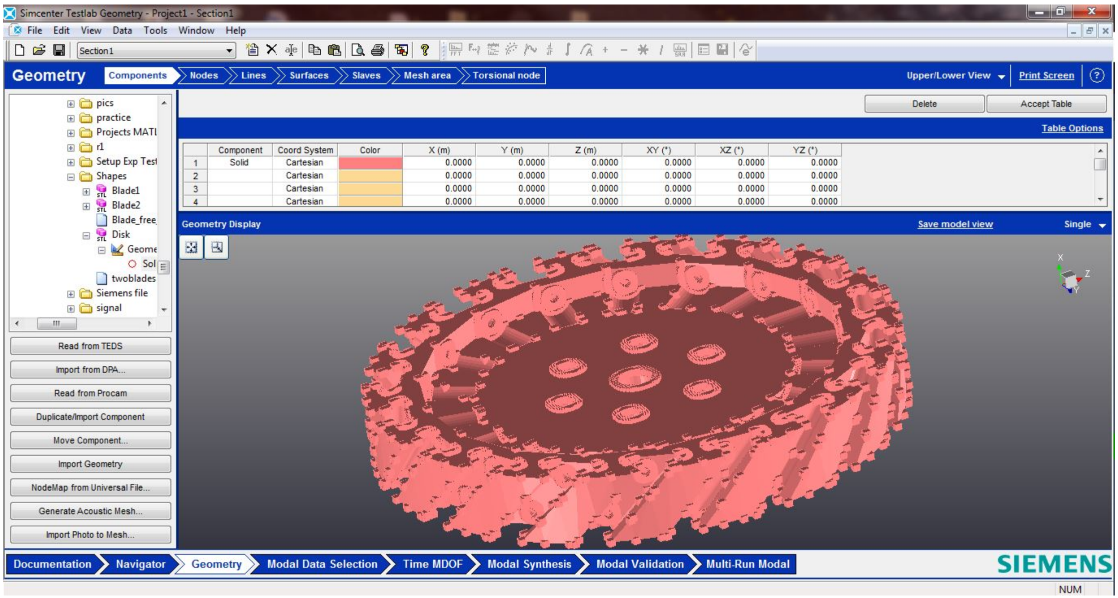

Figure A.12: Import a CAD file to the Geometry workbook.

2. Import the wireframe geometry.

   Now it is important to superimpose the wire frame generated in Simcenter Testlab Geometry onto the CAD geometry.To add the wireframe, highlight the component(s) in the browser tree on the left of the screen and click *Duplicate/Import Component*.

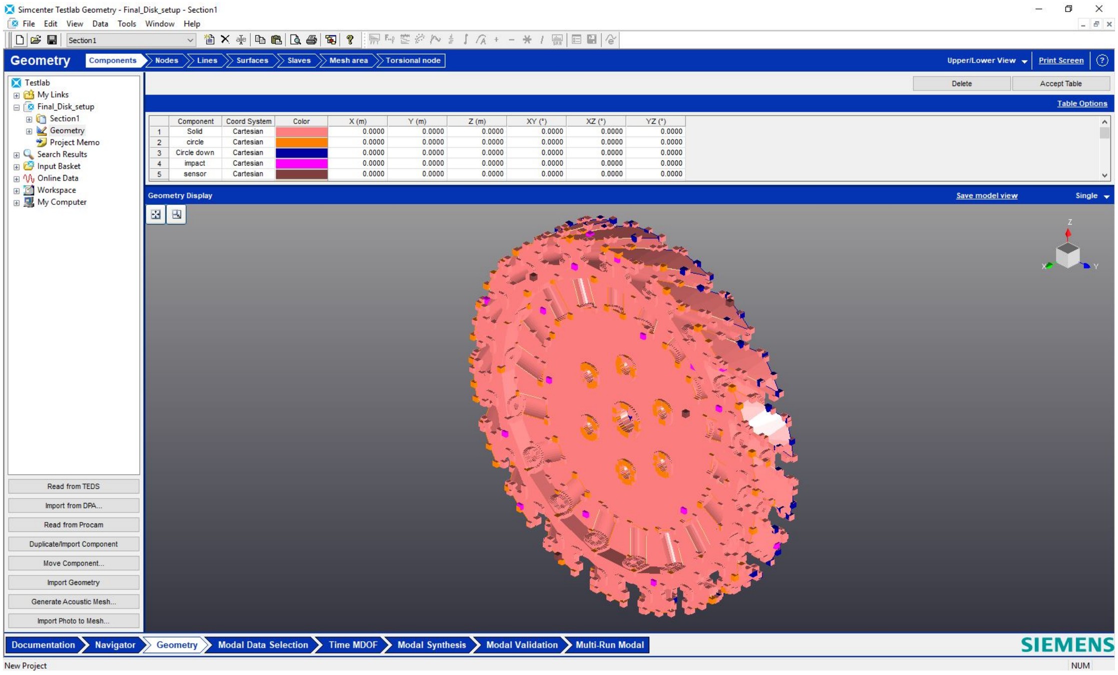

Figure A.13: The wireframe consists of five components. Select all five components in the tree on the left of the screen and then select *Duplicate/Import Component*.

Now both the wireframe and the CAD software appear in the Geometry workbook. See below Figure A.14 The wireframe is overlaid over the CAD.

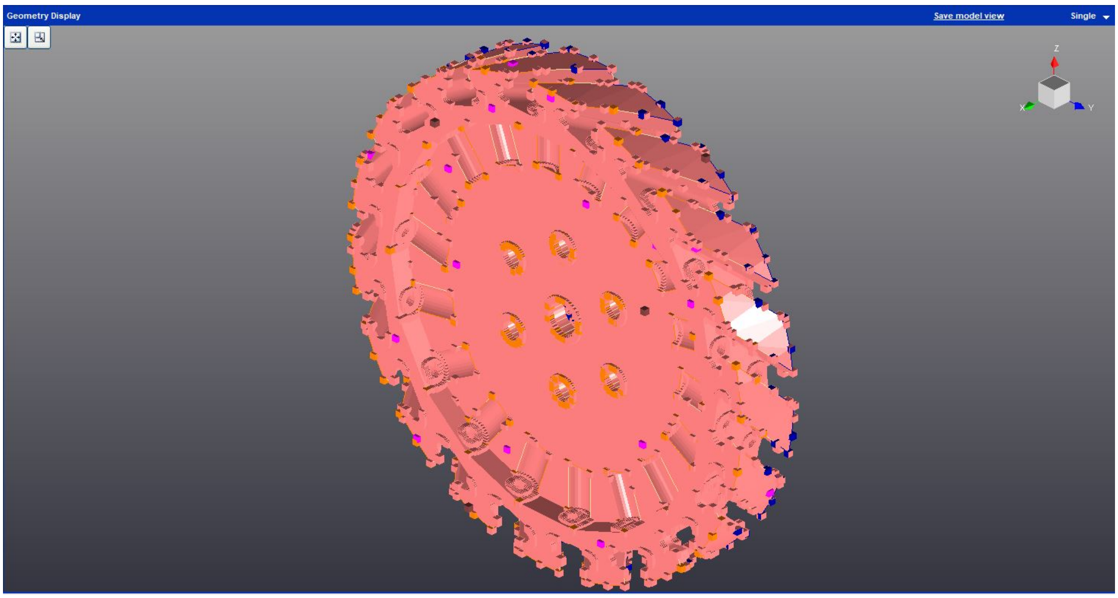

Figure A.14: The wireframe is superimposed over the CAD.

3. Link the CAD and wireframe together.

There has to be an connection between the wireframe nodes and the CAD nodes. This will give the software the information relevant to which wireframe node corresponds to which CAD node. It is needed for proper animation of the CAD geometry [2].

Through drawing lines between the wireframe nodes and the CAD nodes, the connection between the two geometries is complete

Go to the Geometry tab *Lines* sub-worksheet. Add lines between nodes on the wire frame and nodes at the same position on the geometry.

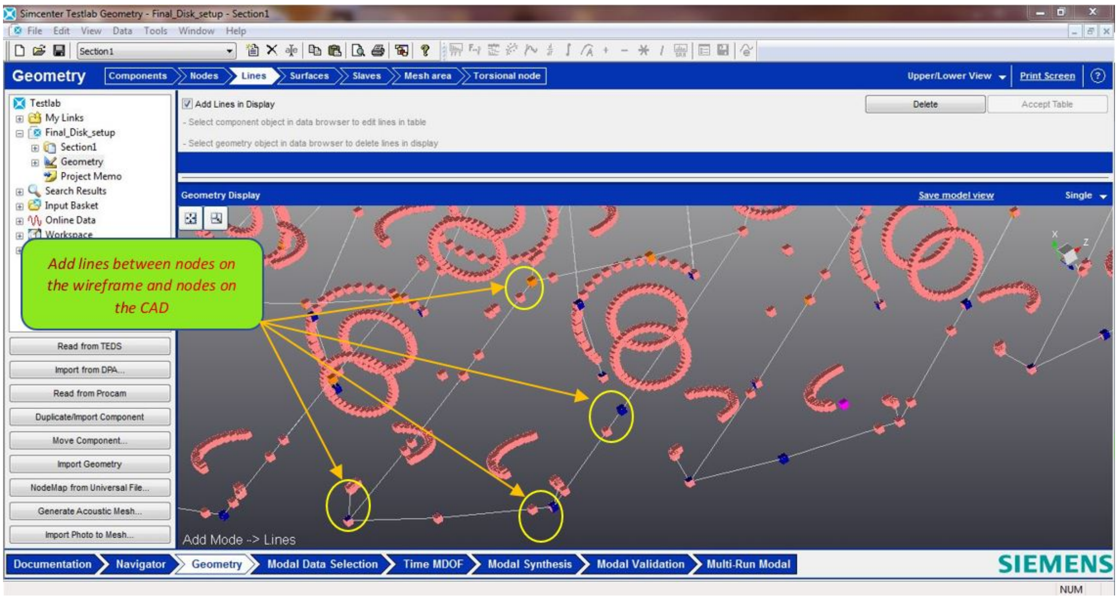

Figure A.15: Add lines between nodes on the wireframe and nodes on the CAD that correspond to the same location on the part.

How to define position of sensors and impacts on the geometry

Open the software through *Impact Testing* then go to *channel setup window* and open *use geometry tab*, choose use geometry , then click on refresh to appear the whole shape. Now the whole shape appear and table corresponding to node name of all the components have already design, the next step is to find the node name correspond to impacts and sensors in the table.

The further step is to select for example *input 1*, choose whole row, also try to find impact 19 assume named *impact: i 19* from the table which have all the coordinate. then after you select both of them (*impact: i 19* coordinate from the table and *input 1* from the channel set up) then click on *insert* to fix that position as impact 19 on the main shape. You can follow the procedure for all the excitation points and sensors.

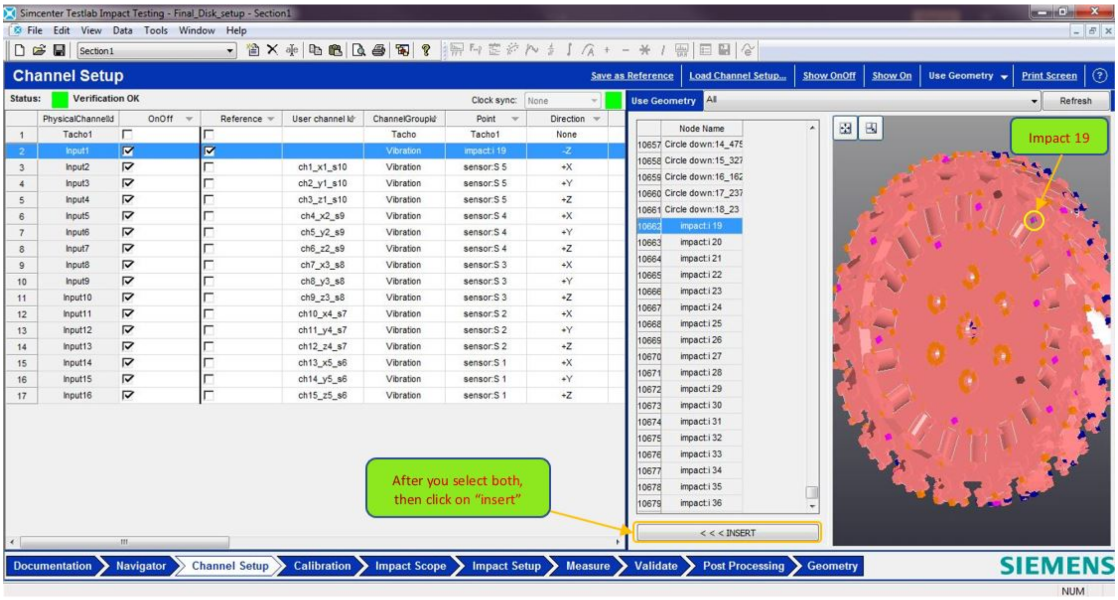

Figure A.16: Define position of sensors and impacts on the geometry.

Note that there might be several impact points on the objects so it is necessary to define all the impact points through *Measure window*. By choosing *edit point* as shown in the bellow picture.

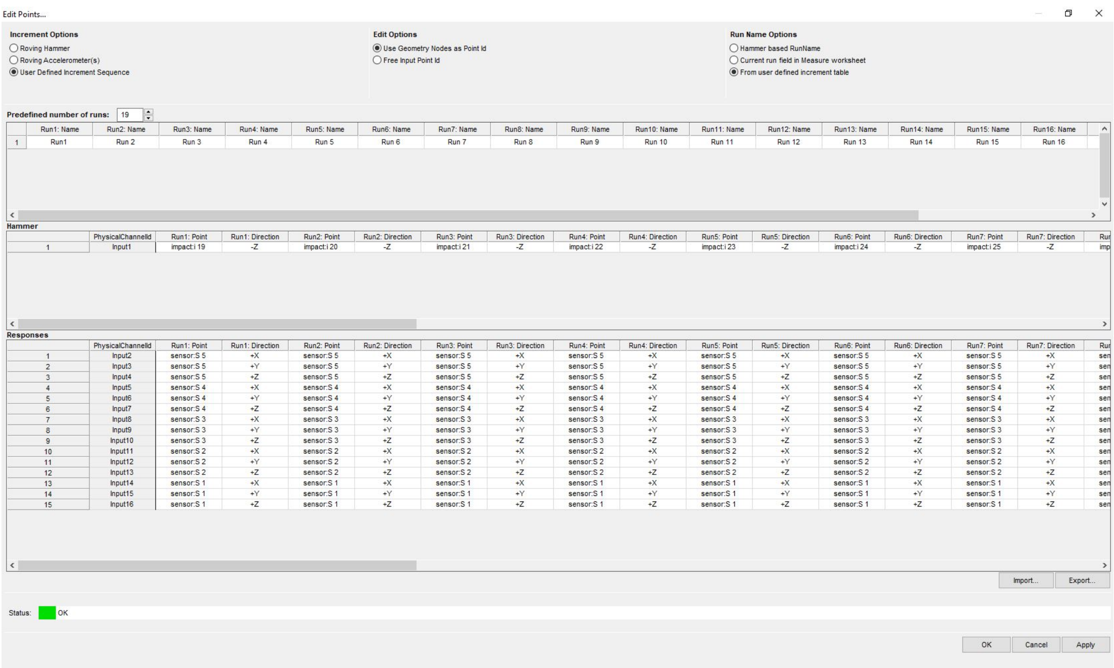

Figure A.17: Edit point window in order to add all excitation points.

Appendix B

Data Sheet

All the data sheet corresponding to Accelerometer, Manual Hammer and Cables provided in this section.

The impact hammer information shown in the following Figures B.1 and B.2. Accelerometer data sheet provided in the Figures B.3 and B.4

Model Number 086C03	ICP® IMPACT HAMMER	Revision: L ECN #: 32387

Performance	ENGLISH	SI	
Sensitivity(± 15 %)	10 mV/lbf	2.25 mV/N	
Measurement Range	± 500 lbf pk	± 2224 N pk	
Resonant Frequency	≥ 22 kHz	≥ 22 kHz	
Non-Linearity	≤ 1 %	≤ 1 %	
Electrical			
Excitation Voltage	20 to 30 VDC	20 to 30 VDC	
Constant Current Excitation	2 to 20 mA	2 to 20 mA	
Output Impedance	<100 ohm	<100 ohm	[1]
Output Bias Voltage	8 to 14 VDC	8 to 14 VDC	
Discharge Time Constant	≥ 2000 sec	≥ 2000 sec	[1]
Physical			
Sensing Element	Quartz	Quartz	
Sealing	Epoxy	Epoxy	
Hammer Mass	0.34 lb	0.16 kg	
Head Diameter	0.62 in	1.57 cm	
Tip Diameter	0.25 in	0.63 cm	
Hammer Length	8.5 in	21.6 cm	
Electrical Connection Position	Bottom of Handle	Bottom of Handle	
Extender Mass Weight	2.6 oz	75 gm	
Electrical Connector	BNC Jack	BNC Jack	

CE [2]

All specifications are at room temperature unless otherwise specified.
In the interest of constant product improvement, we reserve the right to change specifications without notice.

ICP® is a registered trademark of PCB Group, Inc.

OPTIONAL VERSIONS

Optional versions have identical specifications and accessories as listed for the standard model except where noted below. More than one option may be used.

T - TEDS Capable of Digital Memory and Communication Compliant with IEEE P1451.4

TLD - TEDS Capable of Digital Memory and Communication Compliant with IEEE 1451.4

NOTES:
[1] Typical.
[2] See PCB Declaration of Conformance PS068 for details.

SUPPLIED ACCESSORIES:
Model 081B05 Mounting Stud (10-32 to 10-32) (2)
Model 084A08 Extender - Steel, 0.6" Diameter (1)
Model 084B03 Hard Tip- Hard (S.S) (1)
Model 084B04 Hammer Tip- Medium (White Plastic) (1)
Model 084C05 Hammer Tip- Soft (Black) (2)
Model 084C11 Hammer Tip- Supersoft (Red) (2)
Model 085A10 Vinyl Cover For Medium Tip (Blue) (2)
Model HCS-2 Calibration of Series 086 instrumented impact hammers (1)

Entered:	Engineer:	Sales:	Approved:	Spec Number:
Date: 2/24/10	Date: 12/8/09	Date: 2/17/10	Date: 2/17/10	15273

PCB PIEZOTRONICS™
VIBRATION DIVISION
3425 Walden Avenue, Depew, NY 14043

Phone: 716-684-0001
Fax: 716-685-3886
E-Mail: vibration@pcb.com

Figure B.1: Data sheet of manual impact hammer.

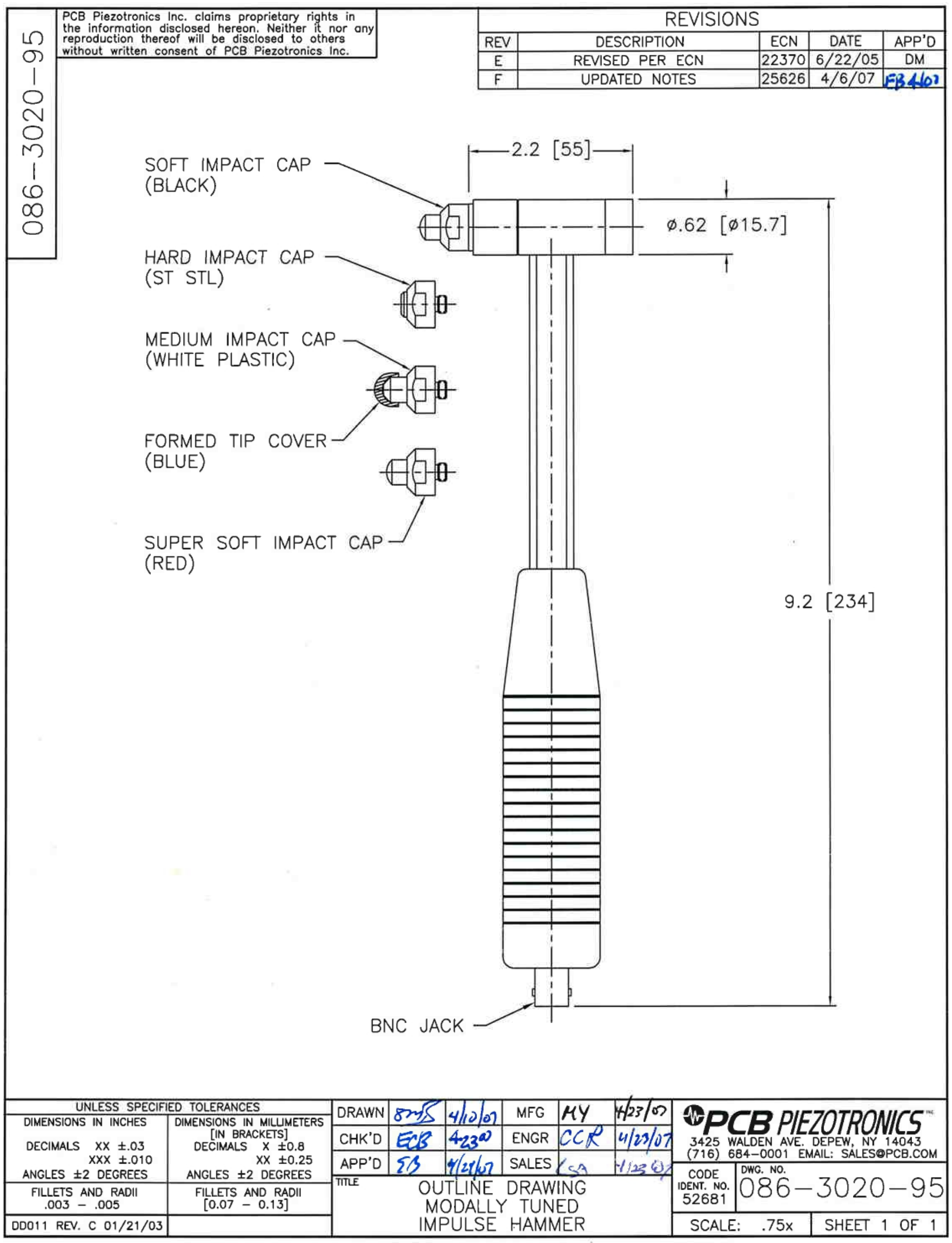

Figure B.2: Data sheet of manual impact hammer.

Model Number 356A03	TRIAXIAL ICP® ACCELEROMETER	Revision: H ECN #: 49419

Performance	ENGLISH	SI	
Sensitivity(± 20 %)	10 mV/g	1.02 mV/(m/s²)	
Measurement Range	± 500 g pk	± 4905 m/s² pk	
Frequency Range(± 5 %)(y or z axis)	2 to 8000 Hz	2 to 8000 Hz	
Frequency Range(± 5 %)(x axis)	2 to 5000 Hz	2 to 5000 Hz	
Frequency Range(+1 dB)(x axis)	≥ 8 kHz	≥ 8 kHz	
Resonant Frequency	≥ 50 kHz	≥ 50 kHz	
Broadband Resolution(1 to 10,000 Hz)	0.003 g rms	0.03 m/s² rms	[1]
Non-Linearity	≤ 1 %	≤ 1 %	[2]
Transverse Sensitivity	≤ 5 %	≤ 5 %	
Environmental			
Overload Limit(Shock)	± 5000 g pk	± 49,050 m/s² pk	
Temperature Range(Operating)	-65 to +250 °F	-54 to +121 °C	
Temperature Response	See Graph	See Graph	[1]
Electrical			
Excitation Voltage	22 to 30 VDC	22 to 30 VDC	
Constant Current Excitation	2 to 20 mA	2 to 20 mA	
Output Impedance	≤ 200 Ohm	≤ 200 Ohm	
Output Bias Voltage	9 to 16 VDC	9 to 16 VDC	
Discharge Time Constant	0.24 to 1.0 sec	0.24 to 1.0 sec	
Settling Time(within 10% of bias)	<3 sec	<3 sec	
Spectral Noise(1 Hz)	1200 μg/√Hz	11,772 (μm/sec²)/√Hz	[1]
Spectral Noise(10 Hz)	300 μg/√Hz	2943 (μm/sec²)/√Hz	[1]
Spectral Noise(100 Hz)	100 μg/√Hz	981 (μm/sec²)/√Hz	[1]
Spectral Noise(1 kHz)	30 μg/√Hz	294 (μm/sec²)/√Hz	[1]
Physical			
Sensing Element	Ceramic	Ceramic	
Sensing Geometry	Shear	Shear	
Housing Material	Titanium	Titanium	
Sealing	Hermetic	Hermetic	
Size (Height x Length x Width)	0.25 in x 0.25 in x 0.25 in	6.35 mm x 6.35 mm x 6.35 mm	
Weight(without cable)	0.04 oz	1.0 gm	[1]
Electrical Connector	Integral Cable	Integral Cable	
Electrical Connection Position	Side	Side	
Cable Termination	1/4-28 4-Pin Jack	1/4-28 4-Pin Jack	
Cable Length	5 ft	1.5 m	
Cable Type	034 4-cond Shielded	034 4-cond Shielded	
Mounting	Adhesive	Adhesive	

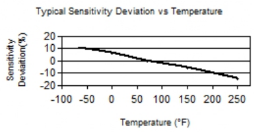

CE [3]

OPTIONAL VERSIONS

Optional versions have identical specifications and accessories as listed for the standard model except where noted below. More than one option may be used.

J - Ground Isolated

Electrical Isolation(Base)	>10⁸ Ohm	>10⁸ Ohm
Size - Height x Length x Width	.28 in x .28 in x .28 in	7.10 mm x 7.10 mm x 7.10 mm
Weight	.04 oz	1.2 gm

W - Water Resistant Cable

Electrical Connector	Sealed Integral Cable	Sealed Integral Cable

NOTES:

[1] Typical.
[2] Zero-based, least-squares, straight line method.
[3] See PCB Declaration of Conformance PS023 for details.

SUPPLIED ACCESSORIES:

Model 034G05 4-cond. shielded cable, 5 ft (1.5M), 4-pin plug to (3) BNC plugs (1)
Model 080A109 Petro Wax (1)
Model 080A90 Quick Bonding Gel (1)
Model ACS-1T NIST traceable triaxial amplitude response, 10 Hz to upper 5% frequency. (1)

Entered: LK	Engineer: SDS	Sales: KK	Approved: JJB	Spec Number:
Date: 4/30/2019	Date: 4/30/2019	Date: 4/30/2019	Date: 4/30/2019	46486

All specifications are at room temperature unless otherwise specified.
In the interest of constant product improvement, we reserve the right to change specifications without notice.

ICP® is a registered trademark of PCB Group, Inc.

PCB PIEZOTRONICS
3425 Walden Avenue, Depew, NY 14043

Phone: 716-684-0001
Fax: 716-684-0987
E-Mail: info@pcb.com

Figure B.3: Data sheet of accelerometer.

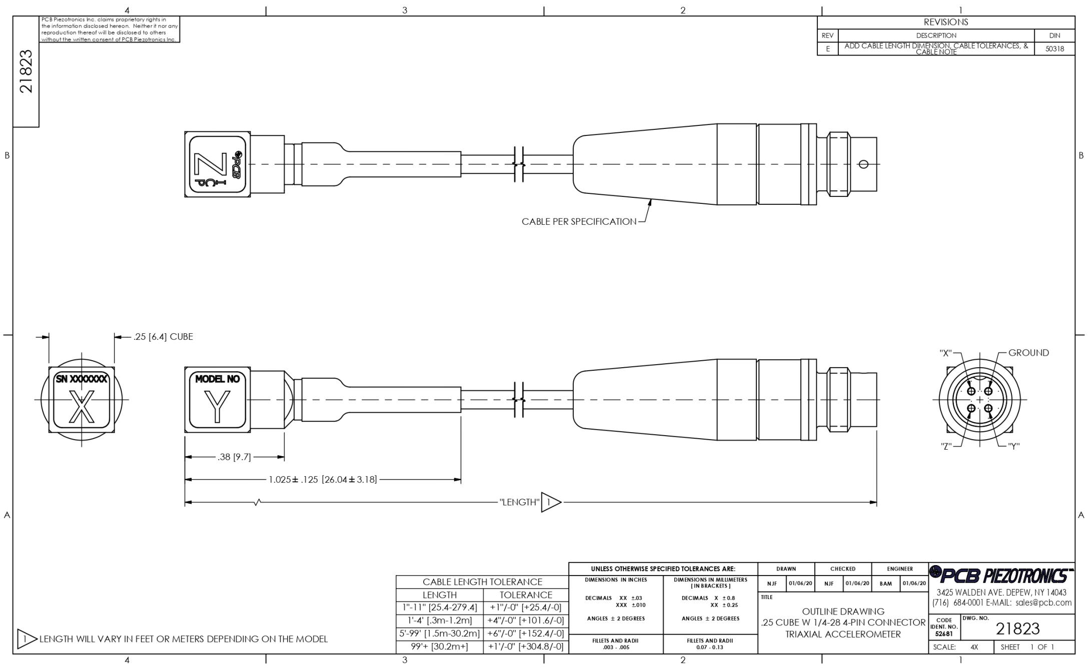

Figure B.4: Data sheet of accelerometer.

Bibliography

[1] A. Fasana S. Marchesiello . *Meccanica delle vibrazioni.* Torino: CLUT, 2006 (cit. on pp. 4–6, 93).

[2] SIEMENS. *SIMCENTER Testlab.* URL: `https://community.sw.siemens.com/` (cit. on pp. 6, 22–26, 29–33, 36–38, 52, 54, 55, 94, 95, 103).

[3] Clarence W. de Silva Farbod Khoshnoud Maoqing Li Saman K. Halgamuge. *Mechatronics Fundamentals and Applications.* Boca Raton: CRC Press, 2015 (cit. on pp. 6–8, 20, 33–35).

[4] M. V. VAN DER SEIJS. «Experimental Dynamic Substructuring: Analysis and Design Strategies for Vehicle Development». PhD thesis. Enschede: Delft University of Technology, 2016 (cit. on pp. 10, 11).

[5] M. Allen D. Rixen P. Tiso R. Mayes M. van der Seijs T. Abrahamsson. *Substructuring in Engineering Dynamics: Emerging Numerical and Experimental Techniques.* Gewerbestrasse 11 6630 Cham. Switzerland: Springer, 2018 (cit. on p. 11).

[6] S.W.B. Klaassen. «Towards Hybrid Modular Design of Structural Dynamic Models». MA thesis. Delft: Delft University of Technology, 2017 (cit. on p. 11).

[7] D. J. Ewins. *Modal Testing: Theory, Practice and Application.* 16 Coach House Cloisters, 10 Hitchin Street, Baldock, Hertfordshire, England, SG7 6AE: RESEARCH STUDIES PRESS LTD, 2000 (cit. on pp. 13–21, 26–29, 35).

[8] PCB. *Sensors and Impact Hammer data sheet.* URL: `https://www.pcb.com/` (cit. on pp. 41, 42, 44, 45).